TÉCNICO LISBOA

The Use of High Strength Steel in Bridge Decks

Pierre Thomas Jacques Lorne

Thesis to obtain the Master of Science Degree in

Civil Engineering

Supervisors

Prof. Dr. José Joaquim Costa Branco de Oliveira Pedro

Prof. Dr. Alain Nussbaumer

Examination Committee

Chairperson: Prof. Jorge Miguel Silveira Filipe Mascarenhas Proença

Supervisor: Prof. Dr. José Joaquim Costa Branco de Oliveira Pedro

Member: Prof. Pedro António Martins Mendes

June 2017

Acknowledgements

The achievement of this work is the conclusion of six years of amazing studies, and allowed me to consolidate and use the knowledge learned throughout the Bachelor and the Master within the civil engineering section of the Ecole Polytechnique Fédérale de Lausanne. The project has been a source of motivation and personal enrichment; it would not have been possible without the participation of a few people.

In the first place, I would like to thank Professors Alain Nussbaumer (EPFL) and José Oliveira Pedro (IST). To them all my gratitude for the support, knowledge and investment they have made throughout the year. It was a real pleasure to study under their guidance to carry out this Master project.

To Maxime Duval, for the time spent working together on our respective theses. His good mood illuminated the days at the office and made the work more enjoyable. To André Biscaya, whose advice and availability were of invaluable help.

To the professors of EPFL, IITM and IST, for all the academic knowledge and methods of work transmitted during these six years, as well as the experience of having been able to study in three exceptional universities.

To my family, whose constant support, patience and encouragement gave me the ideal setting to succeed in my studies and pushed me to surpass myself ever more.

To my friends, from university and elsewhere, from all walks of life, for having accompanied me throughout this journey, and with whom I shared unique moments, among whom François de La Barre, Charles Jeanbart, Camille Jaccard, Thomas Bourany, Nicolas Rey, and so many others.

Abstract

Composite bridges combining steel plates with a concrete slab deck have been widely used due to their economic, constructive and structural advantages. In parallel, High Strength Steels (HSS) have emerged; their use in composite bridge decks could become an interesting option.

Three designs are presented for a composite steel-concrete roadway bridge, based on the Eurocodes: the design A, with two welded I-section girders in S355 steel; the design B, with two welded I-section girders in S690 steel; and the design C, with girders in S690 steel using tubular profiles for the flanges. A comparative analysis of the benefits associated with the three solutions is carried out.

During the design of solutions B and C, it is verified that some rules of EC3-1-5 are very conservative; adaptations are suggested for the case of AAR. By using tubular flanges, it is also possible to consider the webs to be fixed and not simply supported, which is considered in the design C.

The design B presents several advantages compared to the solution A. The weight of the girders reduces consequently; the use of HSS provides more reserve in resistance at ULS. However, problems related to local buckling of the plates in the section and fatigue become critical in the design.

The design C was implemented to try to solve stability and fatigue issues. With a steel weight in the deck similar to solution B, the reserve in resistance at ULS is also high and lateral stability improves greatly. However, the problems related to fatigue remain, and the execution of some constructive details becomes more complex.

Keywords

High strength steel, Composite steel-concrete deck, Tubular flanges, Plate buckling, Lateral-torsional buckling, Fatigue

Resumo

As pontes mistas que combinam placas de aço com um tabuleiro de laje em betão têm sido amplamente utilizadas devido às suas vantagens económicas, construtivas e estruturais. Em paralelo, os Aços de Alta Resistência (AAR) começam a ser utilizados; o seu uso em tabuleiros de pontes mistas pode se tornar uma opção interessante.

São apresentados três soluções para um tabuleiro misto aço-betão, com base nos Eurocódigos: o dimensionamento A, com duas vigas de secção soldada de alma cheia em aço S355; o dimensionamento B, com duas vigas de secção soldada em aço S690; e o dimensionamento C, com vigas em S690 que utilizam banzos com perfis tubulares. Realiza-se uma análise comparativa dos benefícios associados às três soluções.

No decorrer do dimensionamento das soluções B e C verifica-se que algumas regras do EC3-1-5 são muito conservativas, propondo-se adaptações para o caso dos AAR. Utilizando banzos tubulares é também possível considerar as almas encastradas e não apoiadas, o que é considerado no dimensionamento C.

O dimensionamento B apresenta várias vantagens em comparação com a solução A. O peso das vigas reduz-se consideravelmente; o uso de AAR fornece mais reserva em resistência nos ULS. No entanto, os problemas relacionados a encurvadura local das placas que compõe a secção e a fadiga tornam-se determinantes no dimensionamento.

O dimensionamento C foi implementado para procurar resolver os problemas de estabilidade e de fadiga. Com um peso de aço no tabuleiro semelhante à solução B, a reserva na resistência ULS é também elevada e a estabilidade lateral melhora muito. No entanto, os problemas relacionados à fadiga mantêm-se e a execução de alguns detalhes construtivos torna-se mais complexos.

Palavras-chave

Aço de alta resistência, Tabuleiro misto aço-betão, Banzo tubular, Encurvadura de placa, Encurvadura lateral, Fadiga

Contents

List of tables

List of figures

List of abbreviations and symbols

The following list is not exhaustive. Other notations may be introduced locally in the text.

Capital Latin letters

A_c	Cross-sectional area of the half-slab
$A_{f,sup/inf}$	Cross-sectional area of the upper / lower steel flange
A_s	Cross-sectional area of reinforcement
A_{slab}	Cross-sectional area of the concrete slab
A_{tot}	Cross-sectional total area of one main structural steel girder
A_w	Cross-sectional area of the steel web of the girder
C_D	Rigidity of the transverse bracing frame
D_f	Diameter of the flange in the design C
E_a	Modulus of elasticity of structural steel
E_{cm}	Mean value of the modulus of elasticity of concrete
E_s	Modulus of elasticity of reinforcing steel
F	Applied force
G_k	Characteristic value of the action due to permanent loads
I	Second moment of area
$L_{cracked}$	Length of a cracked zone
L_e	Equivalent span length
L_i	Length of span i
L_{tot}	Total length of the bridge
M_{Ed}	Design bending moment
$M_{el,Rd}$	Design value of the elastic resistance moment of the composite section
$M_{f,Rd}$	Design value of the plastic resistance moment without the steel web
$M_{pl,Rd}$	Design value of the plastic resistance moment
M_s	Bending moment in the composite girder due to shrinkage
N_s	Axial force in the composite girder due to shrinkage
P_{Rd}	Design value of the shear resistance of a single connector
Q_k	Characteristic value of the action due to traffic
Q_{ki}	Concentrated traffic load (TSL)
$Q_{k,fat}$	Fatigue load
RH	Ambient relative humidity (in %)
S_k	Characteristic value of the action due to shrinkage
T_{Ed}	Minimum ambient air temperature
T_k	Characteristic value of the action due to temperature variations
$V_{b,Rd}$	Design value of the shear buckling resistance of the steel girder
$V_{bf,Rd}$	Contribution of the flanges to the shear buckling resistance of the web

$V_{bw,Rd}$	Contribution of the web to the shear buckling resistance
V_{cr}	Pre-critical contribution to the shear buckling resistance
V_{Ed}	Design shear force
$V_{pl,a,Rd}$	Design value of the plastic shear resistance of the steel girder
V_{Rd}	Design shear resistance
V_{σ}	Post-critical contribution to the shear buckling resistance
W_{arm}	Section modulus with respect to the mid-plane of the reinforcement
W_{bet}	Section modulus with respect to the extreme fibre of the concrete slab
W_{inf}	Section modulus with respect to the lower fibre of the lower flange
W_{sup}	Section modulus with respect to the upper fibre of the upper flange

Small Latin Letters

a	Length of a web plate between adjacent vertical stiffeners
b	Width of a structural element
b_{eff}	Effective width
d	Diameter of the shank of a stud connector
e	Thickness of the concrete haunch; spacing of rows of connectors
f_{cd}	Design compressive strength of concrete
f_{ck}	Characteristic compressive cylinder strength of concrete at 28 days
f_{cm}	Mean value of concrete cylinder compressive strength
f_{ctm}	Mean value of concrete axial tensile strength
$f_{ctk,0.05}$	5% fractile of the characteristic axial tensile strength of concrete
$f_{ctk,0.95}$	95% fractile of the characteristic axial tensile strength of concrete
f_{sd}	Design yield strength of reinforcement
f_{sk}	Characteristic yield strength of reinforcement
f_{y}	Yield strength of structural steel
f_{yd}	Design yield strength of structural steel
f_{yk}	Characteristic yield strength of structural steel
f_{u}	Ultimate strength of the structural steel
g_{a}	Selfweight of a steel element
$g_{asphalt}$	Selfweight of the asphalt layer
$g_{barrier}$	Selfweight of a safety barrier
g_{c}	Selfweight of the concrete half-slab
h	Height of a plate
h_a	Height of the steel girders
h_c	Height of the steel web in compression
$h_{w,eff}$	Effetive height of the steel web when the steel girder is in class 4
h_0	Notional size of the concrete slab
h_{tot}	Total height of the composite girder

k_σ	Plate buckling coefficient for normal stresses
k_τ	Plate buckling coefficient for shear stresses
n_0	Structural steel / concrete modular ratio for short-term loading
n_L	Structural steel / concrete modular ratio for long-term loading
n_s	Structural steel / concrete modular ratio for shrinkage effects
n_φ	Structural steel / concrete modular ratio for permanent loads
p	Perimeter of the concrete slab section
q_{ki}	Uniformly distributed traffic load (UDL)
s	Spacing between the reinforcing steel bars of a single layer
s_a	Centre-to-centre spacing between the main girders
t	Plate / slab thickness; age
t_0	Mean age of the concrete at loading
v_{Ed}	Design value of the longitudinal shear per unit length
z	Position of the centre of gravity of a section

Capital Greek letters

ΔT_1	Positive variation of the temperature
ΔT_2	Negative variation of the temperature
ΔT_E	Non-linear part of the thermal gradient
ΔT_{My}	Linear thermal gradient following the vertical axis of the deck
ΔT_{Mz}	Linear thermal gradient following the transverse horizontal axis of the deck
ΔT_u	Uniform component of the temperature variation
$\Delta\sigma_c$	Reference value for the fatigue strength at $N_c = 2 \cdot 10^6$ cycles
$\Delta\sigma_{fat}$	Stress range from load $Q_{k,fat}$ (fatigue in structural steel)
$\Delta\sigma_{E,2}$	Equivalent constant amplitude stress range related to 2 million cycles
Ø	Diameter of the reinforcing steel bars
Φ	Damage equivalent impact factor (structural steel)

Small Greek letters

α	Aspect ratio of a web panel
α_Q	Adjustment factor on concentrated load Q_{ki}
α_q	Adjustment factor on distributed load q_{ki}
$\alpha_{th}{}^a$	Coefficient of linear thermal expansion for structural steel
$\alpha_{th}{}^c$	Coefficient of linear thermal expansion for concrete
χ	Reduction factor for instability
ε	Strain; factor for determining the cross-section class
ε_{ca}	Deformation due to autogenous shrinkage

ε_{cd}	Deformation due to drying shrinkage
ε_{cs}	Total deformation due to shrinkage
γ_a	Density of steel
$\gamma_{asphalt}$	Density of asphalt
γ_c	Density of concrete
γ_C	Partial factor for resistance of concrete
γ_{Ff}	Partial factor for equivalent constant amplitude stress range
γ_M	Partial factor for resistance of structural steel
γ_{Mf}	Partial factor for the fatigue strength of a detail
γ_S	Partial factor for resistance of reinforcing steel
γ_V	Partial factor for resistance of a shear connector
λ	Damage equivalent factor (structural steel)
λ_D	Slenderness ratio
$\overline{\lambda}_B$	Slenderness coefficient in the calculation of the plate buckling coefficient
$\overline{\lambda}_p$	Winter's coefficient
ν	Poisson's ratio
ρ	Reinforcement ratio in a concrete cross-section
$\sigma_{c,max}$	Design stress at the extreme fibre of the concrete slab
σ_{cr}	Elastic critical plate buckling stress
σ_{crB}	Elastic critical plate buckling stress in the calculation of the plate buckling coefficient
σ_E	Elastic critical Euler's stress
σ_{Ed}	Design value of a direct stress in a cross-section
$\sigma_{s,moy}$	Design stress in the reinforcement, at the mid-plane of the concrete slab
$\sigma_{y,inf}$	Design stress at the extreme fibre of the lower flange
$\sigma_{y,sup}$	Design stress at the extreme fibre of the upper flange
$\sigma_{w,inf}$	Design stress at the lower fibre of the web
$\sigma_{w,sup}$	Design stress at the upper fibre of the web
τ_{cr}	Elastic critical shear buckling stress
ψ	Stress ratio in the web
ψ_L	Creep multiplier for the modular ratio

1. Introduction

1.1. General considerations

Composite bridges combining steel plates with a concrete slab deck have been widely used due to their economic, constructive and structural advantages. Compared to pure steel bridges, composite bridges are less susceptible to fatigue because the proportion of live load to dead load is much smaller, leading to reduced fatigue stress ranges, and additionally, deflection criterion of road bridges is not so severe in comparison to railway bridges.

In parallel, High Strength Steels (HSS) have emerged and tend to be more widely used, because of their high static yield strength, their good weldability and their high ductility. Using HSS in the design of composite road bridges could become an interesting option.

However, the use of HSS in bridges leads to more slender plate girder elements, which creates new problems due to plate buckling and higher fatigue issues, because of higher stress ranges. Therefore, the fatigue criteria could become decisive for the design of the steel part of the deck.

New forms of plate girders, using tubular or delta beams, can become an alternative to traditional plate girder beams. Their performance still needs to be checked though.

1.2. Objectives of the project

The objective of this Master thesis is to suggest a design of three composite steel-concrete decks for a roadway bridge, based on the Eurocodes:

- Design A: a bridge with traditional plate girder beams, with standard S355 J2/K2 or N/NL steel grades, is used as a control design for comparison purposes. It follows the design of the composite two-girder bridge presented in the “SETRA guidance book for Eurocodes” [1]. Hence, the calculations often refer to this guidance book.

- Design B: a bridge with traditional plate girder beams, in HSS steel (S690 QL or QL1), is calculated to study the influence of the HSS alone, and its advantages on the design.

- Design C: a bridge with tubular flange beams, in HSS steel (S690 QL), is calculated in order to solve the issues related to stability and fatigue that are likely to appear in the design B.

This report summarizes all three designs of a composite two-girder bridge deck, with a final assessment and comparison of the benefits of the three solutions. The calculation of the bridge has been performed with the final version of the Eurocodes, especially EN 1993-1-1, EN 1993-2 and EN 1994-2. Some calculations were also performed with reference to the book “Traité de Génie Civil 12 : Ponts en acier” [2]; especially for the verification against lateral torsional buckling.

1.3. Organization of the work

The work is divided into twelve sections, beginning with this introduction and concluding with the conclusions and future developments. The other ten sections of the paper are organized as follows:

- Section 2 – General design data: the geometry of the deck and the traffic data have been chosen to examine the most general calculation case as possible. The environmental data correspond to Lisbon's climate, where this project has been conducted.

- Section 3 – Description of the deck: the longitudinal elevation, the cross-section of the bridge deck and the bracing frame for all three designs are presented in this section.

- Section 4 – Materials: this section describes the structural steel in the main girders, the concrete in the slab, the reinforcing steel and the shear connectors with their safety factors.

- Section 5 – Actions: all actions that test the bridge resistance are detailed: the permanent loads, corresponding to the selfweight of the elements of the bridge; the internal actions due to shrinkage; the traffic loads and the variation of temperature.

- Section 6 – Global analysis: the bridge is verified to the Ultimate Limit State (ULS) and the Fatigue Limit State (FLS). The internal forces and moments in the critical cross-sections are calculated with a beam model.

- Section 7 – Geometric properties of the cross-sections and design stresses: the design stresses in the elements of the composite girder depend on the cross-section class of the steel girder, and the stage of the bridge life which is considered.

- Section 8 – Safety verification at ULS: all three designs are checked against bending, shear and their interaction. The shear resistance needs to be adapted in the case of the design C, accounting for a fixed connection between the web and the flanges.

- Section 9 – Safety verification of the stability: the flange induced buckling of the web should be verified, as well as the lateral-torsional buckling of the compression flanges at the construction and the final stage of the bridge life.

- Section 10 – Safety verification at fatigue ULS: the steel girder is assessed against web breathing, and three critical details are verified under cyclic loading.

- Section 11 – Shear connection: it is designed elastically in all cross-sections, for all designs.

A list of references can be found at the end of this report.

2. General design data

As defined in [1] § 2.1, a two-lane traffic road 3.5 meter wide takes the bridge. Each lane is bordered by a 2.0 meter wide safety trip on the right-hand side and a normalised safety barrier. The total width of the pavement between safety devices is therefore 11 meter.

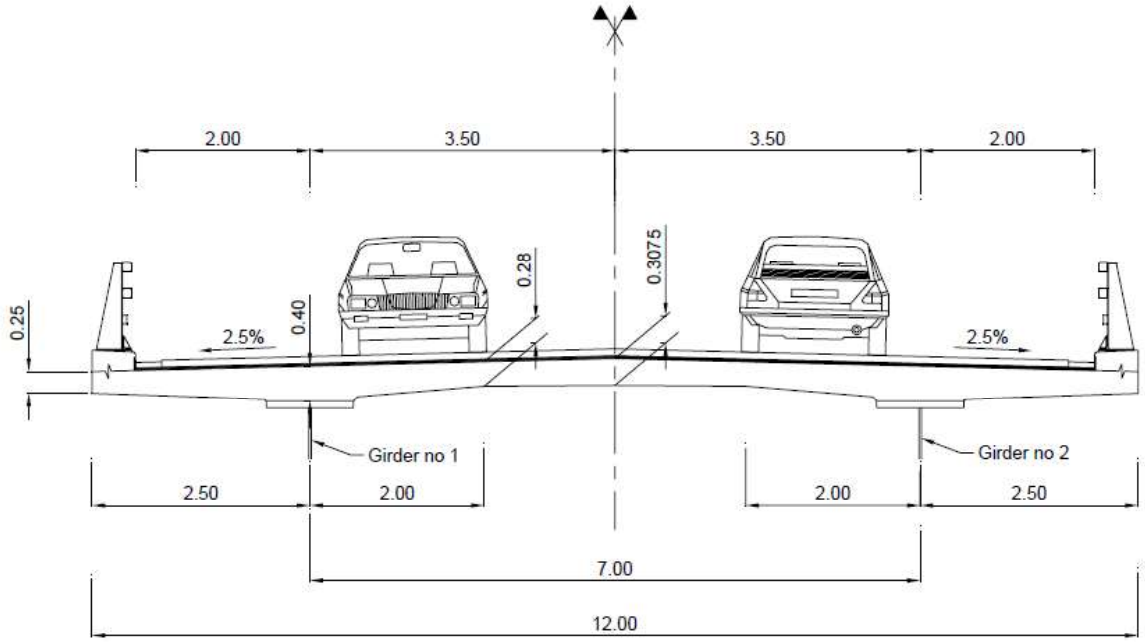

Figure 1: Cross-section of the bridge, [1] Figure 2.1

The Traffic Load Model 1 (LM1), made up of the uniformly distributed load (UDL) and the concentrated loads of the tandem system (TS) is used for the global longitudinal bending analysis. The Fatigue Load Model 3 (FLM3) is used for fatigue verifications, in connection with the simplified method of the equivalent stress range.

The environmental data correspond to the atmospheric conditions in Lisbon. The ambient relative humidity is assumed to be equal to 80%. The minimum ambient air temperature (mean return period of 50 years) to which the structure is subjected is assumed to be equal to -20°C. This information is necessary to determine the structural steel toughness and maximum thickness. Thermal actions are considered with a thermal gradient through the deck depth.

3. Description of the deck

3.1. Longitudinal elevation

As shown in Figure 2, the bridge has a symmetrical composite two-girder superstructure of a total length L_{tot} = 200 m between abutments, divided in three spans of L_1 = 60 m, L_2 = 80 m and L_3 = 60 m. Simplifications have been made as in [1] § 3.1:

- The horizontal alignment is straight.
- The top face of the deck is flat.
- The bridge is straight.
- The structural main girders depth is constant: h_a = 2 800 m.

In the global analysis that will be performed, it is considered that the slab is cracked near internal supports due to the negative bending moment. The cracked zone is considered by taking 15% of the span length near supports P1 and P2:

$$L_{cracked} = 0.15 \cdot (L_1 + L_2) = 0.15 \cdot (L_2 + L_3) \quad (3.1)$$

The length of the cracked zone is therefore $L_{cracked}$ = 21 m. This leads to a variable cross-section along the bridge, with the following distribution:

- A span cross-section of an equivalent length L_e = 0.85 L_1 = 0.85 L_3 = 51 m at side spans.
- A span cross-section of an equivalent length L_e = 0.70 L_2 at the intermediate span.
- A support cross-section of an equivalent length L_e = $L_{cracked}$ near internal supports.

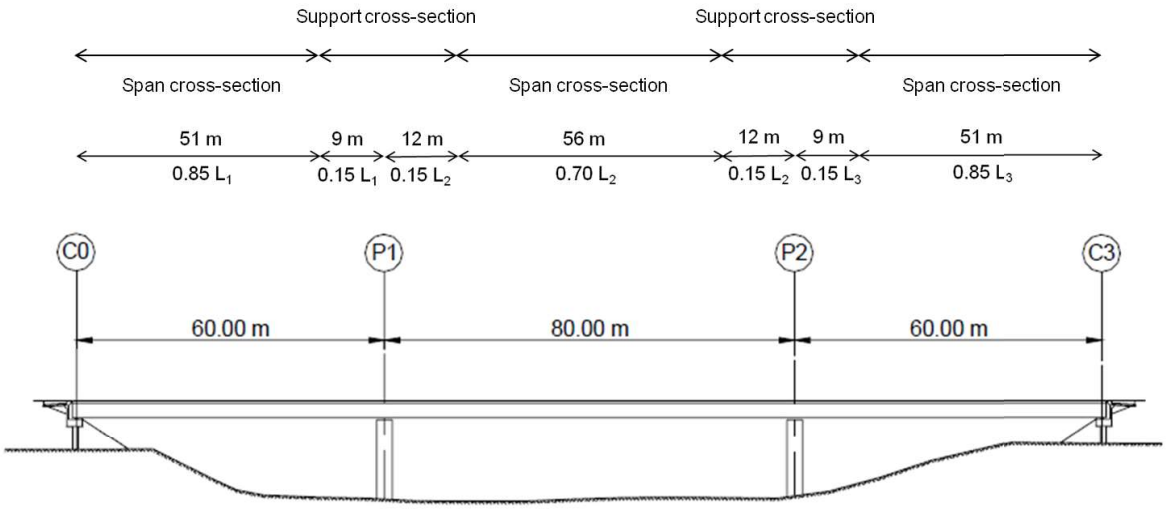

Figure 2: Longitudinal elevation of the bridge

3.2. Transverse cross-section

3.2.1. Reinforced concrete slab

The transverse cross-section of the slab and of the non-structural bridge equipment, as shown in Figure 3, is the same as described in [1] § 3.5. Here are some important characteristics:

- The total slab width b_{slab} is 12 m.
- The centre-to-centre spacing between main girders s_a is 7 m.
- Symmetry with respect to the axis of the bridge.
- The area of the slab A_{slab} is 3.684 m^2. The area of the half-slab A_c is 1.842 m^2.

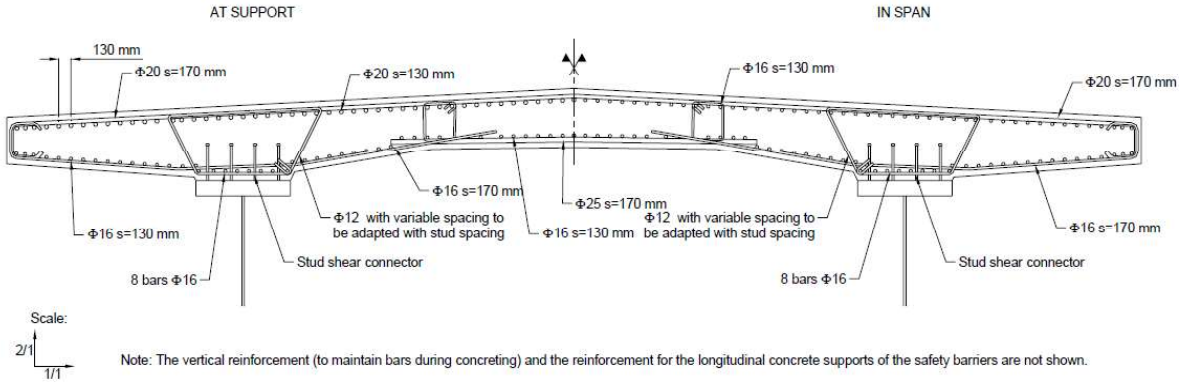

Figure 3: Transverse cross-section of the bridge, [1] Figure 3.6

According to [1] § 3.5.3, the longitudinal reinforcing steel in the slab is as follows:

- In mid-span cross-sections: the total reinforcement is ρ = 0.92% of the concrete section with high bond bars with diameter Ø = 16 mm and spacing s = 130 mm in upper and lower layers: A_s = 16 946 mm^2 for a half-slab.
- In support cross-sections: the total reinforcement is ρ = 1.19% of the concrete section with high bond bars with diameter Ø = 20 mm (respectively 16 mm) and spacing s = 130 mm in upper (respectively lower) layer: A_s = 21 920 mm^2 for a half-slab.

The transverse reinforcing steel is not considered in the analysis.

For simplification reasons, the actual cross-section of the deck is modelled by a main rectangular area to the actual width (12 m), with the same mechanical properties as the actual slab. This gives us a depth t_{slab} = 307 mm, as in [1] § 3.5.4. A haunch of depth e = 109 mm is considered in order to place the centre of gravity of the slab at the right position. The haunch is not considered to be part of the slab in the calculations.

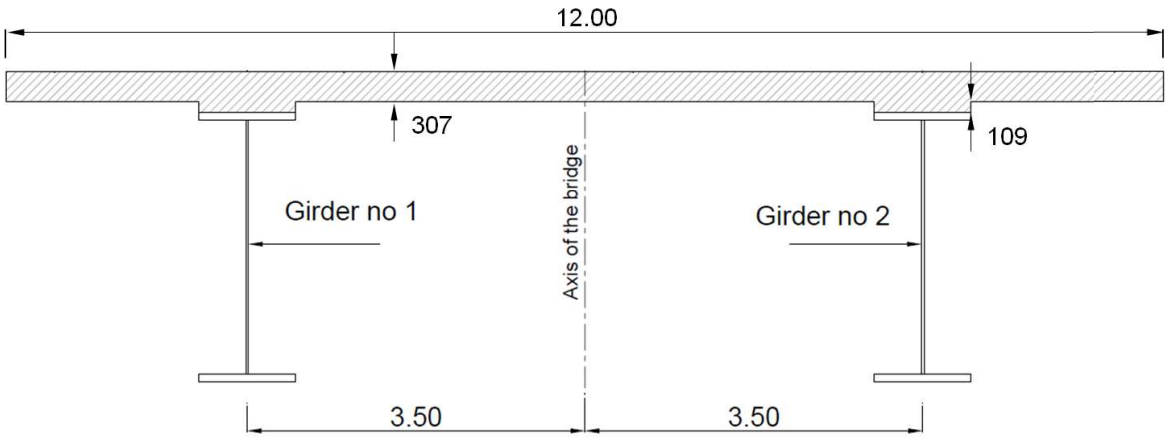

Figure 4: Modelling the concrete slab for the longitudinal bending analysis

3.2.2. Structural steel distribution

The structural steel distributions for each design are detailed in 0 to Annex III. In the longitudinal bending analysis, a simplified steel distribution is considered, with only two cross-sections for each design: a support cross-section at cracked zones, a mid-span cross-section elsewhere. The girders have a constant depth h_a = 2 800 mm in all designs.

All cross-sections dimensions are shown in Figure 5 and detailed in Table 1. The areas of the cross-sections are detailed in
Table 2.

Table 1: Dimensions of the steel girders

[mm]		Support P1			Mid-span P1-P2		
Element		A	B	C	A	B	C
Top flange	$b_{f,sup}$ or D_f	1 000	650	457	1 000	650	457
	$t_{f,sup}$	120	50	30	40	35	17.5
Web	h_w	2 560	2 675	1 886	2 720	2 720	1 886
	t_w	26	20	20	18	14	14
Bottom flange	$b_{f,inf}$ or D_f	1 200	900	457	1 200	900	457
	$t_{f,inf}$	120	75	40	40	45	36

Table 2: Cross-section areas

[mm^2]		Support P1			Mid-span P1-P2		
Element		A	B	C	A	B	C
Total steel area	A_{tot}	330 560	153 500	130 366	136 960	101 330	98 181
Top flange area	$A_{f,sup}$	120 000	32 500	40 244	40 000	22 750	24 163
Web area	A_w	66 560	53 500	37 720	48 960	38 080	26 404
Bottom flange area	$A_{f,inf}$	144 000	67 500	52 402	48 000	40 500	47 614

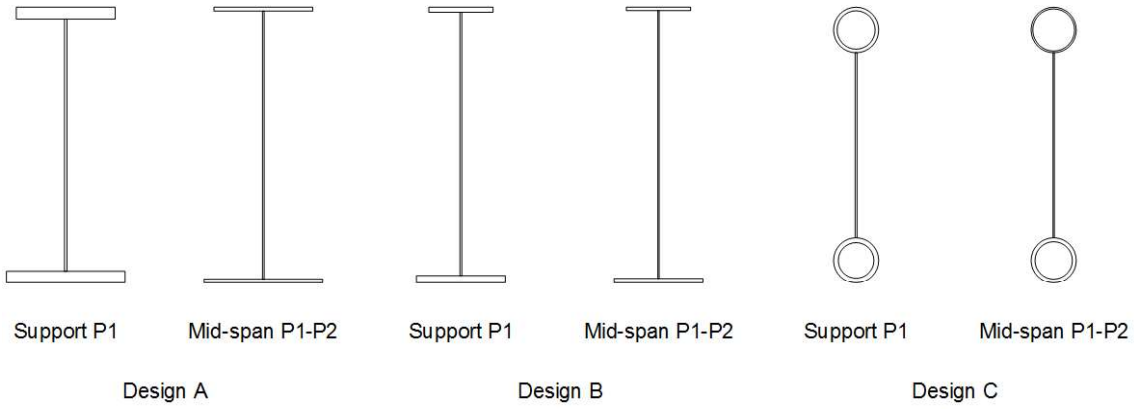

Figure 5: Support and mid-span cross-sections for all designs

The two main girders have light cross-girders made of IPE 600. They are spaced every 7.5 m in end spans (C0-P1 and P2-C3) and every 8 m in the intermediate span (P1-P2). In the designs A and B, the first cross-girder located at each side of the support is replaced with IPE 750x196. The transverse cross-section of the cross-girders is shown in Figure 6.

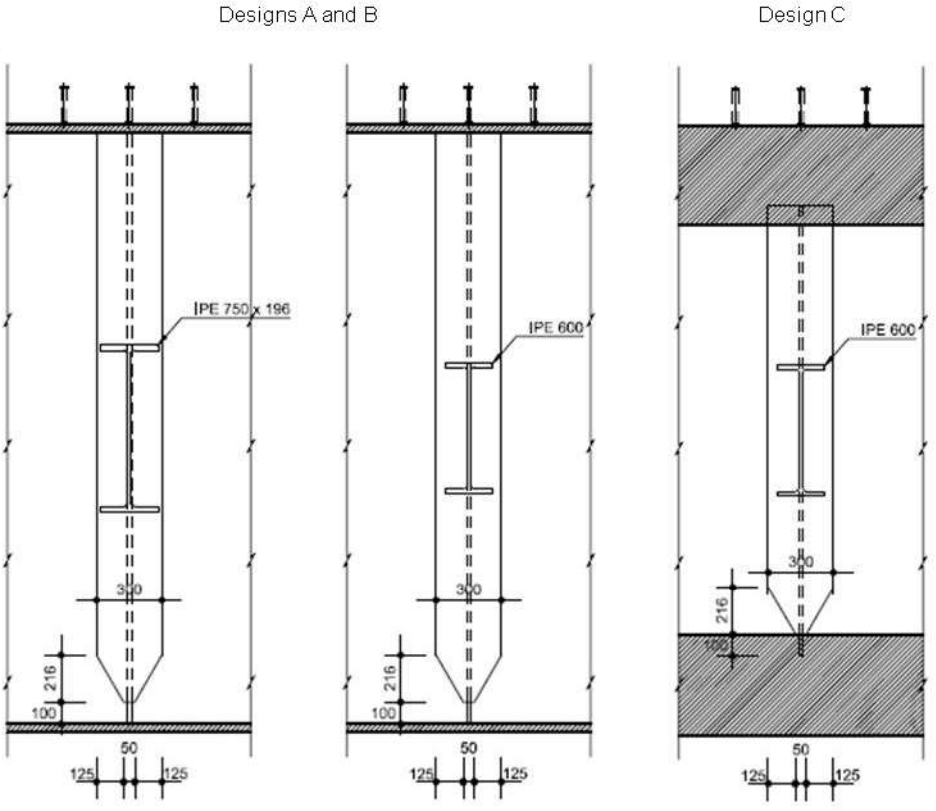

Figure 6: Transverse cross-section of the cross-girders

The choice of the IPE rolled-section depends on the resistance of the main girders against the lateral-torsional buckling of the flanges; it is justified in section 9.2. The flange of the vertical T-shaped stiffeners has a V-shaped cutout for fatigue reasons; it is justified in section 10.3.

The two main girders have heavy support cross-girders at abutments and at internal supports, made of built-up welded sections. In the designs A and B, the vertical T-shaped stiffeners are duplicated and welded on the lower flange. The design C has a specific detailing, in order to allow the transmission of the vertical forces from the girder to the support, while preventing from the punching failure of the lower tubular flange. The transverse cross-section of the stiffeners is shown in Figure 7.

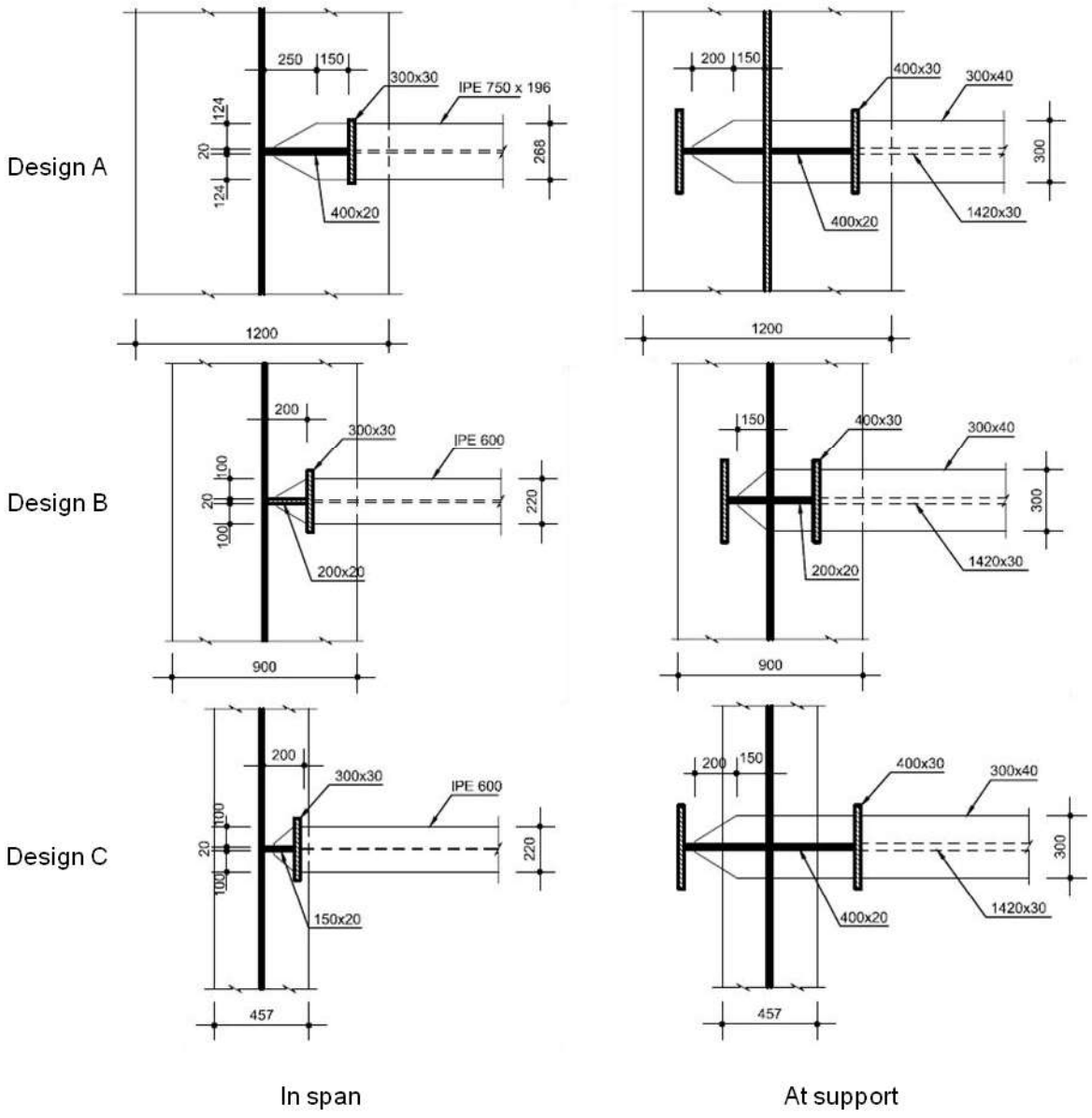

Figure 7: Cross-section of the stiffeners

4. Materials

4.1. Structural steel

The purpose of the project is to compare the use of steel grade S355 and S690 in bridge decks. The yield and ultimate strengths depend on the thickness of the plate or cylindrical element, according to EN 10025-3 [3] Table 5 and EN 10025-6 [4] Table 5. These two normative references can be used for the properties of the materials, according to [5] § 1.2.2.

Table 3: f_y and f_u depending on the element thickness t

Steel	t (mm)	≤ 16	> 16 ≤ 40	> 40 ≤ 50	> 50 ≤ 63	> 63 ≤ 80	> 80 ≤ 100	> 100 ≤ 150
S355	f_y (N/mm^2)	355	345	335	335	325	315	295
	f_u (N/mm^2)	470	470	470	470	470	470	450
S690	f_y (N/mm^2)	690	690	690	650	650	650	630
	f_u (N/mm^2)	770	770	770	760	760	760	710

The structural steel has a modulus of elasticity E_a = 210 GPa from [5] § 3.2.6. The coefficient of linear thermal expansion should be $\alpha_{th}^{a} = 12.10^{-6}$ /°C from [6] § 3.1.3. To simplify the global analysis, it is taken as equal to the concrete coefficient: $\alpha_{th}^{a} = \alpha_{th}^{c} = 10.10^{-6}$ /°C.

The steel quality should be chosen to ensure a good weldability and toughness in the transition or upper shelf of the toughness-temperature relationship, according to [7] Figure 1.1. It depends on the maximum permissible thickness, which is a function of the service temperature T_{Ed} and the stress level σ_{Ed} in the element.

The service temperature T_{Ed} is equal to the minimum ambient air temperature, defined in section 1. It is equal to -20°C. The steel quality and the maximum permissible thickness as a function of σ_{Ed} and T_{Ed} are given in Table 4, according to [7] Table 2.1. The stress level σ_{Ed} is determined with an accidental combination of loads.

Table 4: Maximum permissible thickness [mm]

σ_{Ed}	0.75 · f_y	0.50 · f_y	0.25 · f_y
T_{Ed}	-20°C	-20°C	-20°C
S355 K2 or N	60	95	150
S355 NL	90	135	200
S690 QL	40	65	120
S690 QL1	50	80	140

The steel quality of steel grade S355 for the design A is detailed in Table 5, as defined in [1] § 4.1.

Table 5: Subgrade choice in the design A

Design	A		
Thickness	t ≤ 30 mm	30 ≤ t ≤ 80 mm	80 ≤ t ≤ 135 mm
Subgrade	S355 K2	S355 N	S355 NL

The steel quality for designs B and C is the steel grade S690 QL. There is an exception for the lower flange in the design C, which should be in steel grade S690 QL1 as detailed in Table 6.

Table 6: Subgrade choice for the lower flange in the design B

σ_{Ed}	$0.52 \cdot f_y$	
Thickness	≤ 63.5	63.5 ≤ t ≤ 78.2
Subgrade	S690 QL	S690 QL1

4.2. Concrete

Normal concrete of class C35/45 is used for the reinforced slab. The mechanical properties are resumed in Table 7, according to EC2-1-1 [6] § 3.1.3 and EC4-2 [8] § 2.4.1.2.

Table 7: Mechanical properties of C35/45 concrete from [6] § 3.1.3

Mechanical property	Notation	Value
Characteristic compressive cylinder strength at 28 days	f_{ck}	35 N/mm^2
Mean value of concrete cylinder strength at 28 days	$f_{cm} = f_{ck} + 8$	43 N/mm^2
Design value of compressive strength	$f_{cd} = f_{ck} / \gamma_C$	23.3 N/mm^2
Mean value of axial tensile strength	f_{ctm}	-3.2 N/mm^2
5% fractile of the characteristic axial tensile strength	$f_{ctk,0.05}$	-2.2 N/mm^2
95% fractile of the characteristic axial tensile strength	$f_{ctk,0.95}$	-4.2 N/mm^2
Mean value of the modulus of elasticity	$E_{cm} = 22 (f_{cm} / 10)^{0.3}$	34.077 MPa
Coefficient of linear thermal expansion	$\alpha_{th}{}^{c}$	10.10^{-6} /°C

4.3. Reinforcement

The reinforcement is made of B500B high bond bars from EC2-1-1 [6] § 3.2. The modulus of elasticity of reinforcing steel is E_s = 200 GPa. However, the modulus $E_s = E_a$ = 210 GPa is used for simplification, according to [9] § 3.2.

Table 8: Mechanical properties of B500B reinforcing bar [6] § 3.2

Mechanical property	Notation	Value
Characteristic yield strength	f_{sk}	500 N/mm^2
Design yield strength	$f_{sd} = f_{sk} / \gamma_S$	435 N/mm^2
Modulus of elasticity	$E_s = E_a$	210 GPa

4.4. Shear connectors

Stud shear connectors in S235J2G3 steel grade have been adopted from [10] : f_u = 450 N/mm^2.

4.5. Partial factors for materials

The Ultimate Limit State (ULS), the Fatigue Limit State (FLS) and stability must be justified.
The partial factors at ULS and at FLS are described respectively in Table 9 and
Table 10.

Table 9: Partial factors at ULS

Design situation	Factor	Value	Comment	Reference
Structural steel	γ_{M0}	1.0	Yielding, local instability	EN1993-2, 6.1 EN1993-2, Table 6.2
	γ_{M1}	1.1	Resistance of members to instability	
	γ_{M2}	1.25	Resistance of joints	
Concrete	γ_C	1.5		EN1992-1-1, 2.4.2.4
Reinforcement	γ_S	1.15		
Connectors	γ_V	1.25		EN1994-2, 2.4.1.2

Table 10: Partial factors at fatigue ULS

Design situation	Factor	Value	Comment	Reference
Structural steel	γ_{Mf}	1.0	Damage tolerant, low consequence	EN1993-1-9, Table 3.1
		1.15	Damage tolerant, high consequence	
		1.15	Safe life, low consequence	
		1.35	Safe life, high consequence	
Concrete	$\gamma_{C,fat}$	1.5		EN1992-1-1, 2.4.2.4
Reinforcement	$\gamma_{S,fat}$	1.15		
Connectors	$\gamma_{V,fat}$	1.25		EN1994-2, 6.8.2

5. Actions

5.1. Permanent loads

A distinction is made in the permanent loads between the selfweights of:

- The structural steel girders;
- The reinforced concrete slab;
- The non-structural bridge equipment.

5.1.1. Structural elements

The density of the structural steel is equal to γ_a = 78 kN/m^3 according to [11] Table A.4. The selfweight of one girder depends on the steel distribution along the bridge:

$$g_{a,support} = A_{tot,support} \cdot \gamma_a \quad (5.1)$$

$$g_{a,span} = A_{tot,span} \cdot \gamma_a \quad (5.2)$$

Where $g_{a,support}$ and $g_{a,span}$ are respectively the weights of the girder at the support and the span zones. Hence the average structural steel selfweight $g_{a,av}$ of one girder along the bridge is:

$$g_{a,av} = \frac{(0.85\ L_1 + 0.70\ L_2 + 0.85\ L_3) \cdot g_{a,span} + 2 \cdot L_{cracked} \cdot g_{a,support}}{L_{tot}} \quad (5.3)$$

The selfweight of the cross-girders located over the supports is directly transmitted to the supports and has therefore no influence on the internal forces and moments of the global analysis. The selfweight of the in-span transverse cross-girders is taken into account by considering on each girder a vertical uniformly distributed load of 15% of the average weight of the main girder from the design A:

$$g_{a,trans} = 0.15\ g_{a,av} \quad (5.4)$$

Where $g_{a,trans}$ is the selfweight of the in-span transverse cross-girders. Hence the total structural steel selfweights $g_{a,support,tot}$ and $g_{a,span,tot}$ at support and at mid-span along the bridge are:

$$g_{a,support,tot} = g_{a,support} + g_{a,trans} \quad (5.5)$$

$$g_{a,span,tot} = g_{a,span} + g_{a,trans} \quad (5.6)$$

The results are detailed in Table 11.

Table 11: Selfweight of one steel girder [kN/m]

Design	$g_{a,support}$	$g_{a,span}$	$g_{a,av}$	$g_{a,trans}$	$g_{a,support,tot}$	$g_{a,span,tot}$
A	25.78	10.68	13.85	2.08	27.86	12.76
B	11.97	7.90	8.76	2.08	14.05	9.98
C	10.17	7.66	8.19	2.08	12.25	9.74

The reduction in weight of the steel girders between designs A, B and C is resumed in Table 12.

Table 12: Comparison of the weights of the girders between designs A, B and C

	$g_{a,support,tot}$		$g_{a,span,tot}$		$g_{a,tot}$	
Design	A	B	A	B	A	B
A	0%	-	0%	-	0%	-
B	50%	0%	22%	0%	27%	0%
C	56%	13%	24%	2%	30%	5%

It is visible that the use of HSS allows reducing consequently the weight of the girders. The difference is significant between designs A and B (27%) and between designs A and C (30%). However, the weights of the steel girders are very close between designs B and C. The use of tubular flanges does not allow a significant reduction of the weight.

The density of the reinforced concrete slab is equal to γ_c = 25 kN/m^3 according to [11] Table A.1. Therefore the selfweight of the reinforced concrete slab for one girder is:

$$g_c = \gamma_c \cdot A_c = \gamma_c \cdot \frac{A_{slab}}{2} \tag{5.7}$$

Where A_c is the area of the half-slab of the deck. Therefore the weight of the slab is: g_c = 46.2 kN/m.

5.1.2. Non-structural bridge equipment

The selfweight of one safety barrier is assumed to be equal to $g_{barrier}$ = 1.0 kN/m.

The density of the asphalt layer is equal to $\gamma_{asphalt}$ = 24 kN/m^3 according to [11] Table A.6. Considering half of the width of the asphalt layer $b_{asphalt}$ and the thickness $t_{asphalt}$ = 100 mm for one girder:

$$g_{asphalt} = b_{asphalt} \cdot t_{asphalt} \cdot \gamma_{asphalt} = \frac{b_{slab} - 2 \cdot 0.5}{2} \cdot t_{asphalt} \cdot \gamma_{asphalt} \tag{5.8}$$

Therefore the weight of the asphalt layer is: $g_{asphalt}$ = 13.2 kN/m.

5.2. Concrete shrinkage

The concrete shrinkage introduces an imposed axial deformation ε_{cs} on the concrete slab. In [1] § 5.2 it is the sum of:

- The autogenous shrinkage: the continuing hydration of the cement after the hardening introduces a short-term loading just after the concrete is poured;
- The drying shrinkage: the progressive evaporation of the water contained in the concrete introduces a long-term loading during the bridge life.

The imposed deformation ε_{cs} on the slab must be anchored with shear connectors to the steel girders. Therefore the steel girders are in compression, whereas the slab is in tension. It also creates a negative curvature and introduces flexion in the composite bridge.

These effects on the steel girders only take place after time t_1 of casting the links between the slab and the steel girders. The imposed axial deformation ε_{cs} transmitted from the slab to the steel girders corresponds to the shrinkage that happen between t_1 and t_2 = 100 years (the design life of the bridge).

As in [1] § 3.4, the concrete is considered to be poured on site in several slab segments. Considering the mean value of the ages of all slab segments, the values of t_1 and t_2 are taken as t_1 = 79.25 days and t_2 = 100 · 365 = 36 500 days.

The total shrinkage deformation ε_{cs} is given by the formulas:

$$\varepsilon_{cs} = \varepsilon_{ca} + \varepsilon_{cd} = \varepsilon_{ca}(t_1) - \varepsilon_{ca}(t_2) + \varepsilon_{cd}(t_1) - \varepsilon_{cd}(t_2) \quad (5.9)$$

Where ε_{cs} is the total shrinkage deformation; $\varepsilon_{ca}(t)$ is the autogenous shrinkage deformation; $\varepsilon_{cd}(t)$ is the drying shrinkage deformation.

5.2.1. Autogenous shrinkage

The autogenous shrinkage is calculated with the formulas from [6] § 3.1.4. The results are detailed in Table 13:

$$\varepsilon_{ca}(t) = \beta_{as}(t) \cdot \varepsilon_{ca}(\infty) \quad (5.10)$$

$$\beta_{as}(t) = 1 - \exp(-0.2\sqrt{t}) \quad (5.11)$$

$$\varepsilon_{ca}(\infty) = 2.5 \cdot (f_{ck} - 10) \cdot 10^{-6} \quad (5.12)$$

Where $\varepsilon_{ca}(t)$ is the autogenous shrinkage deformation; *t* is the age of concrete.

Table 13: Results for the autogenous shrinkage

Age of concrete t	79.25 days	36 500 days
β_{as} (t)	0.831	1.000
ε_{ca} (∞)	$6.25 \cdot 10^{-5}$	$6.25 \cdot 10^{-5}$
ε_{ca} (t)	$5.20 \cdot 10^{-5}$	$6.25 \cdot 10^{-5}$

Hence the autogenous shrinkage deformation between t_1 and t_2 is $\varepsilon_{ca} = \varepsilon_{ca}(t_1) - \varepsilon_{ca}(t_2) = 1.05 \cdot 10^{-5}$.

5.2.2. Drying shrinkage

The drying shrinkage deformation is calculated with the formulas from [6] Annex B2. The results are detailed in Table 14:

$$\varepsilon_{cd}(t) = \beta_{ds}(t) \cdot k_h(t) \cdot \varepsilon_{cd,0} \quad (5.13)$$

$$\varepsilon_{cd,0} = 0.85 \cdot \left[(220 + 110 \cdot \alpha_{ds1}) \cdot \exp\left(-\alpha_{ds2} \cdot \frac{f_{cm}}{f_{cm0}}\right)\right] \cdot 10^{-6} \cdot \beta_{RH} \quad (5.14)$$

$$\beta_{RH} = 1.55 \cdot \left(1 - \left(\frac{RH}{100}\right)^3\right) \quad (5.15)$$

$$\beta_{ds}(t) = \frac{t - t_s}{t - t_s + 0.04 \cdot \sqrt{h_0{}^3}} \quad (5.16)$$

$$h_0(t) = \frac{2 \cdot A_c}{u(t)} \tag{5.17}$$

$$u(t) = 0.5 \cdot p(t) \tag{5.18}$$

Where $\varepsilon_{cd}(t)$ is the drying shrinkage deformation; $\varepsilon_{cd,0}$ is the unrestrained drying shrinkage; *t* is the age of concrete; t_s is the starting time of drying; α_{ds1} and α_{ds2} are the coefficients to represent the hardening speed of the cement; RH is the relative humidity; $h_0(t)$ is the notional size; $u(t)$ is the half-slab perimeter exposed to drying effects.

The slab perimeter exposed to drying effects $p(t_1)$ after pre-casting the slab is equal to the actual slab perimeter, according to [1] § 3.5.4: $p(t_1)$ = 24.6 m. The entire slab is exposed to the atmosphere. The slab perimeter exposed to drying effects $p(t_2)$ after executing the finishing works is obtained by subtracting from $p(t_1)$ the lengths that are not in direct contact with the atmosphere: the width of the upper flanges and the width of the asphalt layer.

$$p(t_2) = p(t_1) - 2 \cdot b_{asphalt} - 2 \cdot b_{f,sup} \tag{5.19}$$

Considering the insignificant influence of the change in the width of the upper flange between all designs, it is simpler to take the width of the upper flange of the design A, to calculate the shrinkage deformation in all designs: $p(t_2)$ = 24.6 – 2 · 5.5 – 2 · 1 = 11.6 m.

The relative humidity is assumed to be RH = 80%. A normal type of cement (class N) is used in the construction of the slab. The coefficient $k_h(t)$ depends on the notional size h_0 and is calculated by linear interpolation from [6] Table 3.

Table 14: Results for the drying shrinkage

Age of concrete t	79.25 days	36 500 days
p (t)	24.6 m	11.6 m
u (t)	12.3 m	5.8 m
h_0 (t)	300 mm	635 mm
k_h (t)	0.750	0.700
β_{ds} (t)	0.277	0.983
β_{RH}	0.756	0.756
α_{ds1}	4	4
α_{ds2}	0.12	0.12
$\varepsilon_{cd,0}$	$2.53 \cdot 10^{-4}$	$2.53 \cdot 10^{-4}$
ε_{cd} (t)	$5.26 \cdot 10^{-5}$	$1.74 \cdot 10^{-4}$

The drying shrinkage deformation between t_1 and t_2 is $\varepsilon_{cd} = \varepsilon_{cd}(t_1) - \varepsilon_{cd}(t_2) = 1.22 \cdot 10^{-4}$. The total shrinkage deformation imposed on the concrete slab between t_1 and t_2 is $\varepsilon_{cs} = \varepsilon_{ca} + \varepsilon_{cd} = 1.32 \cdot 10^{-4}$. The total shrinkage deformation is essentially due to the drying shrinkage (92%).

5.3. Concrete creep

The short-term loading applied to a composite structure is resisted by a composite area: the reinforced concrete slab and the steel girders. The value of this composite area is obtained by dividing the concrete area by a modular ratio according to [8] § 5.4.2.2: $n_0 = E_a / E_{cm} = 210\,000 / 34\,077 = 6.16$.

The concrete creep describes the effect of the gradual deformation of a concrete specimen under constant applied load. It only influences long-term loading. The creep effect is taken into account by reducing the concrete area, i.e. increasing the modular ratio.

The modular ratios n_L for long-term calculations (shrinkage, permanent loads) are calculated with a refined formula:

$$n_L = n_0 \cdot (1 + \psi_L \cdot \varphi(t, t_0)) \tag{5.20}$$

The creep multiplier ψ_L from [8] § 5.4.2.2 represents the dependence of the modular ratio on the type of loading:

- For concrete shrinkage: $\psi_L = 0.55$;
- For permanent loads : $\psi_L = 1.1$.

The creep coefficient $\varphi(t, t_0)$ from [6] Annex B represents the dependence of the modular ratio on the creep level at the time considered. It is given by the formulas:

$$\varphi\,(t, t_0) = \varphi_0 \cdot \beta_c(t, t_0) = \varphi_0 \cdot \left(\frac{t - t_0}{\beta_H + t - t_0}\right)^3 \tag{5.21}$$

$$\beta_H = \min(1.5 \cdot (1 + (0.012 \cdot RH)^{18}) \cdot h_0 + 250 \cdot \alpha_3; 1500 \cdot \alpha_3) \tag{5.22}$$

$$\varphi_0 = \varphi_{RH} \cdot \beta(f_{cm}) \cdot \beta(t_0) = \left[1 + \frac{1 - \frac{RH}{100}}{0.10 \cdot \sqrt[3]{h_0}} \cdot \alpha_1\right] \cdot \alpha_2 \cdot \left[\frac{16.8}{f_{cm}}\right] \cdot \left[\frac{1}{0.1 + t_o{}^{0.2}}\right] \tag{5.23}$$

$$\alpha_1 = \left(\frac{35}{f_{cm}}\right)^{0.7}; \alpha_2 = \left(\frac{35}{f_{cm}}\right)^{0.2}; \alpha_3 = \left(\frac{35}{f_{cm}}\right)^{0.5} \tag{5.24}$$

Where $\varphi\,(t, t_0)$ is the creep coefficient; *t* is the age of concrete; t_0 is the first day of casting the concrete; φ_0 is the nominal creep coefficient; α_1, α_2 and α_3 are the coefficients for concrete strength influence.

A normal concrete of class C35/45 is considered, with the relative humidity RH = 80% and the notional size h_0 = 635 mm. Shrinkage effects start at t_0 = 1 day whereas the permanent loads due to non-structural bridge equipment are applied to the steel girders at t_0 = 79.25 days, according to [1] § 5.3.2. The time considered is equal to the bridge design life: t = 36 500 days.

The results are detailed in Table 15.

Table 15: Calculation of the creep coefficients

t_0 (days)	α_1	α_2	α_3	φ_{RH}	β (f_{cm})	β (t_0)	β_H	φ_0	φ (t, t_0)
1	0.87	0.96	0.90	1.15	2.56	0.91	1353.3	2.69	2.66
79.25						0.40		1.18	1.17

Hence the modular ratios for long-term loading are:

- For shrinkage effects: $n_L = n_s = 15.17$;
- For permanent loads: $n_L = n_\varphi = 14.09$.

These values depend strongly on the hypothesis made for t_0, which is an approximation based on the construction phases. It is possible to calculate the modular ratios with a simplified method, according to [2] § 19.2.9:

- Short-term loading: $n_0 = 6$;
- Shrinkage: $n_s = 12$;
- Permanent loads: $n_\varphi = 18$.

Those values are kept, as they are usually conservative as compared to the values calculated with the refined formula, for modelling the slab.

5.4. Variable actions

Three different variable actions are considered:

- The Traffic Load Model 1 (LM1) for the global longitudinal bending analysis;
- The Fatigue Load Model 3 (FLM3) for the fatigue verifications;
- The thermal actions.

5.4.1. Traffic Load Model 1

A straight transverse influence line is used with the assumption that 90% of a vertical load introduced in the web plane of the main girder goes in this girder. It is less conservative than in [1] § 5.4.2, but it is more realistic.

The tandem system and uniformly distributed loads are positioned transversally in the most unfavourable case for the studied girder (n°1), according to [12] § 4.2.3 and § 4.2.4:

- There is 0.5 m free on either side of the deck to consider the safety barriers;
- There are 3 lanes of 3.0 m wide and a remaining area of 2.0 m;
- There is a tandem system with two axles with a load magnitude Q_{ki} on each lane i;
- There is a uniformly distributed load with a load magnitude q_{ki} on each lane i;
- The loads are adjusted by the factors α_Q and α_q.

The values of the loads Q_{ki} and q_{ki} and the adjustments factors α_Q and α_q are detailed in Table 16.

Table 16: Traffic load model 1

Actions	Lane 1	Lane 2	Lane 3	Remaining area
Q_{ki}	300 kN	200 kN	100 kN	-
α_Q	0.9	0.9	0.9	-
q_{ki}	9 kN/m^2	2.5 kN/m^2	2.5 kN/m^2	2.5 kN/m^2
α_q	1.0	1.0	1.0	1.0

It should be noticed that the chosen coefficients α are more conservative than those of [1] § 5.4.3 and § 5.4.4, to account for the change in the influence line:

- The tandem system loads (TSL) are slightly superior to the calculations in [1], where α_{Qi} = 0.9, 0.8 and 0.8 for respectively lanes 1, 2 and 3;
- The uniformly distributed loads (UDL) are slightly superior to the calculations in [1], where α_{qi} = 0.7, 1.0 and 1.0 for respectively lanes 1, 2 and 3. The remaining area is not considered in [1] because of their transverse influence line.

Only 1.88 m of the remaining area is considered. The remaining 0.12 m has a favourable effect according to the influence line and should be neglected. The transverse positioning of the traffic lanes on the deck, the load distribution and the ordinates of the transverse influence line are given in Annex IV Figure 20. Hence the reaction forces on the main girder are:

$$Q_k = \alpha_Q \cdot (1.07 + 0.84) \cdot Q_{k1} + \alpha_Q \cdot (0.73 + 0.50) \cdot Q_{k2} + \alpha_Q \cdot (0.39 + 0.16) \cdot Q_{k3} \quad (5.25)$$

$$q_k = \alpha_q \cdot 0.96 \cdot 3.0 \cdot q_{k1} + \alpha_q \cdot 0.61 \cdot 3.0 \cdot q_{k2} + \alpha_q \cdot 0.27 \cdot 3.0 \cdot q_{k3} + \alpha_q \cdot 0.05 \cdot 1.88 \cdot q_{kr} \quad (5.26)$$

Therefore Q_k = 786.9 kN due to the TSL and q_k = 32.7 kN/m due to the UDL. It should be pointed out that no longitudinal distance of Q_k is considered.

5.4.2. Fatigue Load Model 3

The same transverse influence line as for the LM1 is used for the FLM3.

This time the actual lanes of the bridge are considered; they are located according to the actual painting marks on the pavement. There is a single-vehicle model made up of 4 axles, with a corresponding load of 120 kN per axle, according to [12] § 4.6.4. The model is shown in Annex V Figure 21.

The transverse positioning of the traffic lanes on the deck, the ordinates of the transverse influence line and the load distribution are given in Annex V Figure 22. The loads are Q_{ki} = 4 · 120 / 2 = 240 kN.

Hence the reaction forces on the main girder are: $Q_{k,fat}$ = (0.81 + 0.59) · Q_{ki} = 336 kN.

As in the LM1, no longitudinal distance of $Q_{k,fat}$ is considered.

5.4.3. Thermal actions

The thermal actions can be divided into four components as in [1] § 5.4.6:

- A uniform component ΔT_u;
- A linear thermal gradient following the transverse horizontal axis of the deck ΔT_{My};
- A linear thermal gradient following the vertical axis of the deck ΔT_{Mz};
- A non-linear part of the thermal gradient ΔT_E.

Only the third component ΔT_{Mz} is taken into account in the global longitudinal analysis. It is taken as a linear thermal gradient over the entire depth of the bridge deck according to [13] § 6.1.4.1.

Two values ΔT_1 and ΔT_2 are defined for the variation of temperature, from EC1-1-5 [13] Table 6.1:

- The positive variation ΔT_1 = +15°C is used for the analysis of the deck at mid-span, to maximize the positive bending moment;
- The negative variation ΔT_2 = -18°C is used for the analysis of the deck at supports, to maximize the absolute value of the negative moment.

The total height of the bridge is 3 216 mm from Equation (5.27):

$$h_{tot} = h_a + e + t_{slab} \tag{5.27}$$

Hence the linear thermal gradients are $\Delta T_1 / h_{tot}$ = +4.66 °C/m and ΔT_2 = -5.60 °C/m.

6. Global analysis

6.1. Combination of actions

The bridge is verified under two design combinations of actions, according to [14]:

- The Ultimate Limit State (ULS): $1.35 \cdot G_k + 1.00 \cdot S_k + 1.35 \cdot Q_k + 1.50 \cdot 0.6 \cdot T_k$;
- The Fatigue Ultimate Limit State (FLS): $1.00 \cdot Q_{k,fat}$.

The following notations are considered:

- G_k: characteristic permanent actions
- S_k: characteristic actions due to shrinkage
- Q_k: characteristic traffic actions for verifications at ULS
- $Q_{k,fat}$: characteristic traffic actions for verifications at FLS
- T_k: characteristic thermal actions

6.2. Analysis methods

The internal forces and moments of the bridge are calculated with a global analysis, which is:

- A first order analysis: the deformed geometry has no influence on the internal forces and moments, with a specific verification against lateral-torsional buckling;
- A linear elastic analysis, although the plastic resistance of the composite cross-section at mid-span is considered;
- A cracked analysis: at support, where the concrete slab is assumed to be cracked, the stiffness of the slab is equal to the stiffness of the reinforcing steel at supports.

6.3. Internal forces and stresses

The bridge is modelled as a continuous line of bar elements as in [1] § 7.2.1. This line corresponds to the neutral fibre of the modelled main girder and depends on the mechanical properties of the bar. These correspond to the properties of the cross-section they represent. The girder is simply supported at piles and abutments, with a fixed point at C0.

Several cross-sections are chosen to be at bar element ends, as shown in Annex VI Figure 23:

- At piles and abutments;
- At the thickness changes in the structural steel distribution.

According to [8] § 5.4.1.2, the effective width of the concrete slab should be:

$$b_{eff} = b_0 + \beta_1 \cdot b_{e1} + \beta_2 \cdot b_{e2} \quad (6.1)$$

The following simplification is considered though, since b_{eff} is very close to b_{slab}: $b_{eff} = b_{slab} / 2 = 6$ m. Hence the section A_c of the slab for one girder is considered to be: $A_c = A_{slab} / 2 = 1.842$ m^2.

The reinforced concrete slab is modelled in the uncracked regions as a steel-equivalent area with the modular ratios. Four design models are defined depending on the type of action:

- Design model 0: the structural permanent actions are applied on the steel girder only;
- Design model 1: the non-structural bridge equipment is applied on the composite girder. The modular ratio for long-term actions is n_φ =18. Hence the steel-equivalent width of the slab is b_{eff} / n_φ = 6.00 / 18 = 0.33 m.
- Design model 2: the effects of shrinkage are applied on the composite cross-section. The modular ratio for concrete shrinkage is n_s = 12. Hence the steel-equivalent width of the slab is b_{eff} / n_s = 6.00 / 12 = 0.50 m.
- Design model 3: the traffic and thermal actions are applied on the composite cross-section. The modular ratio for short-term actions is n_0 = 6. Hence the steel-equivalent width of the slab is b_{eff} / n_0 = 6.00 / 6 = 1.00 m.

In the cracked regions, the slab is only modelled by the slab reinforcement at supports:

- Upper layer: Ø 20 mm; s = 130 mm;
- Lower layer: Ø 16 mm; s = 130 mm.

Then the loads are applied on the design models, accounting for the construction stages of the bridge. The model 0 considers the selfweights of the steel girder and the slab: $g_{a,support,tot}$, $g_{a,span,tot}$ and g_c, applied on the girder only. The model 1 includes the selfweight of the asphalt layer and the safety barrier: $g_{perm} = g_{asphalt} + g_{barrier}$.

In the model 2, the shrinkage acts as a normal force N_s applied to the centre of gravity of the slab. It is modelled as a normal force N_s and a bending moment M_s applied to the centre of gravity of the composite cross-section:

$$N_s = E_{cs} \cdot \varepsilon_{cs} \cdot A_c = n_s \cdot E_{cm} \cdot \varepsilon_{cs} \cdot A_c \quad (6.2)$$

$$M_s = N_s \cdot (z_b - z_c) \quad (6.3)$$

Where z_b and z_c are respectively the centres of gravity of the composite cross-section and the reinforced concrete slab. Over internal supports, since the slab is cracked, the stiffness of the slab is much reduced and the imposed deformation due to shrinkage will not create tension. Hence in the cracked analysis, the isostatic effects N_s and M_s are not applied in the cracked zones, but they are introduced only at the end of the uncracked zones.

Lastly, the traffic actions Q_k and q_k and the temperature variation $\Delta T / h_{tot}$ are applied in the model 3 on the composite cross-section, in order to maximize the internal forces at mid-span and at support.

The cross-sections modelled in SAP 2000 are resumed in Annex VI Figure 24, Figure 25 and Figure 26. The loads applied on the girder are shown in Annex VII Figure 27 to Figure 30. They are resumed in Table 17.

Table 17: Actions applied in SAP 2000

Action	Design A	Design B	Design C	Safety factor
$g_{a,support,tot}$	12.8 kN/m	10.0 kN/m	9.7 kN/m	1.35
$g_{a,span,tot}$	27.9 kN/m	14.1 kN/m	12.3 kN/m	1.35
g_c	46.1 kN/m			1.35
g_{perm}	14.2 kN/m			1.35
N_s	4 262 kN	4 270 kN	4 262 kN	1.00
M_s	3 503 kNm	3 227 kNm	3 229 kNm	1.00
Q_k	786.9 kN			1.35
q_k	32.7 kN/m			1.35
$\Delta T_1 / h_{tot}$	+4.66 °C/m			0.90
$\Delta T_2 / h_{tot}$	-5.60 °C/m			0.90

6.4. Maximum shear forces and bending moments

The values of the maximum bending moment and the maximum shear forces at ULS are detailed respectively in Table 18 and Table 19. The bending moment and shear force diagrams at ULS are shown respectively in Annex VIII and Annex IX.

Table 18: Maximum bending moments at the studied cross-sections

[kNm]	Support P1			Mid-span P1-P2		
Design	A	B	C	A	B	C
Model 0	-47 774	-41 439	-40 664	17 335	19 547	19 853
Model 1	-10 231	-8 673	-8 038	5 105	6 663	7 298
Model 2	-3 063	-2 129	-1 767	440	1 098	1 329
Model 3	-39 297	-30 609	-27 199	39 259	41 172	42 086
Total: M_{Ed}	-100 335	-82 851	-77 669	62 139	68 479	70 565

The value of the bending moment decreases at support P1 from design A to design C. This should be favourable at ULS, and in the justification against lateral-torsional buckling at support. At mid-span P1-P2, the values of the bending moment increase despite the reduction in weight, because of the change in the geometric properties.

Table 19: Maximum shear forces at the studied cross-sections

[kN]	Support P1			Mid-span P1-P2		
Design	A	B	C	A	B	C
Model 0	3 425	3 096	3 055	0	0	0
Model 1	767	767	767	0	0	0
Model 2	0	0	0	0	0	0
Model 3	2 974	2 935	2 921	1 062	1 062	1 062
Total: V_{Ed}	7 166	6 797	6 743	1 062	1 062	1 062

7. Geometric properties of the cross-sections and design stresses

The purpose of this section is to determine the neutral axis, the second moment of inertia and the section modulus of the cross-sections for all designs, at all stages. These properties are necessary to calculate the design stresses in the elements of the girder, from the maximum bending moments.

7.1. Cross-section classes in the Eurocode

According to [5] § 5.5, the elements of the girder can be classified into four classes of cross-sections:

- Class 1: the cross-section can reach its plastic strength without buckling. The rotation capacity of the plastic hinge is sufficient to perform a global plastic analysis of the structure.
- Class 2: the cross-section can reach its plastic moment resistance without buckling. The rotation capacity of the plastic hinge is not sufficient to perform a global plastic analysis.
- Class 3: the cross-section can reach its elastic resistance but not its plastic moment resistance due to buckling.
- Class 4: local buckling occurs in the cross-section before it can reach its elastic resistance.

The limits between cross-section classes are determined with [5] Table 5.2. Several issues should be considered about the limit between class 3 and class 4 of the web, which depends on the boundary conditions of the web and the stress distribution. It is necessary to understand the theory behind the limits given in the Eurocode between the cross-section classes 3 and 4, in order to adapt these limits.

According to [15] § 12.3.2, the critical buckling stress σ_{crB} of a plate with a height h_w is:

$$\sigma_{crB} = k_\sigma \cdot \sigma_E = k_\sigma \cdot \frac{\pi^2 \cdot E_a}{12 \cdot (1-\nu^2)} \cdot \left(\frac{t_w}{h_w}\right)^2 = k_\sigma \cdot \frac{1}{1.052^2} \cdot E_a \cdot \left(\frac{t_w}{h_w}\right)^2 \quad (7.1)$$

Where ν is the Poisson's coefficient of steel; σ_E is the elastic critical Euler's stress; k_σ is the plate buckling coefficient. The limit between classes 3 and 4 occurs when the effective height $h_{w,eff}$ is equal to the actual height h_w of the web:

$$h_{w,eff} = \frac{h_w}{\bar{\lambda}_B} = h_w \cdot \sqrt{\frac{\sigma_{crB}}{\sigma_{max}}} = h_w \cdot \sqrt{\frac{\sigma_{crB}}{f_{yk}}} \quad (7.2)$$

$$\bar{\lambda}_B = \sqrt{\frac{f_{yk}}{\sigma_{crB}}} = 1.052 \cdot \sqrt{\frac{f_{yk}}{k_\sigma \cdot E_a}} \cdot \frac{h_w}{t_w} = 1.052 \cdot \sqrt{\frac{235}{k_\sigma \cdot E_a}} \cdot \frac{1}{\varepsilon} \cdot \frac{h_w}{t_w} \quad (7.3)$$

Where $\bar{\lambda}_B$ is the slenderness coefficient of the plate. To avoid local buckling, this coefficient should be inferior to the Winter's coefficient $\bar{\lambda}_p$ defined in [16] § 4.4, which depends on the stress ratio ψ. Hence the limiting slenderness of the web is defined by the general formulas:

$$\bar{\lambda}_B \leq \bar{\lambda}_p = 0.5 + \sqrt{(0.085 - 0.055 * \psi)} \quad (7.4)$$

$$\frac{h_w}{t_w} \leq \bar{\lambda}_p \cdot \frac{1}{1.052} \cdot \sqrt{\frac{k_\sigma \cdot E_a}{235}} \cdot \varepsilon \quad (7.5)$$

7.1.1. Calculation of the plate buckling coefficient k_σ

In the Eurocodes, the steel girders used in the composite steel-concrete bridges are assumed to be formed with 3 plates: the web and two flanges. Hence the web is considered to be hinged to the flanges, and according to [16] Table 4.1:

- Pure compression with ψ = 1: k_σ = 4.00.
- Bending and compression with ψ = 0: k_σ = 7.81.
- Pure bending with ψ = -1: k_σ = 23.90.

For other values of ψ, [16] Table 4.1 gives:

- Equation (7.6) for $1 \geq \psi \geq 0$.
- Equation (7.7) for $0 \geq \psi \geq -1$.
- Equation (7.8) for $-1 \geq \psi \geq -3$.

$$k_\sigma = \frac{8.2}{1.05 + \psi} = \frac{(1 + 1.05) * 4.00}{1.05 + \psi} \quad (7.6)$$

$$k_\sigma = 7.81 - 6.29 * \psi + 9.78 * \psi^2 = 7.81 - 6.29 * \psi + \big((23.90 - 7.81) - 6.29\big) * \psi^2 \quad (7.7)$$

$$k_\sigma = 5.98 * (1 - \psi)^2 = \frac{23.90}{4} * (1 - \psi)^2 \quad (7.8)$$

A first issue concerns the validity range of the Equations (7.6) to (7.8): $0 \geq \psi \geq -3$. An analysis is done with the software EBPlate [17] to test the validity of the equations when $\psi \leq -3$. The input data correspond to a web panel between two cross-bracings of the girder:

- Plate of thickness t = 20 mm, length a = 8 000 mm, height = 2 800 mm, hinged on four sides.
- Positive upper stress (compression): σ = +10 MPa.
- Variable lower stress: +10 MPa ≥ σ ≥ -50 MPa. Hence the stress ratio is: $1 \geq \psi \geq -5$.
- Analysis of the first 20 modes of buckling.

Specific values of the plate buckling coefficient k_σ are also given [15] Table 12.7. They depend on the stress ratio ψ and on the boundary conditions. For comparison purposes, the values of k_σ obtained with [15] Table 12.7, the Eurocode and EBPlate are detailed in Table 20.

According to Table 20, the validity of Equation (7.8) can be extended to cases when $\psi \leq -3$.

A second issue concerns the adaptation of the Equations (7.6) to (7.8) when the web is considered to be fixed to the flanges, as it is in the design C. The torsional stiffness of the flanges is indeed much higher because of the tubular shape. According to [15] Table 12.7:

- Pure compression with ψ = 1: k_σ = 6.97.
- Bending and compression with ψ = 0: k_σ = 13.54.
- Pure bending with ψ = -1: k_σ = 39.52.

Therefore new formulas are suggested for other values of ψ:

- Equation (7.9) for $1 \geq \psi \geq 0$.
- Equation (7.10) for $0 \geq \psi \geq -1$.
- Equation (7.11) for $\psi \leq -1$.

$$k_\sigma = \frac{(1 + 1.06) * 6.97}{1.06 + \psi} \tag{7.9}$$

$$k_\sigma = 13.54 - 6.29 * \psi + \big((39.52 - 13.54) - 6.29\big) * \psi^2 \tag{7.10}$$

$$k_\sigma = \frac{39.52}{4} * (1 - \psi)^2 \tag{7.11}$$

Another analysis with EBPlate is performed to test the validity of Equations (7.9) to (7.11). The input data is the same than for the first analysis, except that the plate is fixed on the upper and lower sides.

According to Table 20, the values given by the new formulas are slightly conservative as compared to those given by EBPlate, when the stress ratio is: $0 \geq \psi \geq -1$. The difference tend to increase when $\psi \leq -1$, as shown in the graph below.

Table 20: Calculation of the plate buckling coefficient k_σ

	Hinged connection			Fixed connection		
ψ	TGC 10, [15] Table 12.7	EC3	EBPlate [17]	TGC 10, [15] Table 12.7	EC3 adapted	EBPlate [17]
1.0	4.00	4.00	4.010	6.97	6.97	7.424
0.5	5.32	5.29	5.330	9.27	9.20	9.872
0.0	7.81	7.81	7.817	13.54	13.55	14.455
-0.5	13.40	13.40	13.419	24.50	21.61	24.099
-1.0	23.90	23.90	23.952	39.52	39.52	42.722
-2.0	-	53.78	54.000	-	88.92	100.822
-3.0	-	95.60	95.852	-	158.08	189.212
-4.0	-	149.38	149.557	-	247.00	315.171
-5.0	-	215.10	215.261	-	355.68	491.952

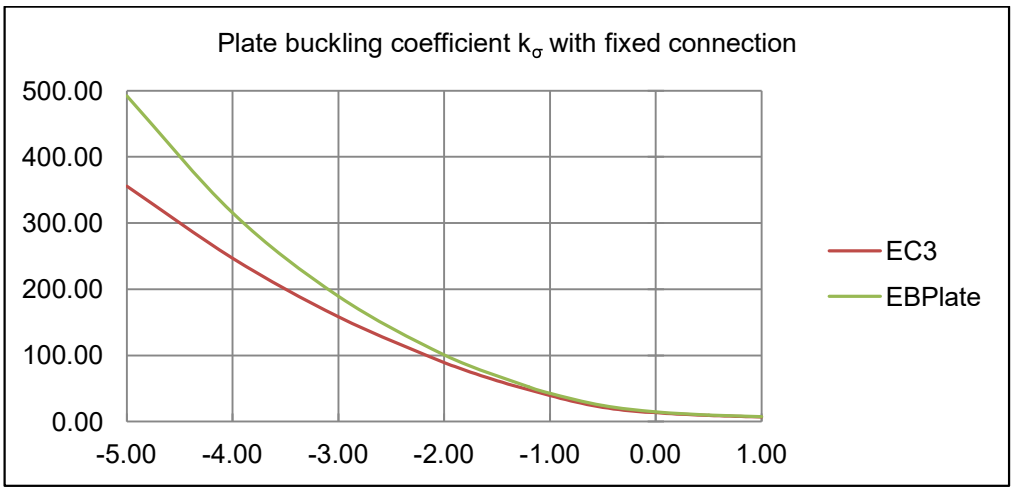

7.1.2. Limit between cross-section classes 3 and 4 of the web

The limit between the cross-section classes 3 and 4 of the web should be calculated with Equation (7.5). It depends on the plate buckling coefficient k_σ and the Winter's coefficient $\bar{\lambda}_p$, which both depend on the stress ratio ψ. For pure compression and pure bending, $\bar{\lambda}_p$ is respectively equal to 0.673 and 0.874 with Equation (7.4). However, the Eurocode uses different values (respectively 0.74 and 0.89), and defines Equations (7.12) and (7.13) for other values of ψ.

Hence according to [5] Table 5.2, the limit between the cross-section classes 3 and 4 of the web is:

- Pure compression (ψ = 1): $h_w / t_w \leq 42 \cdot \varepsilon$.
- Pure bending (ψ = -1): $h_w / t_w \leq 124 \cdot \varepsilon$.
- Equation (7.12) for $1 \geq \psi \geq -1$.
- Equation (7.13) for $\psi \leq -1$.

$$\frac{h_w}{t_w} \leq \frac{42 * \varepsilon}{0.67 + 0.33 * \psi} \tag{7.12}$$

$$\frac{h_w}{t_w} \leq \frac{124}{2} * \varepsilon * (1 - \psi) * \sqrt{-\psi} \tag{7.13}$$

For the designs A and B, with hinged connections between the web and the flanges of the main girders, the limits defined in [5] Table 5.2 are used. For the design C, new limits are defined with Equation (7.5) when the stress ratio is $1 \geq \psi \geq -1$. In case $\psi \leq -1$, a new formula is suggested:

$$\frac{h_w}{t_w} \leq \frac{156}{2} * \varepsilon * (1 - \psi) * \sqrt{-\psi} \tag{7.14}$$

All results are detailed in Table 21. The limit between the cross-section classes 3 and 4 of the web is:

- Pure compression (ψ = 1): $h_w / t_w \leq 51 \cdot \varepsilon$.
- Pure bending (ψ = -1): $h_w / t_w \leq 156 \cdot \varepsilon$.
- Equation (7.5) for $1 \geq \psi \geq -1$.
- Equation (7.14) for $\psi \leq -1$.

Table 21: Limits between classes 3 and 4 of the web

	EC3		Hinged connection		Fixed connection	
ψ	h_w/t_w	$\bar{\lambda}_p$	k_σ	h_w/t_w	k_σ	h_w/t_w
1.0	42.1 · ε	0.673	4.00	38.3 · ε	6.97	50.5 · ε
0.5	50.4 · ε	0.740	5.29	48.5 · ε	9.20	64.0 · ε
0.0	62.8 · ε	0.792	7.81	62.8 · ε	13.55	82.7 · ε
-0.5	83.3 · ε	0.835	13.40	86.4 · ε	21.61	113.1 · ε
-1.0	123.6 · ε	0.874	23.90	121.4 · ε	39.52	156.2 · ε
-1.5	189.3 · ε	0.909	37.34	185.9 · ε	61.75	239.1 · ε
-2.0	262.3 · ε	0.942	53.78	257.6 · ε	88.92	331.3 · ε
-2.5	342.1 · ε	0.972	73.19	336.0 · ε	121.03	432.1 · ε

7.2. Elastic geometric properties of the gross cross-sections

Table 22, Table 23 and Table 24 give respectively the second moment of inertia I, the neutral axis z and the section modulus W of all gross cross-sections, for all designs, at all stages. The neutral axis is given with respect to lower fibre of the bottom flange. The section modulus is given with respect to the extreme fibres of the flanges and the slab, and to the mid-plane of the reinforcement.

Table 22: Elastic second moment of area of the gross cross-sections

I [10^9 mm4]	Support P1			Mid-span P1-P2		
Model	A	B	C	A	B	C
0	508	205	139	197	138	100
1	571	279	198	376	323	290
2				418	360	327
3				487	416	383

Table 23: Elastic neutral axis of the gross cross-sections

z [mm]	Support P1			Mid-span P1-P2		
Model	A	B	C	A	B	C
0	1 303	1 096	1 291	1 319	1 162	1 120
1	1 412	1 342	1 546	2 065	2 117	2 111
2				2 241	2 307	2 305
3				2 525	2 591	2 592

Table 24: Elastic section modulus of the gross cross-sections

W [10^6 mm^3]		Support P1			Mid-span P1-P2		
Design	Model	W_{inf}	W_{sup}	W_{arm}	W_{inf}	W_{sup}	W_{bet}
A	0	390	-339	-	149	-133	-
	1	405	-412	-346	182	-511	-326
	2				187	-747	-429
	3				193	-1 770	-705
B	0	187	-120	-	119	-84	-
	1	208	-191	-162	153	-473	-294
	2				156	-729	-396
	3				160	-1 987	-665
C	0	108	-92	-	90	-58	-
	1	128	-158	-130	137	-421	-263
	2				142	-661	-359
	3				148	-1 842	-614

The stress distribution in the gross cross-section of the main girder is given in Annex X, in Figure 31 at support P1 and in Figure 32 at mid-span P1-P2, for all designs, at all stages.

7.3. Determination of the cross-section class

The class of a cross-section depends on the stage of life of the bridge. At the construction stage, the main steel girder resist alone to the structural permanent actions: the weight of the steel girder and of the concrete slab (Model 0). At the final stage, the composite girder resist to shrinkage, permanent and variable actions (Models 0 to 3).

7.3.1. Design A, support P1

The elastic stress distribution at support P1 at all stages is given in Table 25. The stress ratio ψ is calculated from the design stresses at the extreme fibres of the web, with Equation (7.15) to (7.17). The part of the web in compression can be calculated with Equation (7.18):

$$\sigma_{w,sup} = \sigma_{y,sup} - \frac{\sigma_{y,sup} - \sigma_{y,inf}}{h_a} \cdot t_{f,sup} \quad (7.15)$$

$$\sigma_{w,inf} = \sigma_{y,inf} + \frac{\sigma_{y,sup} - \sigma_{y,inf}}{h_a} \cdot t_{f,inf} \quad (7.16)$$

$$\psi = \sigma_{w,sup}/\sigma_{w,inf} \quad (7.17)$$

$$h_c = h_w/(1-\psi) \quad (7.18)$$

Where $\sigma_{y,sup}$ is the design stress at the extreme fibre of the upper flange; $\sigma_{y,inf}$ is the design stress at the extreme fibre of the lower flange; $\sigma_{w,sup}$ is the design stress at the upper fibre of the web; $\sigma_{w,inf}$ is the design stress at the lower fibre of the web; h_a is the height of the steel girder; h_w is the height of the web; h_c is the compression height of the web.

Table 25: Elastic stress distribution at support P1 (design A)

Model	$\sigma_{y,sup}$	$\sigma_{y,inf}$	$\sigma_{w,sup}$	$\sigma_{w,inf}$	ψ	h_c
0	+141 MPa	-123 MPa	+130 MPa	-111 MPa	-1.165	1 183 mm
1	+24.9 MPa	-25.3 MPa	+22.7 MPa	-23.1 MPa	-0.981	1 292 mm
2	+7.4 MPa	-7.6 MPa	+6.8 MPa	-6.9 MPa		
3	+95 MPa	-97 MPa	+87 MPa	-89 MPa		
Total	+269 MPa	-253 MPa	+246 MPa	-230 MPa	-1.070	1 237 mm

At the construction stage, no plastification of the cross-section is allowed. The upper flange is in tension and therefore in class 1. The lower flange is in compression; it is in class 1 from [5] Table 5.2:

$$\frac{b_{f,inf} - t_w}{2 \cdot t_{f,inf}} = \frac{1\,200 - 26}{2 \cdot 120} = 4.89 \leq 9 \cdot \varepsilon = 8.03$$

According to Table 25, less than half of the web is in compression. It is at least in class 3, according to Equation (7.13):

$$\frac{h_c}{h_w} = \frac{1\,183}{2\,560} = 0.46; \quad \frac{h_w}{t_w} = \frac{2\,560}{26} = 98.5 \leq 62 * \varepsilon * (1 + 1.165) * \sqrt{1.165} = 119.5$$

Hence the cross-section of the main girder at support P1, at the construction stage, is in class 3.

At the final stage, the plastification of the cross-section is allowed. The design plastic resistance of the elements of the main girder are detailed in Table 26:

Table 26: Design plastic resistance at support P1 (design A)

Design plastic resistance	Force	Value
Reinforcement	$F_s = A_s \cdot f_{sk}/\gamma_s$	9.53 MN
Upper flange	$F_{y,sup} = A_{f,sup} \cdot f_{yk,sup}/\gamma_{M0}$	35.40 MN
Web	$F_{y,w} = A_w \cdot f_{yk,w}/\gamma_{M0}$	22.96 MN
Lower flange	$F_{y,inf} = A_{f,inf} \cdot f_{yk,inf}/\gamma_{M0}$	42.48 MN

Since $F_s + F_{y,sup} \leq F_{y,w} + F_{y,inf}$ and $F_s + F_{y,sup} + F_{y,w} \geq F_{y,inf}$, the plastic neutral axis (PNA) is located in the steel web at a distance x = 1 143 mm from the lower fibre of the upper flange, as shown in Annex XII Figure 34:

$$x = \frac{F_{y,inf} + F_{y,w} - F_{y,sup} - F_s}{2 \cdot t_w \cdot h_w} \tag{7.19}$$

The upper flange and the lower flange are still in class 1. Over half of the web would be in plastic compression; it is in class 3 or 4, according to [5] Table 5.2:

$$\frac{h_w - x}{h_w} = \frac{2\,560 - 1\,143}{2\,560} = 0.55; \quad \frac{h_w}{t_w} = \frac{2\,560}{26} = 98.5 \geq \frac{456 \cdot \varepsilon}{13 \cdot \frac{2\,560 - 1\,143}{2560} - 1} = 60.8$$

According to Table 25, less than half of the web is in elastic compression. It is in class 3, according to Equation (7.13):

$$\frac{h_c}{h_w} = \frac{1\,237}{2\,560} = 0.48; \quad \frac{h_w}{t_w} = \frac{2\,560}{26} = 98.5 \leq 62 * \varepsilon * (1 + 1.070) * \sqrt{1.070} = 109.5$$

Hence the cross-section of the main girder at support P1, at the final stage, is in class 3.

7.3.2. Design A, mid-span P1-P2

The elastic stress distribution at mid-span P1-P2 at all stages is given in Table 27. The calculation of the stress ratio ψ has to be adapted from Equation (7.17) to Equation (7.20):

$$\psi = \sigma_{w,inf}/\sigma_{w,sup} \tag{7.20}$$

Table 27: Elastic stress distribution at mid-span P1-P2 (design A)

Model	$\sigma_{y,sup}$	$\sigma_{y,inf}$	$\sigma_{w,sup}$	$\sigma_{w,inf}$	ψ	h_c
0	-130 MPa	+116 MPa	-127 MPa	+113 MPa	-0.888	1 441 mm
1	-10.0 MPa	+28.1 MPa	-9-4 MPa	+27.5 MPa	-2.913	695 mm
2	-0.6 MPa	+2.4 MPa	-0.5 MPa	+2.3 MPa	-4.237	519 mm
3	-22 MPa	+204 MPa	-19 MPa	+200 MPa	-10.563	235 mm
Total	-163 MPa	+350 MPa	-156 MPa	+343 MPa	-2.200	850 mm

At the construction stage, no plastification of the cross-section is allowed. The lower flange is in tension and therefore in class 1. The upper flange is in compression; it is in class 4 from [5] Table 5.2:

$$\frac{b_{f,sup} - t_w}{2 \cdot t_{f,sup}} = \frac{1\,000 - 18}{2 \cdot 40} = 12.28 \geq 14 \cdot \varepsilon = 11.55$$

According to Table 27, over than half of the web is in compression. It is in class 4, according to Equation (7.12):

$$\frac{h_c}{h_w} = \frac{1\,441}{2\,720} = 0.53; \quad \frac{h_w}{t_w} = \frac{2\,720}{18} = 151.1 \geq \frac{42 * \varepsilon}{0.67 + 0.33 * (-0.888)} = 92.0$$

Hence the cross-section of the main girder at mid-span P1-P2, at the construction stage, is in class 4. It must be checked by an elastic section analysis using the effective reduced area of the web and of the compression flange, from [2] Equation (12.9) and (12.28):

$$b_{f,eff} = \min\left(b_f; 2 \cdot 0.56 \cdot \sqrt{\frac{E_a}{f_{yk,f}}} \cdot t_f\right) \tag{7.21}$$

$$h_{c,eff} = \min\left(h_c; 0.86 \cdot \sqrt{\frac{k_\sigma \cdot E_a}{f_{yk,w}}} \cdot \frac{h_c}{h_w} \cdot t_w\right) \tag{7.22}$$

Where $b_{f,eff}$ is the effective width of the upper flange; $h_{c,eff}$ is the effective compression height of the web; $f_{yk,f}$ is the yield stress of the upper flange; $f_{yk,w}$ is the yield stress of the web.

Equation (7.21) accounts for the local buckling of the compression flange. According to [2] § 12.2.3, when the slenderness of the compression flange of a welded I-section is too high, it can buckle around its connection to the web, and only the effective part of the compression flange resists to the design stresses at ULS.

The results for $h_{c,eff}$ and $b_{f,sup,eff}$ are detailed in Table 28.

Table 28: $h_{c,eff}$ and $b_{f,sup,eff}$ of the web at mid-span P1-P2, at the construction stage (design A)

Model	h_c	Equation (7.22)	$h_{c,eff}$	$b_{f,sup}$	Equation (7.21)	$b_{f,sup,eff}$
0	1 441 mm	929 mm	929 mm	1 000 mm	1 105 mm	1 000 mm

The new stress distribution at the construction stage is shown in Annex XI Figure 33.

At the final stage, the plastification of the cross-section is allowed. The design plastic resistance of the elements of the main girder are detailed in Table 29:

Table 29: Design plastic resistance at mid-span P1-P2 (design A)

Design plastic resistance	Force	Value
Slab	$F_c = A_c \cdot f_{ck}/\gamma_c$	36.53 MN
Upper flange	$F_{y,sup} = A_{f,sup} \cdot f_{yk,sup}/\gamma_{M0}$	13.80 MN
Web	$F_{y,w} = A_w \cdot f_{yk,w}/\gamma_{M0}$	16.89 MN
Lower flange	$F_{y,inf} = A_{f,inf} \cdot f_{yk,inf}/\gamma_{M0}$	16.56 MN

Since $F_c \leq F_{y,sup} + F_{y,w} + F_{y,inf}$ and $F_c + F_{y,sup} \geq F_{y,w} + F_{y,inf}$, the PNA is located in the upper steel flange at a distance x = 15.5 mm from the upper fibre of the upper flange:

$$x = \frac{F_{y,inf} + F_{y,w} + F_{y,sup} - F_c}{2 \cdot b_{f,sup} \cdot t_{f,sup}} \tag{7.23}$$

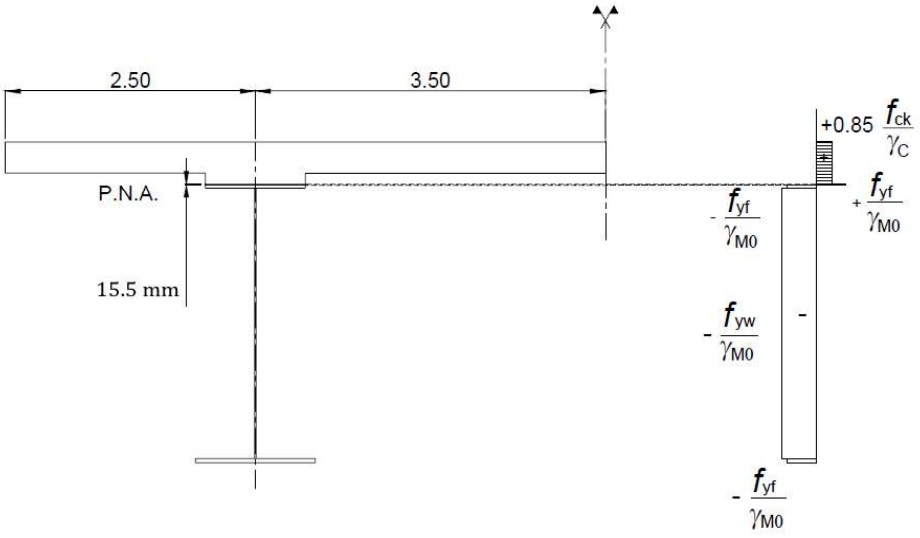

Figure 8: PNA of the cross-section at mid-span P1-P2 (design A)

The lower flange is still in class 1. The upper flange is composite and connected to the slab, therefore in class 1. The steel web would be entirely in plastic tension since the PNA is in the upper flange; therefore in class 1.

Hence the cross-section of the main girder at mid-span P1-P2, at the final stage, is in class 1.

7.3.3. Design B, support P1

As for the design A, no plastification of the cross-section is allowed at the construction stage. At the final stage in design B, the yield stress is much higher than the design stress in the web; buckling would occur before the plastification of the web. Therefore neither at the final stage is the plastification allowed, and the cross-section has to be checked with an elastic analysis.

The elastic stress distribution at support P1 at all stages is given in Table 30. The stress ratio ψ is calculated with Equation (7.17).

Table 30: Elastic stress distribution at support P1 (design B)

Model	$\sigma_{y,sup}$	$\sigma_{y,inf}$	$\sigma_{w,sup}$	$\sigma_{w,inf}$	ψ	h_c
0	+345 MPa	-222 MPa	+335 MPa	-207 MPa	-1.619	1 021 mm
1	+45.4 MPa	-41.8 MPa	+43.8 MPa	-39.4 MPa	-1.111	1 267 mm
2	+11.1 MPa	-10.3 MPa	+10.8 MPa	-9.7 MPa		
3	+160 MPa	-147 MPa	+155 MPa	-139 MPa		
Total	+562 MPa	-422 MPa	+544 MPa	-395 MPa	-1.377	1 125 mm

At the construction stage, the upper flange is in tension and therefore in class 1. The lower flange is in compression; it is in class 2 from [5] Table 5.2:

$$\frac{b_{f,inf} - t_w}{2 \cdot t_{f,inf}} = \frac{900 - 20}{2 \cdot 75} = 5.87 \leq 10 \cdot \varepsilon = 8.42$$

According to Table 30, less than half of the web is in compression. It is in class 4, according to Equation (7.13):

$$\frac{h_c}{h_w} = \frac{1\,021}{2\,675} = 0.38; \quad \frac{h_w}{t_w} = \frac{2\,675}{20} = 133.8 \geq 62 * \varepsilon * (1 + 1.619) * \sqrt{1.619} = 120.6$$

Hence the cross-section of the main girder at support P1, at the construction stage, is in class 4 and must be checked by an elastic section analysis, using the effective reduced area of the web. With Equation (7.22):

Table 31: $h_{c,eff}$ of the web at support P1, at the construction stage (design B)

Model	h_c	Equation (7.22)	$h_{c,eff}$
0	1 021 mm	734 mm	734 mm

The new stress distribution at the construction stage is shown in Figure 33.

At the final stage, the upper and lower flanges are still in class 1 and 2. According to Table 30, less than half of the web is in elastic compression. It is in class 4, according to Equation (7.13):

$$\frac{h_c}{h_w} = \frac{1\,125}{2\,675} = 0.42; \quad \frac{h_w}{t_w} = \frac{2\,675}{20} = 133.8 \geq 62 * \varepsilon * (1 + 1.377) * \sqrt{1.377} = 100.9$$

Hence the cross-section of the main girder at support P1, at the final stage, is in class 4 and must be checked by an elastic section analysis, using the effective reduced area of the web at all stages. From Table 30 and with Equation (7.22):

Table 32: $h_{c,eff}$ of the web at support P1, at the final stage (design B)

Model	h_c	Equation (7.22)	$h_{c,eff}$
0	1 021 mm	734 mm	734 mm
1, 2, 3	1 267 mm	734 mm	734 mm
Total	1 125 mm	734 mm	734 mm

The new stress distribution at the final stage is shown in Figure 33.

7.3.4. Design B, mid-span P1-P2

The elastic stress distribution at mid-span P1-P2 at all stages is given in Table 33. The calculation of the stress ratio ψ is calculated with Equation (7.20).

Table 33: Elastic stress distribution at mid-span P1-P2 (design B)

Model	$\sigma_{y,sup}$	$\sigma_{y,inf}$	$\sigma_{w,sup}$	$\sigma_{w,inf}$	ψ	h_c
0	-232 MPa	+164 MPa	-227 MPa	+158 MPa	-0.697	1 603 mm
1	-14.1 MPa	+43.7 MPa	-13.4 MPa	+42.8 MPa	-3.196	648 mm
2	-1.5 MPa	+7.0 MPa	-1.4 MPa	+6.9 MPa	-4.935	458 mm
3	-21 MPa	+257 MPa	-17 MPa	+252 MPa	-14.615	174 mm
Total	-268 MPa	+472 MPa	-259 MPa	+460 MPa	-1.775	980 mm

At the construction stage, the lower flange is in tension and therefore in class 1. The upper flange is in compression; it is in class 4 from [5] Table 5.2:

$$\frac{b_{f,sup} - t_w}{2 \cdot t_{f,sup}} = \frac{650 - 14}{2 \cdot 35} = 9.09 \geq 14 \cdot \varepsilon = 8.17$$

According to Table 33, over half of the web is in compression. It is in class 4, according to Equation (7.12):

$$\frac{h_c}{h_w} = \frac{1\,603}{2\,720} = 0.59; \quad \frac{h_w}{t_w} = \frac{2\,720}{14} = 194.3 \geq \frac{42 * \varepsilon}{0.67 + 0.33 * (-0.697)} = 55.7$$

Hence the cross-section of the main girder at mid-span P1-P2, at the construction stage, is in class 4. It must be checked by an elastic section analysis, using the effective reduced area of the web and of the compression flange. From Table 33 and with Equation (7.21) and (7.22):

Table 34: $h_{c,eff}$ of the web at mid-span P1-P2, at the construction stage (design B)

Model	h_c	Equation (7.22)	$h_{c,eff}$	$b_{f,sup}$	Equation (7.21)	$b_{f,sup,eff}$
0	1 603 mm	510 mm	510 mm	650 mm	684 mm	650 mm

The new stress distribution at the construction stage is shown in Figure 33.

At the final stage, the lower flange is still in class 1. The upper flange is composite and connected to the slab, therefore in class 1. According to Table 33, less than half of the web is in compression. It is in class 4, according to Equation (7.13):

$$\frac{h_c}{h_w} = \frac{980}{2\,720} = 0.36; \quad \frac{h_w}{t_w} = \frac{2\,720}{14} = 194.3 \geq 62 * \varepsilon * (1 + 1.377) * \sqrt{1.377} = 133.8$$

Hence the cross-section of the main girder at mid-span P1-P2, at the final stage, is in class 4 and must be checked by an elastic section analysis, using the effective reduced area of the web at all stages. From Table 33 and with Equation (7.22):

Table 35: $h_{c,eff}$ of the web at mid-span P1-P2, at the final stage (design B)

Model	h_c	Equation (7.22)	$h_{c,eff}$
0	1 603 mm	510 mm	510 mm
1	648 mm	514 mm	514 mm
2	458 mm	514 mm	458 mm
3	174 mm	514 mm	174 mm
Total	980 mm	514 mm	514 mm

The new stress distribution at the final stage is shown in Figure 33.

7.3.5. Design C, support P1

As for the design B, plastification of the cross-section is allowed neither at the construction nor the stages. The cross-section has to be checked with an elastic analysis. The elastic stress distribution at support P1 at all stages is given in Table 36. The stress ratio ψ is calculated with Equation (7.17).

Table 36: Elastic stress distribution at support P1 (design C)

Model	$\sigma_{y,sup}$	$\sigma_{y,inf}$	$\sigma_{w,sup}$	$\sigma_{w,inf}$	ψ	h_c
0	+442 MPa	-378 MPa	+308 MPa	-244 MPa	-1.262	834 mm
1	+51 MPa	-63 MPa	+32 MPa	-44 MPa	-0.732	1 089 mm
2	+11.2 MPa	-13.8 MPa	+7.1 MPa	-9.7 MPa		
3	+173 MPa	-213 MPa	+110 MPa	-150 MPa		
Total	+677 MPa	-667 MPa	+457 MPa	-448 MPa	-1.021	933 mm

At the construction stage, the upper flange is in tension and therefore in class 1. The lower flange is in compression; it is in class 1 from [5] Table 5.2:

$$\frac{D_{f,inf}}{t_{f,inf}} = \frac{457}{40} = 11.4 \leq 50 \cdot \varepsilon^2 = 17.03$$

According to Table 36, less than half of the web is in compression. It is in class 3, according to Equation (7.14):

$$\frac{h_c}{h_w} = \frac{834}{1\,886} = 0.44; \quad \frac{h_w}{t_w} = \frac{1\,886}{20} = 94.3 \leq 78 * \varepsilon * (1 + 1.262) * \sqrt{1.262} = 115.7$$

Hence the cross-section of the main girder at support P1, at the construction stage, is in class 3.

At the final stage, the upper flange and the lower flange are still in class 1. According to Table 36, less than half of the web is in compression. It is in class 4, according to Equation (7.14):

$$\frac{h_c}{h_w} = \frac{933}{1\,886} = 0.49; \quad \frac{h_w}{t_w} = \frac{1\,886}{20} = 94.3 \geq 78 * \varepsilon * (1 + 1.262) * \sqrt{1.262} = 93.0$$

Hence the cross-section of the main girder at support P1, at the final stage, is in class 4 and must be checked by an elastic section analysis, using the effective reduced area of the web at all stages. From Table 36 and with Equation (7.22):

Table 37: $h_{c,eff}$ of the web at support P1, at the final stage (design C)

Model	h_c	Equation (7.22)	$h_{c,eff}$
0	834 mm	943 mm	834 mm
1, 2, 3	1 089 mm	928 mm	928 mm
Total	933 mm	943 mm	933 mm

The new stress distribution at the final stage is shown in Figure 33.

7.3.6. Design C, mid-span P1-P2

The elastic stress distribution at mid-span P1-P2 at all stages is given in Table 38. The calculation of the stress ratio ψ is calculated with Equation (7.20).

Table 38: Elastic stress distribution at mid-span P1-P2 (design C)

Model	$\sigma_{y,sup}$	$\sigma_{y,inf}$	$\sigma_{w,sup}$	$\sigma_{w,inf}$	ψ	h_c
0	-333 MPa	+222 MPa	-242 MPa	+131 MPa	-0.542	1 223 mm
1	-17 MPa	+53 MPa	-6 MPa	+42 MPa	-7.145	232 mm
2	-2.0 MPa	+9.4 MPa	-0.2 MPa	+7.5 MPa	-48.371	38 mm
3	-23 MPa	+285 MPa	+27 MPa	+234 MPa	+8.579	-249 mm
Total	-375 MPa	+569 MPa	-221 MPa	+415 MPa	-1.879	655 mm

At the construction stage, the lower flange is in tension and therefore in class 1. The upper flange is in compression; it is in class 3 from [5] Table 5.2:

$$\frac{D_{f,sup}}{t_{f,sup}} = \frac{457}{17.5} = 26.1 \leq 90 \cdot \varepsilon^2 = 30.65$$

According to Table 38, over half of the web is in compression. It is in class 4, according to Equation (7.5) and (7.10):

$$\frac{h_c}{h_w} = \frac{1\,223}{1\,886} = 0.54; \quad \frac{h_w}{t_w} = \frac{1\,886}{14} = 134.7 \geq 0.84 \cdot \frac{1}{1.052} \cdot \sqrt{\frac{22.74 \cdot E_a}{235}} \cdot \varepsilon = 113.7$$

Hence the cross-section of the main girder at mid-span P1-P2, at the construction stage, is in class 4. It must be checked by an elastic section analysis, using the effective reduced area of the web. From Table 38 and with Equation (7.22):

Table 39: $h_{c,eff}$ of the web at mid-span P1-P2, at the construction stage (design C)

Model	h_c	Equation (7.22)	$h_{c,eff}$
0	1 223 mm	649 mm	649 mm

The new stress distribution at the construction stage is shown in Figure 33.

At the final stage, the lower flange and the upper flange are still in class 1 and 3. According to Table 38, over half of the web is in compression. It is in class 3, according to Equation (7.14):

$$\frac{h_c}{h_w} = \frac{980}{2\,720} = 0.36; \quad \frac{h_w}{t_w} = \frac{2\,720}{14} = 194.3 \geq 0.84 \cdot \frac{1}{1.052} \cdot \sqrt{\frac{k_\sigma \cdot E_a}{235}} \cdot \varepsilon = 133.8$$

Hence the cross-section of the main girder at mid-span P1-P2, at the final stage, is in class 3.

7.4. Elastic geometric properties of the effective cross-sections

Table 40, Table 41 and Table 42 give the effective properties of the cross-sections. The stress distribution in the main girder is given in Figure 31 and Figure 32 when the girder is in class 3 or higher, with the effective cross-section equal to the gross-cross-section. The stress distribution is given in Figure 33, when the girder is in class 4.

Table 40: Elastic second moment of area of the effective cross-sections

I [10^9 mm^4]		Support P1			Mid-span P1-P2		
Stage	Model	A	B	C	A	B	C
Construction	0	508	203	139	191	125	97
Final	0	508	203	139	197	125	100
	1	571	274	197	376	323	290
	2				418	360	327
	3				487	416	383

Table 41: Elastic neutral axis of the effective cross-sections

z [mm]		Support P1			Mid-span P1-P2		
Stage	Model	A	B	C	A	B	C
Construction	0	1 303	1 117	1 291	1 267	1 017	1 065
Final	0	1 303	1 117	1 291	1 319	1 017	1 120
	1	1 412	1 384	1 558	2 065	2 114	2 111
	2				2 241	2 307	2 305
	3				2 525	2 591	2 592

Table 42: Elastic section modulus of the effective cross-sections

W [10^6 mm^3]			Support P1			Mid-span P1-P2		
	Stage	Model	W_{inf}	W_{sup}	W_{arm}	W_{inf}	W_{sup}	W_{bet}
Design A	Construction	0	390	-339	-	151	-125	-
	Final	0	390	-339	-	149	-133	-
		1	405	-412	-346	182	-511	-326
		2				187	-747	-429
		3				193	-1 770	-705
Design B	Construction	0	182	-121	-	123	-70	-
	Final	0	182	-121	-	123	-70	-
		1	198	-193	-163	153	-470	-293
		2				156	-729	-396
		3				160	-1 987	-665
Design C	Construction	0	108	-92	-	91	-56	-
	Final	0	108	-92	-	90	-58	-
		1	126	-158	-131	137	-421	-263
		2				142	-661	-359
		3				148	-1 842	-614

8. Safety verification at ULS

8.1. Bending resistance

8.1.1. Verification principles

The verification of the bending resistance depends on the cross-section class:

- Class 1 or 2 cross-sections are checked by using the plastic bending resistance;
- Class 3 cross-sections are checked by using the elastic bending resistance;
- Class 4 cross-sections are checked by using the elastic bending resistance, considering the effective cross-section due to buckling.

For the plastic verification, the bending moment M_{Ed} at ULS is checked against the plastic moment resistance $M_{pl,Rd}$ according to [8] § 6.2.1.2. $M_{pl,Rd}$ depends on the position of the PNA; both are calculated by using the design yield strengths of the materials:

- Structural steel: $f_{yd} = f_{yk}/\gamma_{M0}$;
- Reinforcing steel: $f_{sd} = f_{sk}/\gamma_{M0}$ only in tension; it is neglected in compression;
- Concrete: $0.85 \cdot f_{cd} = 0.85 \cdot f_{ck}/\gamma_C$ only in compression; it is neglected in tension.

For the elastic verification, the design stresses in the elements due to the bending moment at ULS are checked against the limiting stresses of the materials, according to [8] § 6.2.1.3:

- Structural steel: f_{yd};
- Reinforcing steel in tension: f_{sd};
- Concrete in compression: f_{cd}.

The elastic verifications are performed with the stresses in the extreme fibres of the structural steel flanges and the concrete slab from [5] § 6.2.1, and at the average position of the reinforcing steel.

8.1.2. Verification calculations

The mid-span cross-section of the design A is in class 1. Therefore the bending moment at ULS can be checked with a plastic verification. The design plastic bending resistance $M_{pl,Rd}$ is calculated from the PNA = 2 784 mm: $M_{pl,Rd}$ = 79.47 MNm ≥ M_{Ed} = 62.14 MNm.

Hence the mid-span cross-section of the design A is verified against the bending moment at ULS. All other cross-sections should be checked with an elastic verification. The design stresses are shown in Annex X and Annex XI. The results are resumed in Table 43.

Table 43: Elastic stress distribution

[MPa]		Support P1			Mid-span P1-P2		
Design		A	B	C	A	B	C
Class at final stage		3	4	4	1	4	3
Concrete slab	$\sigma_{c,max}$	-	-	-	-10	-12	-13
	f_{ck}/γ_c	-	-	-	-23	-23	-23
Reinforcing steel	$\sigma_{s,moy}$	+152	+254	+283	-	-	-
	f_{sk}/γ_s	+435	+435	+435	-	-	-
Upper flange	$\sigma_{y,sup}$	+269	+558	+676	-163	-316	-375
	$f_{yk,sup}/\gamma_{M0}$	+295	+690	+690	-345	-690	-690
Lower flange	$\sigma_{y,inf}$	-253	-438	-671	+350	+467	+569
	$f_{yk,inf}/\gamma_{M0}$	-295	-650	-690	+345	+690	+690

The cross-section at support P1 in design A is not justified against the bending moment at ULS with an elastic verification, but it is with a plastic verification. All other cross-sections are justified with an elastic verification.

Compared to the design A, the design B provides more reserve in the resistance of the lower flange, with an utilisation ratio in both flanges of 67% and 68%, against 86% and 100% in the design A.

Compared to the design A, the design C also provides more reserve in the resistance of the flange. The working coefficient of 97% and 82% is more than in the design B, but the lower tubular flange is in class 1; therefore, the partial plastification of the tube could be considered in the resistance.

It should be noticed that with respect to solution A, the design stresses increase in the concrete slab of 20% and 30% respectively in the designs B and C. The increase of the design stresses in the reinforcing steel is respectively 67% and 86%; therefore the cracking control should be checked.

8.2. Shear resistance

8.2.1. Eurocode calculations

In the designs A and B, the criterion $V_{Ed} \leq V_{Rd}$ is checked according to [8] § 6.2.2, with V_{Rd} the design shear resistance of the composite cross-section. It is the minimum between the plastic design shear resistance of the web $V_{pl,a,Rd}$ and the design shear buckling resistance $V_{b,Rd}$, considering that the web is too slender and could buckle:

$$V_{Ed} \leq V_{Rd} = \min\left(V_{pl,a,Rd}; V_{b,Rd}\right) \tag{8.1}$$

$$V_{pl,a,Rd} = \frac{\eta \cdot f_y}{\gamma_{M0} \cdot \sqrt{3}} \cdot h_w \cdot t_w \tag{8.2}$$

$$V_{b,Rd} = V_{bw,Rd} + V_{bf,Rd} \leq \frac{\eta \cdot f_{y,w}}{\gamma_{M1} \cdot \sqrt{3}} \cdot h_w \cdot t_w \tag{8.3}$$

Where $V_{bw,Rd}$ and $V_{bf,Rd}$ are respectively the contributions from the web and the flanges to $V_{b,Rd}$; η is a coefficient to account for the steel grade of the main girder. $\eta = 1.2$ for steel grades up to and including S460; $\eta = 1.0$ for higher steel grades, according to [16] § 5.1.

$V_{bw,Rd}$ depends on the spacing a of the vertical stiffeners at the transverse bracing frames, according to [16] § 5.3. The vertical stiffeners are assumed to be rigid (see section 8.2.3):

$$\alpha = a/h_w \tag{8.4}$$

$$k_\tau = 5.34 + 4/\alpha^2 \tag{8.5}$$

$$\sigma_E = \frac{\pi^2 \cdot E_a \cdot {t_w}^2}{12 \cdot (1 - \nu^2) \cdot {h_w}^2} \tag{8.6}$$

$$\tau_{cr} = k_\tau \cdot \sigma_E \tag{8.7}$$

$$\bar{\lambda}_w = \sqrt{\frac{f_{yk,w}}{\tau_{cr} \cdot \sqrt{3}}} \tag{8.8}$$

$$\chi_w = \frac{1.37}{0.7 + \bar{\lambda}_w} \tag{8.9}$$

$$V_{bw,Rd} = \frac{\chi_w \cdot f_{yk,w}}{\gamma_{M1} \cdot \sqrt{3}} \cdot h_w \cdot t_w \tag{8.10}$$

Where *a* is the spacing between transverse cross-bracings at the studied cross-section; α is the aspect ratio of the web panel; k_τ is the plate buckling coefficient for shear stresses; σ_E is the elastic critical Euler's stress; τ_{cr} is the elastic critical shear buckling stress; $\bar{\lambda}_w$ is the reduced slenderness; χ_w is the reduction factor for instability, for $\bar{\lambda}_w \geq 1.08$ and rigid stiffeners.

The contribution from the flanges $V_{bf,Rd}$ is negligible compared to $V_{bw,Rd}$ and should be neglected.

All calculations are resumed in Table 44. The dimensions h_w, t_w and *a* come from Annex I, Annex II and Annex III.

Table 44: Shear justification

	Support P1			Mid-span P1-P2			
Design	A	B	C	A	B	C	
h_w	2 560	2 675	1 886	2 720	2 720	1 886	mm
t_w	26	20	20	18	14	14	mm
a	8.0	4.0	8.0	8.0	8.0	8.0	m
α	3.125	1.495	4.242	2.941	2.941	4.242	[-]
k_τ	5.75	7.13	5.56	5.80	5.80	5.56	[-]
σ_E	19.6	10.6	21.3	8.31	5.03	10.5	MPa
τ_{cr}	112.6	75.6	118.7	48.2	29.2	58.2	MPa
$\bar{\lambda}_w$	1.33	2.29	1.83	2.03	3.70	2.62	[-]
χ_w	0.675	0.457	0.541	0.501	0.312	0.413	[-]
$V_{bw,Rd}$	8.13	8.86	7.39	4.45	4.30	3.95	MN
$V_{bf,Rd}$	0.00	0.00	0.00	0.00	0.00	0.00	MN
$V_{b,Rd}$	8.13	8.86	7.39	4.45	4.30	3.95	MN
$V_{pl,a,Rd}$	15.91	21.31	15.03	11.70	15.17	10.52	MN
V_{Rd}	8.13	8.17	7.39	4.45	4.30	3.95	MN
V_{Ed}	7.17	6.80	6.74	1.06	1.06	1.06	MN

All cross-sections of all designs are justified. The design C provides the least reserve in resistance; however, some assumptions used in the calculations do not apply to the design C.

The calculations of the shear resistance in the Eurocodes come from the rotated stress field theory, which gives good results for web panels with high aspect ratios α, according to [18] § 2.5.2. It considers that the tension field can be anchored in the plate flanges.

In the design C though, the behaviour of the tubular flanges under shear force is not well-known, and the tubes could fail under punching shear. Another model, Basler's theory, makes it possible to calculate the shear resistance of the cross-section, while considering that the tension field in the web can only be anchored in the next web panel through the transverse stiffeners. Those are assumed to be rigid according to [2] § 12.3.3.

8.2.2. Basler's model

Because of the slenderness of the web, the behaviour of a web panel is decomposed into two phases:

- The pre-critical contribution to the shear resistance V_{cr}.
- The post-critical contribution to the shear resistance V_{σ}.

$$V_{cr} = h_w \cdot t_w \cdot \tau_{cr} \tag{8.11}$$

$$V_{\sigma} = h_w \cdot t_w \cdot \left(\frac{f_{y,w} - \sqrt{3} \cdot \tau_{cr}}{2 \cdot \sqrt{1 + \alpha^2}} \right) \tag{8.12}$$

Where V_{cr} is the pre-critical shear resistance; V_{σ} is the post-critical shear resistance. The aspect ratio has a limiting value: $\alpha \leq 3$ from [2] § 12.3.3.

The theory is detailed in [18] § 2.5.1. Before the web buckling, the shear stresses are determined with the theory of the linear elastic buckling. They correspond to a tensile stress σ_1 and a compressive stress σ_2 in the web, with an inclination of 45° with respect to the x-axis of the steel girder. After the web buckling, the tension field brings a post-critical contribution to the shear resistance of the web panel, with an increase of the tensile stresses σ_1.

Besides the shear model, the plate buckling coefficient k_{τ} has to be adapted. In the designs A and B, the web is assumed to be hinged to the plate flanges; in the design C, it is considered to be fixed to the tubular flanges, as specified in section 7.1.1. According to [15] Table 12.7:

$$k_{\tau} = 9.0 + 3.3/\alpha^2 \tag{8.13}$$

An analysis with EBPlate is performed to check the validity of Equation (8.13). The input data is:

- Plate of thickness t = 20 mm, length 1000 mm ≤ a ≤ 5 000 mm, height = 1 000 mm, hinged on four sides for designs A and B, fixed on two sides for design C.
- Shear stress: τ = 10 MPa.
- Analysis of the first 20 modes of buckling.

All results are detailed in Table 45. For comparison purposes, the values given by Equation (8.5) are also detailed. The difference between the formulas and EBPlate is generally less than 1% for a hinged connection, and around 6% for a fixed connection. Hence the formulas are considered to be valid.

Table 45: Calculation of the plate buckling coefficient k_{τ}

	Hinged connection		Fixed connection	
α	EC3 / TGC 10	EBPlate [17]	TGC 10	EBPlate [17]
1	9.34	9.325	12.30	12.837
2	6.34	6.546	9.83	10.378
3	5.78	5.840	9.37	9.925
4	5.59	5.625	9.21	9.755
5	5.50	5.530	9.13	9.733

The design shear buckling resistance of the web $V_{b,Rd}$ calculated with Basler's theory becomes:

$$V_{b,Rd} = V_{cr} + V_{\sigma} \tag{8.14}$$

The calculations are resumed in Table 46. The comparison is made between the methods from the Eurocode and from Basler's theory, for hinged and fixed connections.

Table 46: Shear justification of the design C

	Support P1				Mid-span P1-P2				
	Hinged		Fixed		Hinged		Fixed		
	EC3	Basler	EC3	Basler	EC3	Basler	EC3	Basler	
k_{τ}	5.56		9.18		5.56		9.18		[-]
σ_E	21.3		21.3		10.5		10.5		MPa
τ_{cr}	118.7		196.0		58.2		96.0		MPa
V_{cr}	-	4.48	-	7.39	-	1.54	-	2.54	MN
V_{σ}	-	2.89	-	2.09	-	2.46	-	2.19	MN
V_{Rd}	7.39	7.37	8.80	9.48	3.95	4.00	4.79	4.72	MN
V_{Ed}	6.74				1.06				MN

It can be seen that the shear resistance increases consequently, due to the change of boundary condition between the web and the flanges, and its influence on the plate buckling coefficient k_{τ}. In Basler's model, it can be noticed that the increase in resistance concerns the pre-critical contribution, whereas the post-critical contribution slightly reduces.

The Eurocode and Basler's theory give very close results for a hinged connection between the web and the flanges. The difference is more significant between the two models for a fixed connection. It could be explained by the fact that the formulas from the rotated stress field theory were calibrated only for a hinged connection. Therefore the results from Basler's theory are kept.

8.2.3. Verification of the rigidity of the stiffeners

The section of a stiffener is shown in Figure 9, with a part of the web acting, as in [16] § 9.1.

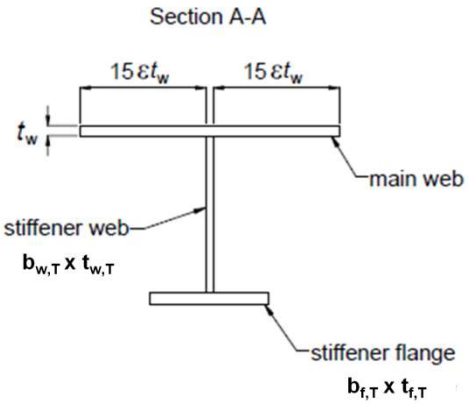

Figure 9: Section of a vertical stiffener, adapted from [1] Figure 8.12

The shear resistance verification is based on the assumption that the vertical stiffeners are rigid. This assumption must be justified according to [16] § 9.3.3:

$$\frac{a}{h_w} \geq \sqrt{2}: \quad I_m \geq 0.75 \cdot h_w \cdot {t_w}^3 \tag{8.15}$$

$$\frac{a}{h_w} < \sqrt{2}: \quad I_m \geq 1.5 \cdot \frac{{h_w}^3 \cdot {t_w}^3}{a^2} \tag{8.16}$$

Where *a* is the spacing between the vertical stiffeners; I_m is the second moment of inertia of a stiffener. The criterion is checked at the critical cross-sections for shear verification, at support P1 and at mid-span P1-P2; the results are detailed in Table 47.

Table 47: Minimum rigidity under shear force

	Support P1			Mid-span P1-P2			
Design	A	B	C	A	B	C	
h_w	2 560	2 675	1 886	2 720	2 720	1 886	mm
t_w	26	20	20	18	14	14	mm
a	8.0	4.0	8.0	8.0	8.0	8.0	m
a/h_w	3.13 ≥ $\sqrt{2}$	1.50 ≥ $\sqrt{2}$	4.24 ≥ $\sqrt{2}$	2.94 ≥ $\sqrt{2}$	2.94 ≥ $\sqrt{2}$	4.24 ≥ $\sqrt{2}$	[-]
I_m	$1.22 \cdot 10^9$	$2.20 \cdot 10^8$	$1.31 \cdot 10^8$	$8.88 \cdot 10^8$	$1.51 \cdot 10^8$	$8.79 \cdot 10^7$	mm^4
Criterion	$3.37 \cdot 10^7$	$1.61 \cdot 10^7$	$1.13 \cdot 10^7$	$1.19 \cdot 10^7$	$5.60 \cdot 10^6$	$3.88 \cdot 10^6$	mm^4

Hence the criterion is verified for all designs.

8.3. Bending and shear interaction

In case $V_{Ed} \geq 0.5 \cdot V_{Rd}$, the bending and shear interaction in the web should be considered. It happens at support P1 for all designs. The internal forces and moments considered for the verification should be taken at a distance $h_w/2$ from the support. The interaction criterion is:

$$\overline{\eta}_1 = \frac{M_{Ed,\frac{h_w}{2}}}{M_{pl,Rd}} \geq \frac{M_{f,Rd}}{M_{pl,Rd}} \tag{8.17}$$

$$\overline{\eta}_3 = \frac{V_{Ed,\frac{h_w}{2}}}{V_{Rd}} \tag{8.18}$$

$$\overline{\eta}_1 + \left(1 - \frac{M_{f,Rd}}{M_{pl,Rd}}\right) \cdot \left(2 \cdot \overline{\eta}_3 - 1\right)^2 \geq 1 \tag{8.19}$$

Where $\overline{\eta}_1$ and $\overline{\eta}_3$ are the ratios of respectively the design bending moment on the plastic bending resistance and the design shear force on the shear resistance; $M_{f,Rd}$ is the design plastic bending resistance while neglecting the contribution of the web. The design plastic resistance of the elements is detailed in Table 48, for the calculation of $M_{pl,Rd}$ and $M_{f,Rd}$. The position of the PNA of the cross-sections for $M_{pl,Rd}$ and $M_{f,Rd}$ is shown in Figure 34.

Table 48: Design plastic resistance at support P1

		Support P1			
Element	Force	A	B	C	
Reinforcement	$F_s = A_s \cdot f_{sk}/\gamma_s$	9.53	9.53	9.53	MN
Upper flange	$F_{y,sup} = A_{f,sup} \cdot f_{yk,sup}/\gamma_{M0}$	35.40	22.43	27.77	MN
Web	$F_{y,w} = A_w \cdot f_{yk,w}/\gamma_{M0}$	22.96	36.92	26.03	MN
Lower flange	$F_{y,inf} = A_{f,inf} \cdot f_{yk,inf}/\gamma_{M0}$	42.48	43.88	36.16	MN

The results for the justification of the cross-sections against the bending and shear interaction in the web are detailed in Table 49.

Table 49: Bending and shear interaction justification

	Support P1			
	A	B	C	
$M_{Ed,h_w/2}$	91.00	74.02	68.91	MNm
$V_{Ed,h_w/2}$	6.55	6.21	6.15	MN
$M_{pl,Rd}$	117.06	89.77	89.63	MNm
$M_{f,Rd}$	134.73	128.72	102.98	MNm
$\overline{\eta}_1$	0.869	0.697	0.870	[-]
$\overline{\eta}_3$	0.806	0.759	0.649	[-]
Criterion	0.918	0.779	0.882	[-]

Hence the criterion is verified for all designs.

9. Safety verification of the stability

9.1. Flange induced buckling

When a girder is subjected to a bending moment M, this results in a curvature ϕ and axial forces N_f in the flanges, as shown in Figure 10. Because of the curvature ϕ, the forces N_f induce deflection forces in the girder, which result in a uniform compression stress σ_z in the web of the girder:

$$\sigma_z = \frac{N_f}{t_w} \cdot \phi = \frac{\sigma_f \cdot A_f}{r \cdot t_w} \tag{9.1}$$

Where *r* is the radius of curvature of the girder; σ_f is the stress in the most used flange. In a composite cross-section, the compression stress σ_z is governed by the axial force N_f in the lower flange (in tension at mid-span, in compression at support).

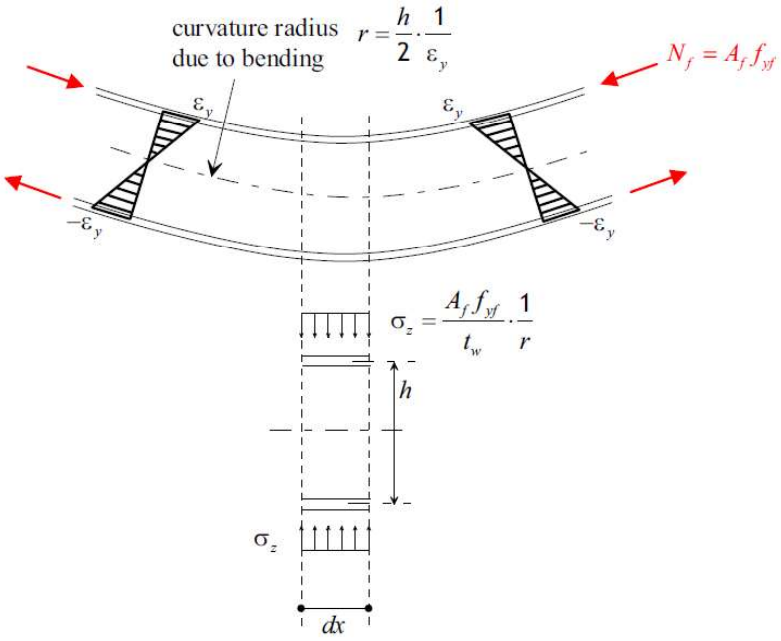

Figure 10: Flange induced buckling, [18] Figure 2.61

According to [2] § 12.2.2 and [18] § 2.8, it is assumed that the residual compression stresses σ_{0f} in the flange are equal to half of the characteristic resistance. At mid-span, it should have a favourable effect, which is neglected by considering that σ_{0f} is in tension as σ_f. Hence the residual deformation ε_{0f} is:

$$\varepsilon_{0f} = \frac{\sigma_{0f}}{E_a} = \frac{f_{yk,inf}}{2 * E_a} \tag{9.2}$$

The stress σ_f in the lower flange correspond to a certain proportion m of the characteristic resistance $f_{yk,inf}$ of the flange. Hence the total deformation ε_f that the flange must be able to bear is:

$$\sigma_f = \sigma_{y,inf} = m \cdot f_{yk,inf} \tag{9.3}$$

$$\varepsilon_f = \frac{\sigma_f}{E_a} + \varepsilon_{0f} = (m + \frac{1}{2}) \cdot \frac{f_{yk,inf}}{E_a} \tag{9.4}$$

The position of the neutral axis of the section can be determined by the ratio h_i/h_w. The height h_i correspond to the compression height h_c of the web at support, and to the tension height h_t of the web at mid-span. Then the total deformation ε_f, the curvature ϕ of the girder and the compression stress σ_z in the web become:

$$\varepsilon_f = \phi \cdot h_w \cdot \frac{h_i}{h_w} = \frac{h_w}{r} \cdot \frac{h_i}{h_w} \tag{9.5}$$

$$\phi = \frac{1}{r} = \varepsilon_f \cdot \frac{h_w}{h_i} \cdot \frac{1}{h_w} = \left(m + \frac{1}{2}\right) \cdot \frac{f_{yk,inf}}{E_a} \cdot \frac{h_w}{h_i} \cdot \frac{1}{h_w} \tag{9.6}$$

$$\sigma_z = \frac{m \cdot f_{yk,inf} \cdot A_{f,inf}}{t_w \cdot h_w} \cdot \frac{f_{yk,inf}}{E_a} \cdot \left(m + \frac{1}{2}\right) \cdot \frac{h_w}{h_i} \tag{9.7}$$

To avoid the flange induced buckling of the web, the compression stress σ_z should be less than the critical Euler's stress σ_E:

$$\sigma_z \leq \sigma_E = \frac{\pi^2 \cdot E_a}{12 \cdot (1 - \nu^2)} \cdot \left(\frac{t_w}{h_w}\right)^2 = \frac{\pi^2}{36 \cdot (1 - \nu^2)} \cdot 3 \cdot E_a \cdot \left(\frac{t_w}{h_w}\right)^2 = k \cdot 3 \cdot E_a \cdot \left(\frac{t_w}{h_w}\right)^2 \tag{9.8}$$

Where k = 0.55 is the factor to account for the utilisation of the elastic moment resistance. Hence the ruin of the web of the girder by flange induced buckling is avoided by respecting the following criterion:

$$\frac{h_w}{t_w} \leq k \cdot \frac{E}{f_{yk,inf}} \cdot \sqrt{\frac{A_w}{A_{f,inf}}} \cdot \sqrt{\frac{h_i}{h_w} \cdot \frac{3}{m \cdot \left(m + \frac{1}{2}\right)}} \tag{9.9}$$

Table 50: t_w minimum against flange induced buckling

	Support P1			Mid-span P1-P2			
Design	A	B	C	A	B	C	
$\sigma_{y,inf}$	-253	-438	-671	(+350)	+467	+569	MPa
$f_{yk,inf}$	-295	-650	-690	+345	+690	+690	MPa
m	0.86	0.67	0.97	1.00	0.68	0.82	[-]
h_i	1 237	1 156	938	850	1 095	655	mm
$t_{w,min}$	10.4	14.0	13.0	7.2	11.2	11.3	mm
t_w	26	20	20	18	14	14	mm

The results for all designs are resumed in Table 50. All cross-sections in all designs are verified against the flange induced buckling. As the design stress $\sigma_{y,inf}$ is considered at the extreme fibre of the lower flange instead of the mid-plane, the results are conservative.

It is interesting to notice that when the lower flange is considered to be fully plastified (m = 1) and the steel girder is symmetrical with respect to its z-axis ($h_w/h_i = 2$), then the criterion from [16] § 8 is met:

$$\frac{h_w}{t_w} \leq k \cdot \frac{E}{f_{yk,inf}} \cdot \sqrt{\frac{A_w}{A_{f,inf}}} \tag{9.10}$$

9.2. Lateral-torsional buckling of the flanges

The compression flange must be justified against lateral-torsional buckling (LTB). A distinction is made between the construction stage and the final stage of the bridge life.

At the construction stage, only the permanent structural actions apply: the weights of the structural steel girder and the concrete slab. LTB can occur in the upper flange at mid-span P1-P2 because it is in compression and not yet connected to the slab.

At the final stage, all permanent and variable actions apply. The upper flange is connected to the slab and therefore is prevented from buckling. Hence LTB can occur in the lower flange at support P1.

The justification is performed with the simplified method using the Engesser's formula. Uniform resisting section and load over the whole length of the deck are assumed.

The resisting section is the effective area of the flange in compression and the effective part of the web near the flange, according to [19] § 6.3.4.2. The height h of the acting web and the area of the resisting section are:

$$h = \min\left(\frac{h_{c,eff}}{2}; \frac{h_c}{3}\right) \tag{9.11}$$

$$A_D = A_{f,eff} + h \cdot t_w \tag{9.12}$$

Where $h_{c,eff}$ is the effective compression height of the web; h_c is the compression height of the web; $A_{f,eff}$ is the effective area of the compression flange.

The resisting section at mid-span P1-P2, at the construction stage, is shown in Figure 11. The resisting section at support P1, at the final stage, is shown in Figure 12.

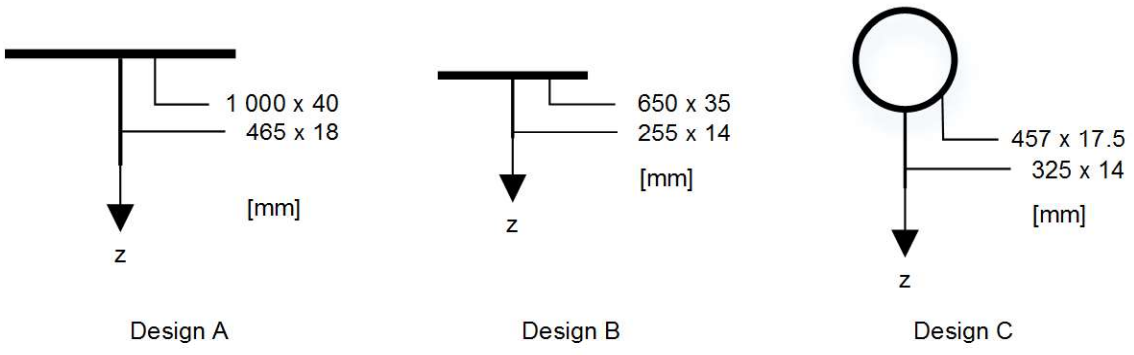

Figure 11: Geometry of the compression upper flanges

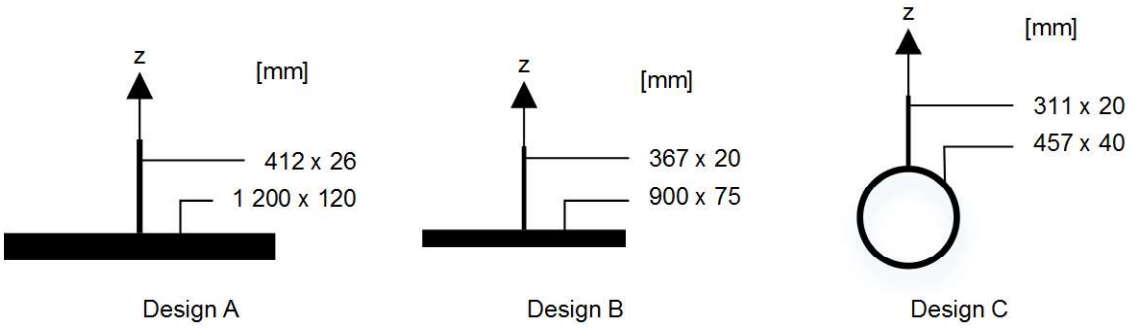

Figure 12: Geometry of the compression lower flanges

Considering the second moment of inertia I_z of the resisting section, the radius of gyration i_D is:

$$i_D = \sqrt{\frac{I_z}{A_D}} \tag{9.13}$$

Table 51: Geometric properties of the resisting section to LTB

	Support P1			Mid-span P1-P2			
Design	A	B	C	A	B	C	
h_c	1 237	1 125	933	1 441	1 603	1 223	mm
$h_{c,eff}$	1 237	734	943	929	510	649	mm
h	412	367	311	465	255	325	mm
A_D	154 719	74 838	58 623	48 364	26 317	28 709	mm^2
I_z	$1.73 \cdot 10^{10}$	$4.56 \cdot 10^9$	$1.15 \cdot 10^9$	$3.33 \cdot 10^9$	$8.01 \cdot 10^8$	$5.84 \cdot 10^8$	mm^4
i_D	334	247	140	263	174	143	mm

The resisting section is assumed to be laterally simply supported at piles and abutments. At the construction stage, the girders are also assumed to be laterally simply supported by erection bracings.

The bracing frames constituted of the cross-girders and the transverse vertical stiffeners rigidify the main steel girders by providing a lateral elastic support. Hence the lateral stability of the resisting section depends on the frame rigidity C_D.

9.2.1. Rigidity of the cross-bracing frame at the construction stage

The upper flange at mid-span P1-P2 is critical at the construction stage. The erection bracings are assumed to be rigid enough to provide a lateral support. Therefore the bracing frame consists of the cross-girder and the upper part of the steel girder, as shown in Figure 13:

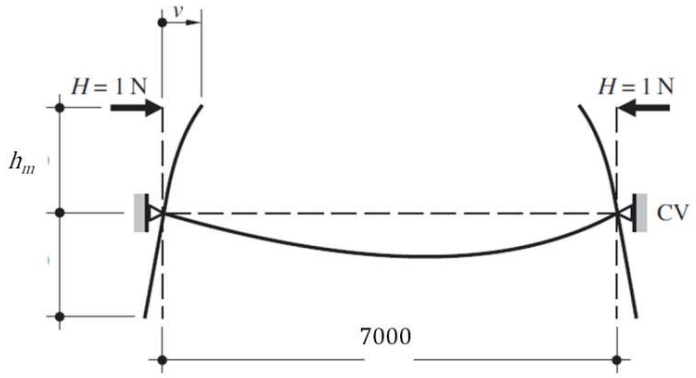

Figure 13: Bracing frame at the construction stage, adapted from [2] Figure 19.18

The lateral displacement ν of the upper flange under a unit force, and the rigidity C_D of the frame are:

$$\nu = \frac{h_m{}^3}{3 \cdot E_a \cdot I_m} + \frac{h_m{}^2 \cdot s_a}{2 \cdot E_a \cdot I_t} \tag{9.14}$$

$$C_D = \frac{1}{\nu} \tag{9.15}$$

Where h_m is the vertical distance between the neutral axis of the cross-girder and the neutral axis of the upper flange; I_m is the second moment of inertia of the stiffener from Table 47; I_t is the second moment of inertia of the cross-girder; s_a is the centre-to-centre spacing between the main girders. The results are detailed in Table 52.

Table 52: Stiffness of the upper flange at the construction stage

	Mid-span P1-P2			
Design	A	B	C	
h_m	1 380	1 383	1 172	mm
I_m	$8.88 \cdot 10^8$	$1.51 \cdot 10^8$	$8.79 \cdot 10^7$	mm^4
I_t	$9.21 \cdot 10^8$	$9.21 \cdot 10^8$	$9.21 \cdot 10^8$	mm^4
δ	$3.70 \cdot 10^{-5}$	$6.09 \cdot 10^{-5}$	$5.30 \cdot 10^{-5}$	mm/N
C_D	27.0	16.4	18.9	MN/m

The rigidity C_D of the transverse bracing frame much greater for the design A than for designs B and C. This is due to the reduction of width $b_{w,T}$ of the vertical stiffeners web:

- Design A: $b_{w,T}$ = 400 mm.
- Design B: $b_{w,T}$ = 200 mm.
- Design C: $b_{w,T}$ = 150 mm.

9.2.2. Rigidity of the cross-bracing frame at the final stage

The lower flange at support P1 is critical at the final stage. The rigidity C_D of the bracing frame is calculated according to [20], with the notations from [2]. The flexibility of the slab is neglected. Therefore the bracing frame consists of the cross-girder and the steel girders, as shown in Figure 14.

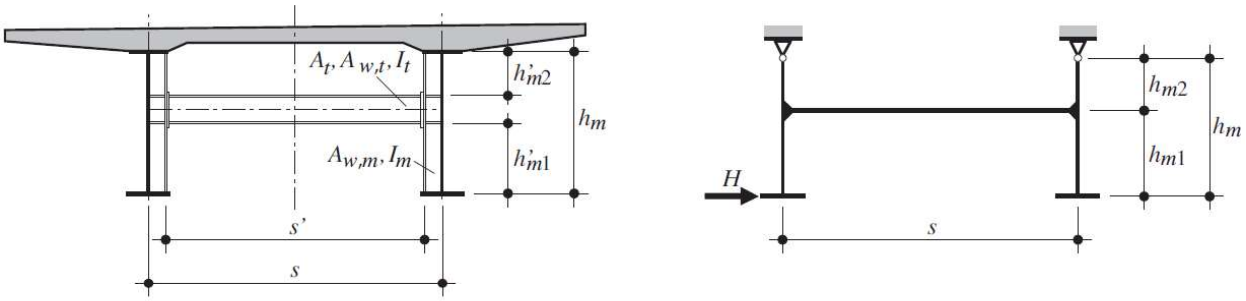

Figure 14: Bracing frame at the final stage, [2] Figure 14.7

The calculation of the rigidity from Equation (9.17) to (9.22) is valid in the cases of flat flanges. It is also applied in the case of tubular flanges, since no other way to calculate the rigidity exists. The notations are then adapted as shown in Figure 15.

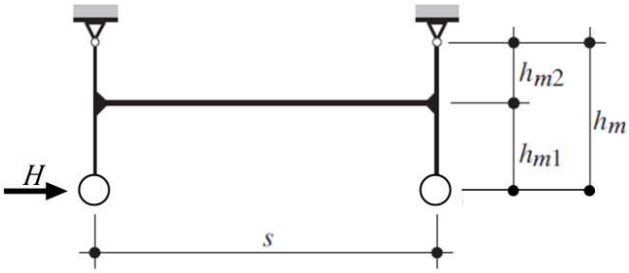

Figure 15: Static system of the bracing frame in the design C

As shown in Figure 16, two load cases should be considered: the symmetric mode with same direction forces, and the anti-symmetric mode with opposite direction forces.

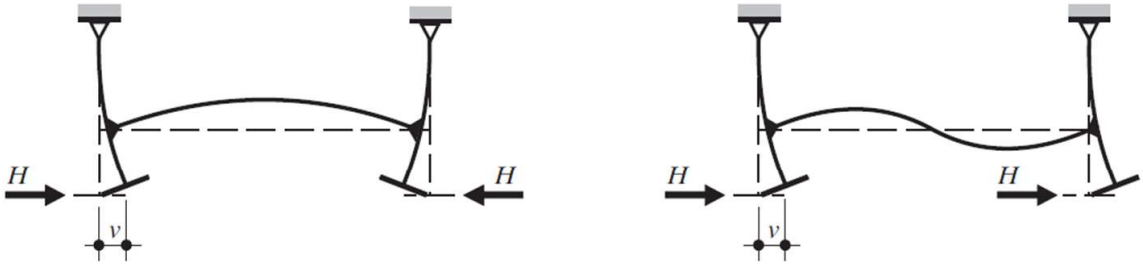

Figure 16: Load cases for the calculation of the rigidity C_D, [2] Table 14.8

The geometric properties of the bracing frame are $A_{w,m}$, $A_{w,t}$ and A_t:

$$A_{w,m} = t_{w,T} \cdot \left(\frac{t_w}{2} + b_{w,T} + \frac{t_{f,T}}{2}\right) \tag{9.16}$$

Where $t_{w,T}$ and $b_{w,T}$ are respectively the thickness and the width of web of the stiffener; $t_{f,T}$ is the thickness of the flange of the stiffener; $A_{w,m}$ and $A_{w,t}$ are respectively the shear section of the stiffener and the cross-girder; A_t is the total section of the cross-girder. $A_{w,t}$ and A_t are given by the IPE producers.

The flexibilities of the vertical stiffeners and of the cross-girders are:

$$K_{m1} = \frac{h'^3_{m1}}{3 \cdot E_a \cdot I_m};\ K_{V,m1} = \frac{h_{m1}}{G_a \cdot A_{w,m}} \tag{9.17}$$

$$K_{m2} = \frac{h'^3_{m2}}{3 \cdot E_a \cdot I_m};\ K_{V,m2} = \frac{h_{m2}}{G_a \cdot A_{w,m}} \tag{9.18}$$

$$K_{t1} = \frac{s' \cdot h^2_{m1}}{2 \cdot E_a \cdot I_t};\ K_t = \frac{s' \cdot h^2_m}{2 \cdot E_a \cdot I_t};\ K_{t2} = \frac{s' \cdot h^2_{m2}}{2 \cdot E_a \cdot I_t};\ K_{tN} = \frac{s'}{2 \cdot E_a \cdot A_t};\ K_{V,t} = \frac{2 \cdot s'}{G_a \cdot A_{w,t}} \tag{9.19}$$

Where I_t and I_m are respectively the second moment of area of the cross-girder and the stiffener.

K_{m1} and $K_{V,m1}$ are the flexibility coefficients to bending and shear of the lower part of a stiffener; K_{m2} and $K_{V,m2}$ are the flexibility coefficients to bending and shear of the upper part of a stiffener. They are influenced by the height of the stiffeners h_m, h_{mi} and h'_{mi}, and by the dimensions of the stiffeners.

K_{ti} and K_t are the flexibility coefficients to bending of the cross-girder; K_{tN} is the extensibility coefficient of the cross-girder; $K_{V,t}$ is the flexibility coefficient to shear of the cross-girder.

Hence, the lateral displacements for the anti-symmetric and symmetric modes δ_1 and δ_2, and the rigidity C_D of the bracing frame are:

$$\nu = \delta_1 = K_{m1} + K_{V,m1} + K_{m2} + K_{V,m2} + \frac{K_t}{3} + K_{V,t} \cdot \left(\frac{h_m}{s_a}\right)^2 \tag{9.20}$$

$$\nu = \delta_2 = K_{m1} + K_{V,m1} + K_{t1} + K_{tN} - \frac{\left(K_{tN} - K_{t2} \cdot \frac{h_{m1}}{h_{m2}}\right)^2}{K_{t2} + K_{tN} + K_{m2} + K_{V,m2}} \tag{9.21}$$

$$C_D = \min\left(\frac{1}{\delta_1}; \frac{1}{\delta_2}\right) \tag{9.22}$$

The cross-girders are first assumed to be IPE 600 with a spacing a = 8.0 m in the intermediate span for all designs. The characteristics of IPE 600 are:

- Shear section: $A_{w,t}$ = 8 378 mm^2.
- Total section: A_t = 15 600 mm^2.
- Second moment of area of the section: I_t = 9.21 · 10^8 mm^4.

The results are detailed in Table 53.

Table 53: Stiffness of the lower flange at the final stage

	Support P1			
Design	A	B	C	
h_m	2 740	2 763	2 572	mm
h_{m1}	1 340	1 363	1 172	mm
h_{m2}	1 400	1 400	1 400	mm
h'_{m1}	955	1 063	872	mm
h'_{m2}	1 015	1 100	1 100	mm
$A_{w,m}$	8 560	4 500	3 500	mm^2
I_m	$1.22 \cdot 10^9$	$2.20 \cdot 10^8$	$1.31 \cdot 10^8$	mm^4
δ_1	$4.89 \cdot 10^{-5}$	$7.03 \cdot 10^{-5}$	$7.16 \cdot 10^{-5}$	mm/N
δ_2	$8.88 \cdot 10^{-6}$	$2.30 \cdot 10^{-5}$	$2.22 \cdot 10^{-5}$	mm/N
C_D	20.4	14.2	14.0	MN/m

The rigidity C_D of the transverse bracing frame is reduced by around 30% from the design A to designs B and C. This is due to the reduction of the width $b_{w,T}$ of the vertical stiffeners web, as it was at the construction stage concerning the compression upper flange at mid-span P1-P2.

The rigidity C_D is very close for designs B and C. The reduction of $b_{w,T}$, which decreases the geometric cross-sectional properties I_m and $A_{w,m}$ of the stiffener, is compensated by the reduction of the heights h_m, h_{mi} and h'_{mi} in the design C. Hence the flexibility coefficients of the vertical stiffeners remain very close for designs B and C, and thus the lateral displacement ν.

9.2.3. Simplified check method

The critical axial load $N_{cr,D}$ can be calculated according to [19] § 6.3.4.2. The influence of the bracing frame on $N_{cr,D}$ has be expressed in other terms in [2] Equation (12.21). It defines a buckling length L_D of the laterally elastically supported compression flange, which depends on the rigidity C_D of the bracing frame. L_D should not be less than the distance a between the cross-girders, which correspond to the case where the compression flange is laterally simply supported by the bracing frame.

$$L_D = \sqrt[4]{\frac{\pi^4}{4} * E_a * I_z * \frac{a}{C_d}} \geq a \tag{9.23}$$

Therefore the critical axial load $N_{cr,D}$ is calculated with the formulas:

$$L_K = \frac{L_D}{\sqrt{\eta}} \tag{9.24}$$

$$\lambda_K = \frac{L_K}{i_D} \tag{9.25}$$

$$N_{cr,D} = \frac{\pi^2 \cdot E_a \cdot I_z}{{\lambda_K}^2} \tag{9.26}$$

Where L_K is the stable length between adjacent torsional restraints; λ_K is the slenderness ratio of the member in compression; η is the reduction factor to account for the variation of the moment between the restraints. It is taken as $\eta = 1$ to be conservative.

The critical lateral-torsional buckling stress $\sigma_{cr,D}$ can be divided into the uniform and the non-uniform component σ_{Dv} and σ_{Dw}. For the designs A and B, the small contribution of σ_{Dv} from the flat flanges should be neglected; it is taken into account for the design C.

$$K = 2 \cdot \pi \cdot t_f \cdot \left(D_f - \frac{t_f}{2}\right)^3 + h * \frac{t_w^3}{3} \tag{9.27}$$

$$\sigma_{Dv} = \eta \cdot \pi \cdot \frac{\sqrt{E_a \cdot G_a \cdot K \cdot I_z}}{L_D \cdot W} \tag{9.28}$$

$$\sigma_{Dw} = \frac{N_{cr,D}}{A_D} \tag{9.29}$$

$$\sigma_{cr,D} = \sqrt{\sigma_{Dv}^2 + \sigma_{Dw}^2} \tag{9.30}$$

Where K is the St.Venant torsional constant of the flange. The critical LTB load $\sigma_{cr,D}$ is calculated with the method from the SIA 263 of the Swiss codes [21] Annex B.

Hence the design stress σ_{Ed} at the mid-plane of the flange should be less than the lateral-torsional buckling stress σ_D:

$$\lambda_D = \sqrt{\frac{f_{yk,inf}}{\sigma_{cr,D}}} \tag{9.31}$$

$$\phi_D = 0.5 \cdot \left(1 + \alpha_D \cdot (\lambda_D - 0.2) + {\lambda_D}^2\right) \quad (9.32)$$

$$\chi_D = \frac{1}{\phi_D + \sqrt{{\phi_D}^2 - {\lambda_D}^2}} \quad (9.33)$$

$$\sigma_{Ed} \leq \sigma_D = \frac{\chi_D \cdot f_{y,inf}}{\gamma_{M1}} \quad (9.34)$$

Where λ_D is the slenderness ratio; ϕ_D is the imperfection coefficient; α_D is the imperfection factor; χ_D is the reduction factor for lateral-torsional buckling; σ_{Ed} is the design stress at the mid-plane of the flange.

According to [5] Table 6.2 and Table 6.3:

- The buckling curve d is used for a welded I-section, in designs A and B: $\alpha_D = 0.76$.
- The buckling curve a_0 is used for a hot finished hollow section, in the design C: $\alpha_D = 0.13$.

The results are detailed in Table 54.

Table 54: Calculation of the buckling stress in the resisting section

	Support P1			Mid-span P1-P2			
Design	A	B	C	A	B	C	
L_D	13 636	10 698	7 618	8 430	6 684	5 968	mm
L_K	13 636	10 698	8 000	8 430	8 000	8 000	mm
λ_K	40.8	43.4	57.1	32.1	45.9	56.1	[-]
$N_{cr,D}$	192 626	82 511	37 233	97 216	25 942	18 926	kN
σ_{Dw}	1 245	1 103	635	2 010	986	659	MPa
σ_{Dv}	0	0	1 989	0	0	2 206	MPa
$\sigma_{cr,D}$	1 245	1 103	2 088	2 010	986	2 302	MPa
λ_D	0.49	0.77	0.57	0.41	0.84	0.55	[-]
α_D	0.76	0.76	0.13	0.76	0.76	0.13	[-]
ϕ_D	0.727	1.011	0.690	0.667	1.092	0.672	[-]
χ_D	0.789	0.600	0.934	0.840	0.558	0.941	[-]
σ_D	211	354	586	263	350	590	MPa
σ_{Ed}	241	424	561	137	277	309	MPa

First, it should be noticed that the design C provides more resistance against lateral-torsional buckling than the other designs. It is due to the important contribution of the uniform component σ_{Dv} of the critical stress $\sigma_{cr,D}$, which was neglected in designs A and B.

At the construction stage, there is no problem of stability of the upper flange. The stress in the compression flange is induced by the weights of the steel girder and the slab only, and the lateral supports provided by the erection bracings rigidifies the frame enough to avoid LTB.

At the final stage, the designs A and B have insufficient resistance at support P1, against LTB of the lower flange. The bracing frame is not rigid enough, or the spacing between the cross-girders needs to be reduced.

The choice is made to strengthen the bracing frame by replacing the IPE 600 by IPE 750x196, in order to increase the rigidity C_D. The characteristics of IPE 750x196 are:

- Shear section: A_t = 25 100 mm^2.
- Total section: $A_{w,t}$ = 12 730 mm^2.
- Second moment of area of the section: I_t = 2.40 · 10^9 mm^4.

The new rigidity of the bracing frame and the LTB stress are detailed in Table 55.

Table 55: Buckling stress with IPE 750x196

	Support P1		
Design	A	B	
C_D	44.4	26.1	MN/m
L_D	11 232	9 191	mm
$N_{cr,D}$	283 919	111 785	kN
$\sigma_{cr,D}$	1 835	1 494	MPa
χ_D	0.850	0.670	[-]
σ_D	228	396	MPa
σ_{Ed}	241	424	MPa

The rigidity C_D is improved by a factor 2, and the lateral-torsional buckling stress σ_D increases by around 10%, but it is still not great enough to resist against the design stress σ_{Ed}.

The simplified method is a conservative way to justify the compression flange against LTB. It considers a constant distribution of the moment along the bridge, with the maximum value of the stresses (at support P1). On the contrary, the actual compression stresses reduce almost proportionally with the distance from the support. They reach the null value at an approximate distance of 13 m from the support P1 and become tensile stresses beyond that point.

The general check method would be a more accurate way to assess the lower compression flanges against LTB, by approaching the critical stresses as precisely as possible in the section. It allows accounting for different sections of cross-girders in the intermediate span, and the spacing of 7.5 m between the bracing frames in side spans.

9.2.4. General check method

The general check method consists in performing critical load calculations as exactly as possible. A model of a continuous simplified T-section girder is modelled with an area equal to the sum of the lower flange area and a sixth of the web, as shown in Table 56.

Table 56: Dimensions of the simplified girders

	Support P1		Mid-span P1-P2		
Design	A	B	A	B	
$b_{f,inf}$	1 200	900	1 200	900	mm
$t_{f,inf}$	120	75	40	45	mm
$h_w/6$	425	445	455	455	mm
t_w	26	20	18	14	mm
A_D	155 050	76 400	56 190	46 870	mm^2

The combination of actions which gives the maximum bending moment at support P1 is considered. The critical stresses at the lower fibre of the girder correspond to the design stresses at the extreme fibre of the lower flange, which is conservative. The longitudinal distribution of the normal force in the continuous simplified girder is obtained by multiplying the critical stresses by the area of the girder. The graphs are shown in Annex XIII.

Six different girders are studied; for designs A and B:

- Case a): transverse cross-girders with IPE 600.
- Case b): transverse cross-girders with IPE 750x196.
- Case c): cross-girders with IPE 600 in span and IPE 750x196 near supports P1 and P2.

The girders are modelled in SAP 2000 as in Figure 17, with the characteristics:

- Lateral elastic springs are defined in the global direction u2 every 8 m in the intermediate span, and every 7.5 m in the side spans, with the corresponding rigidity C_D.
- A fixed point in the u1 direction is defined at the mid-span of the intermediate span.
- The piles and abutments are defined as lateral supports, with no torsion allowed.

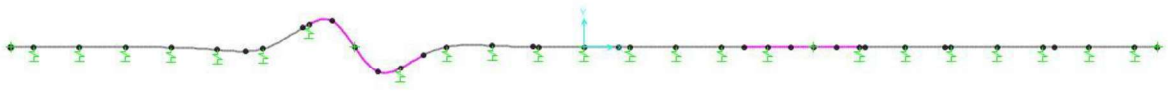

Figure 17: First lateral-torsional buckling mode of the simplified girder

The load case type buckling gives the minimum amplification factor $\alpha_{cr,op}$ to apply to the critical forces to reach the critical elastic resistance of the girder with regard to the lateral-torsional buckling. The general check method also considers the reserve in elastic resistance at ULS in the lower flange, which is taken into account by the minimum amplification factor $\alpha_{ult,k}$ to apply to the design stresses to reach the characteristic resistance of the cross-section.

Therefore the global non-dimensional slenderness $\bar{\lambda}_{op}$, the imperfection coefficient ϕ_{op} and the global reduction factor χ_{op} are:

$$\bar{\lambda}_{op} = \sqrt{\frac{\alpha_{ult,k}}{\alpha_{cr,op}}} \tag{9.35}$$

$$\phi_{op} = 0.5 * \left[1 + \alpha_D * \left(\bar{\lambda}_{op} - 0.2\right) + \bar{\lambda}_{op}^2\right] \tag{9.36}$$

$$\chi_{op} = \frac{1}{\phi_{op} + \sqrt{\phi_{op}^2 - \bar{\lambda}_{op}^2}} \tag{9.37}$$

$$\chi_{op} * \frac{\alpha_{ult,k}}{\gamma_{M1}} \geq 1.0 \tag{9.38}$$

Where α_D is the imperfection factor as defined in section 9.2.3. The buckling curve d for a welded I-section is used: $\alpha_D = 0.76$.

The results are detailed in Table 57.

Table 57: LTB verification with the general check method

	Design A			Design B			
Case	a)	b)	c)	a)	b)	c)	
$\alpha_{cr,op}$	8.59	12.21	12.05	4.55	5.59	5.56	[-]
σ_{Ed}	241	241	241	424	424	424	MPa
$f_{yk,inf}$	295	295	295	690	690	690	MPa
$\alpha_{ult,k}$	1.22	1.22	1.22	1.53	1.53	1.53	[-]
χ_{op}	0.87	0.91	0.91	0.72	0.76	0.76	[-]
Criterion	0.963 < 1	1.013 > 1	1.011 > 1	1.008 > 1	1.062 > 1	1.061 > 1	

It should be noticed that it is not necessary to replace all the cross-girders by IPE 750x196 to increase the resistance of the lower flange against lateral-torsional buckling. Similar results are obtained by strengthening only the two bracing frames near each support P1 and P2.

In the design A, it is necessary to replace these two cross-girders from IPE 600 to IPE 750x196. In the design B, the IPE 600 are enough to resist against lateral-torsional buckling. However, it is safer to strengthen the two cross-girders near the supports, as in the design A.

With the general check method, the use of high strength steel is an advantage against lateral-torsional buckling. Although the lower flange is slenderer in the design B than A, the reserve in resistance represented by the factor $\alpha_{ult,k}$ provides more safety to the design B, in all cases a), b) and c).

9.3. Stability of the cross-bracings

The shear resistance check and the LTB verification assume that the vertical stiffeners are prevented from torsional buckling. It should be justified in case of open stiffeners like flat or T-shaped stiffeners. The verification is explained from [18] § 2.9.4. The critical buckling stress σ_{cr} of the stiffener should respect the following condition:

$$\sigma_{cr} = \frac{G_a \cdot I_T}{I_p} \geq \theta \cdot f_{yk,T} \tag{9.39}$$

Where I_T is the St. Venant torsional constant of the stiffener; I_p is the second moment of area of the stiffener around the edge fixed to the web of the girder; $f_{yk,T}$ is the characteristic yield strength of the stiffener; θ is a parameter to ensure class 3 behaviour. I_T and I_p are calculated for the stiffener alone, without the web of the girder.

The verification with Equation (9.39) is conservative because it does not consider the warping stiffness of the transverse stiffener. For flat stiffeners, the parameter θ is equal to 2. Hence the criterion has been rewritten in the Eurocode in another form, according to [16] § 9.2.1:

$$\frac{I_T}{I_p} \geq 5.3 \cdot \frac{f_{yk,T}}{E_a} \tag{9.40}$$

The verification with Equation (9.40) applies for flat stiffeners, but its use has been extended to vertical T-shaped stiffeners in [1] § 8.5.2. However, when the criterion is not verified, the warping stiffness could be considered. Then the criterion becomes:

$$\sigma_{cr} = \frac{1}{I_p} \cdot \left(\frac{\pi^2 \cdot E_a \cdot I_w}{l^2} + G_a \cdot I_T \right) \geq \theta \cdot f_{yk,T} \tag{9.41}$$

Where $l = h_w$ is the length of the stiffener; I_w is the warping cross-section constant of the stiffener around the edge fixed to the web of the girder. The parameter θ is equal to 6.

The verification with Equation (9.41) is still conservative, because it assumes that the stiffener if fully loaded axially, which is not the case for vertical transverse stiffeners. Hence it is possible to replace the yield strength $f_{yk,T}$ in Equation (9.41) with the actual stress $\sigma_{act,Ed}$:

$$N_{Ed} = V_{Ed} - \frac{1}{\bar{\lambda}_w^2} \cdot \frac{h_w \cdot t_w \cdot f_{yk,w}}{\sqrt{3} \cdot \gamma_{M1}} \tag{9.42}$$

$$\sigma_{act,Ed} = \frac{N_{Ed}}{A_T} \geq 0.3 \cdot f_{yk,T} \tag{9.43}$$

Where A_T is the cross-section of the stiffener alone; $\bar{\lambda}_w$ is the relative slenderness of the web calculated with Equations (8.4) to (8.8); V_{Ed} is the design shear force from Table 19 in the studied cross-section; N_{Ed} is the axial load in the vertical stiffener. The actual stress $\sigma_{act,Ed}$ should be taken with a minimum value of $0.3 \cdot f_{yk,T}$.

All the results are detailed in Table 58.

Table 58: Torsional buckling of the vertical stiffeners

	Support P1			Mid-span P1-P2			
Design	A	B	C	A	B	C	
A_T	17 000	13 000	12 000	17 000	13 000	12 000	mm^2
I_T	$3.77 \cdot 10^6$	$3.23 \cdot 10^6$	$3.10 \cdot 10^6$	$3.77 \cdot 10^6$	$3.23 \cdot 10^6$	$3.10 \cdot 10^6$	mm^4
I_p	$2.04 \cdot 10^9$	$5.37 \cdot 10^8$	$3.35 \cdot 10^8$	$2.04 \cdot 10^9$	$5.37 \cdot 10^8$	$3.35 \cdot 10^8$	mm^4
I_w	$1.16 \cdot 10^{13}$	$3.12 \cdot 10^{12}$	$1.84 \cdot 10^{12}$	$1.16 \cdot 10^{13}$	$3.12 \cdot 10^{12}$	$1.84 \cdot 10^{12}$	mm^6
$\bar{\lambda}_w$	1.35	2.55	1.83	2.06	3.70	2.62	[-]
V_{Ed}	7 166	6 797	6 153	1 062	1 062	1 062	kN
N_{Ed}	355	3 811	2 082	(-1 084)	52	(-334)	kN
$\sigma_{Ed,act}$	104	293	207	104	207	207	MPa
σ_{cr} (9.39)	149	486	747	149	486	747	MPa
$2 \cdot f_{yk,T}$	690	1 380	1 380	690	1 380	1 380	MPa
σ_{cr} (9.41)	1 947	2 170	3 944	1 742	2 115	3 944	MPa
$6 \cdot f_{yk,T}$	2 070	4 140	4 140	2 070	4 140	4 140	MPa
$6 \cdot \sigma_{Ed,act}$	621	1 759	1 242	621	1 242	1 242	MPa

The negative values of N_{Ed} mean that the stiffener is in tension. Then the actual stress has been considered to be $\sigma_{act,Ed} = 0.3 \cdot f_{yk,T}$ in the verification.

The stiffeners are more critical at support P1 than at mid-span P1-P2. The criteria from Equations (9.39) and (9.41) are never fulfilled, and it is necessary to account for the actual stress $\sigma_{act,Ed}$ in the justification. With this requirement, the vertical stiffeners are checked against torsional buckling.

10. Safety verification at fatigue ULS

Traffic actions can be assimilated to cycle loads, which provoke repeated stress variations in the bridge deck. The stress variation could lead to a crack initiation and propagation inside a deck component, and eventually to the collapse of the bridge.

The fatigue verification according to [22] consists in ensuring that the probability of such a collapse remains low. In a composite bridge, several components must be checked under fatigue load according to [8] § 6.8:

- The structural steel;
- The concrete slab;
- The reinforcing steel bars;
- The shear connection between the structural steel and the concrete slab.

In this report, important details are justified against fatigue: (1) the butt weld in the lower flange for the change in thickness; (2) the transverse weld of the vertical T-shaped stiffener web on the lower flange at mid-span P1-P2; (3) the butt weld of the lower flange to the vertical plate at support P1, in design C.

The cross-section should also be checked against the web breathing.

10.1. Web breathing

Under cyclic loading due to the traffic actions, the initial out-of-plane imperfections can increase or decrease and induce stress variations in the web. These stress variations can produce damages due to fatigue in the welds between the web and the flanges of the girder. According to [2] § 12.7.3, the compression height h_c of the web should be limited, based on the empiric formula:

$$\frac{h_c}{t_w} \leq 100 \tag{10.1}$$

The Eurocode defines another criterion, depending on the length L of the span, from [19] § 7.4:

$$\frac{h_w}{t_w} \leq \min(30 + 4 \cdot L; 300) \tag{10.2}$$

Table 59: Justification against the web breathing

	Support P1			Mid-span P1-P2		
Design	A	B	C	A	B	C
h_c	1 237	1 125	933	850	980	655
h_w/t_w	98.5	133.8	94.3	151.1	194.3	134.7
h_c/t_w	47.6	56.3	46.7	47.2	70.0	46.8
$h_w/t_w \leq$	300	300	300	300	300	300

All the cross-sections are verified against the web breathing, from Table 59. It should be pointed out that in the side spans, the criterion from Equation (10.2) is equal to 270, which is still respected.

10.2. Fatigue verification principles

The FLM3 and the equivalent stress ranges simplified method (ESRSM) from [8] § 6.8.4 can be used for fatigue calculations. According to [19] § 9.5, the fatigue assessment is:

$$\gamma_{Ff} \cdot \Delta\sigma_{E,2} \leq \frac{\Delta\sigma_c}{\gamma_{Mf}} \tag{10.3}$$

Where $\Delta\sigma_{E,2}$ is the equivalent constant amplitude stress range related to 2 million cycles; $\Delta\sigma_c$ is the reference value of the fatigue strength at 2 million cycles, defined in Figure 18; $\gamma_{Ff} = 1.0$ is the partial factor for the fatigue loads; γ_{Mf} is the partial factor for the fatigue strength of the detail.

The maximum stress variation in the cross-section, due to the moving loads, is needed. The FLM3 is used to determine the influence lines and the internal moments, in the cross-sections of the bridge where the details are most critical. The fatigue traffic load $Q_{k,fat}$ was already calculated in section 5.4.2: $Q_{k,fat}$ = 336 kN. The influence line represents the value of the internal moment for a specific cross-section, depending on the position of the moving load $Q_{k,fat}$. Hence the maximum and minimum values of the bending moment $M_{max,fat}$ and $M_{min,fat}$ are obtained at any cross-section of the bridge deck.

The ESRSM requires the calculation of the stress $\Delta\sigma_{E,2}$ according to [8] § 6.8.6:

$$\Delta\sigma_{E,2} = \lambda \cdot \Phi \cdot \Delta\sigma_{fat} = \lambda \cdot \Phi \cdot \left(\sigma_{max,fat} - \sigma_{min,fat}\right) = \lambda \cdot \Phi \cdot \left(\frac{M_{max,fat} - M_{min,fat}}{W_b}\right) \tag{10.4}$$

Where $\Delta\sigma_{fat}$ is the stress variation due to $Q_{k,fat}$; W_b is the elastic section modulus defined with the modular ratio n_0 = 6.0 in section 5.3; Φ is the damage equivalent impact factor; λ is the damage equivalent factor.

The damage equivalent factor Φ accounts for the dynamic effects of the traffic loads near expansion joints. It may be taken as $\Phi = 1.00$ according to [8] § 6.8.6.1. The damage equivalent factor λ is calculated according to [17] § 9.5.2 :

$$\lambda = \lambda_1 \cdot \lambda_2 \cdot \lambda_3 \cdot \lambda_4 \tag{10.5}$$

The factor λ_1 accounts for the damage effects due to the traffic volume. It depends on the internal force which is considered (bending moment, shear force, reaction), on the cross-section (at internal support, in central or intermediate span) and on the length of the span. Considering the bending moment and span lengths L_i greater than 30 m:

$$\lambda_1 = 2.55 - 0.70 \cdot \frac{L_i - 10}{70} \tag{10.6}$$

$$\lambda_1 = 1.70 + 0.50 \cdot \frac{L_{i,moy} - 30}{50} \tag{10.7}$$

The formula (10.6) applies in span cross-sections. The formula (10.7) applies at support cross-sections. Table 60 shows the values of λ_1 for the cross-sections of the case study.

Table 60: Values of the factor λ_1

	Length of the influence line	Factor λ_1
End-span	$L_i = L_1 = 60$ m	2.05
Internal support	$L_{i,moy} = 0.5 \cdot (L_1 + L_2) = 70$ m	2.10
Intermediate span	$L_i = L_2 = 80$ m	1.85

The factor λ_2 accounts for the traffic composition, which is assumed to be identical than in [1] § 9.1.3:

$$\lambda_2 = \frac{Q_{m1}}{Q_0} \cdot \left(\frac{N_{obs}}{N_0}\right)^{\frac{1}{5}} = 0.927 \tag{10.8}$$

A class 2 traffic with two slow lanes is considered. Hence the number of heavy vehicles per year for each slow lane is $N_{obs} = 0.5 \cdot 10^6$, according to [12] Table 4.5. The average gross weight of the lorries per slow lane is $Q_{m1} = 445$ kN, using the information from [12] Table 4.6. The reference number of vehicles from the FLM3 is $N_0 = 0.5 \cdot 10^6$ with a weight $Q_0 = 480$ kN.

The factor λ_3 accounts for the required design life of the structure t_{Ld} =100 years:

$$\lambda_3 = \left(\frac{t_{Ld}}{100}\right)^{\frac{1}{5}} = 1.0 \tag{10.9}$$

The factor λ_4 accounts for the effects of the heavy traffic on the other additional slow lanes defined in the design. It depends on the transverse influence line of each slow lane on the internal forces and moments in the main girder:

$$\lambda_4 = \left(1 + \frac{N_2}{N_1} \cdot \left(\frac{\eta_2 \cdot Q_{m2}}{\eta_1 \cdot Q_{m1}}\right)^5\right)^{\frac{1}{5}} = 1.0 \tag{10.10}$$

$$\eta_1 = \frac{1}{2} + \frac{e}{b} = 0.75 \quad ; \quad \eta_2 = \frac{1}{2} - \frac{e}{b} = 0.25 \tag{10.11}$$

Where e = 1.75 m is the eccentricity of the FLM3 load with respect to the bridge axis (Figure 22); b = 7 m is the centre-to-centre spacing of the girders; η_1 and η_2 are the maximum influence of the transverse location of the traffic slow lanes on the main girder; $Q_{m1} = Q_{m2}$ and $N_1 = N_2 = N_{obs}$ are taken as in the calculations for the factor λ_2.

For the bending moment, the equivalent damage factor λ should remain lower than a limit value λ_{max}. Considering the span lengths L_i greater than 30 m:

$$\lambda_{max} = 1.80 + 0.90 \cdot \frac{L_{i,moy} - 30}{50} = 2.52 \tag{10.12}$$

The formula (10.12) applies at support cross-sections. In span: $\lambda_{max} = 2.0$. According to Equation (10.5) to (10.12), the value of the equivalent damage factor λ is equal to 1.95 at support P1 and 1.72 at mid-span P1-P2; these values are below the upper limit λ_{max}. The value of the partial factor for the fatigue strength of the details is taken as $\gamma_{Mf} = 1.35$ to be conservative.

10.3. Fatigue calculations

The influence lines at the cross-sections of the details are given in Annex XIV. The stresses are taken:

- At the lower fibre of the lower flange for the details 1 and 3.
- At the upper fibre of the lower flange in designs A and B, and at a distance $D_f/4$ from the upper fibre of the lower flange in the design C, for the detail 2.

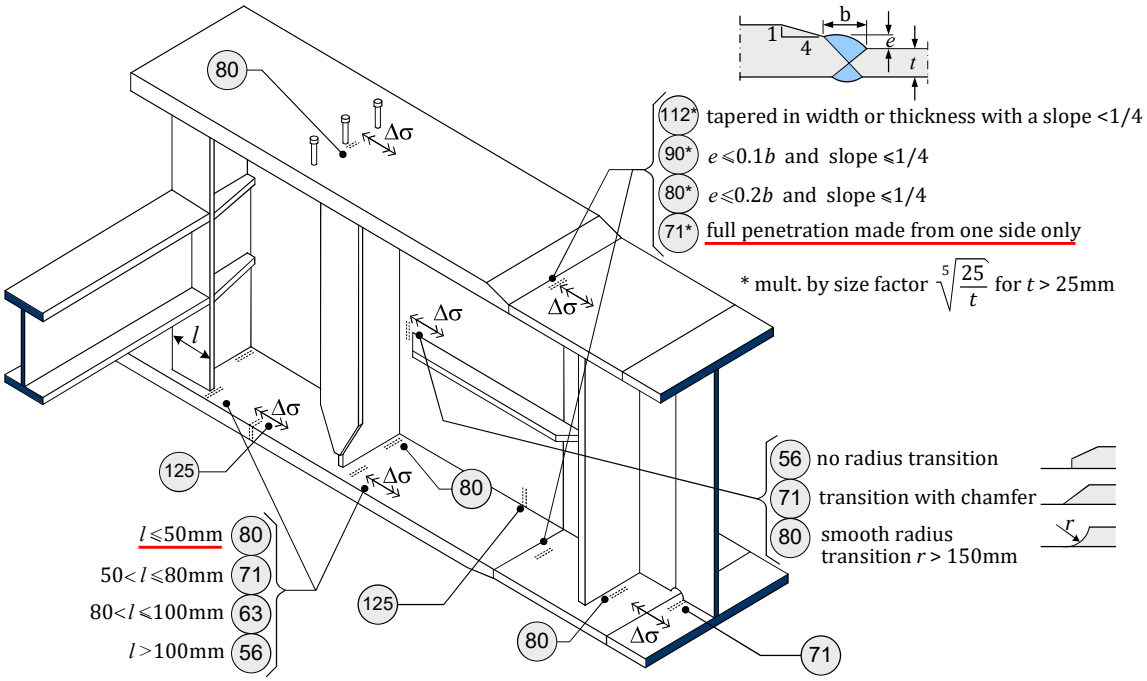

Figure 18: Typical FAT detail categories, adapted from [1] Figure 9.10

The results are given in Table 61. The fatigue strength of details 2 and 3 is equal to 80 MPa. The fatigue strength of the detail 1 is shown in Figure 18:

$$\Delta\sigma_c = 71 \cdot \sqrt[5]{\frac{25}{t_{f,inf}}} \tag{10.13}$$

Table 61: Fatigue assessment of all details

	Detail 1			Detail 2			Detail 3	
Design	A	B	C	A	B	C	C	
$M_{max,fat}$	1 953	2 108	2 172	4 463	4 892	5 073	241	kNm
$M_{min,fat}$	-1 455	-1 108	-977	-691	-558	-502	-1 785	kNm
$\Delta\sigma_{fat}$	17.7	20.0	21.3	26.3	33.4	32,7	12.0	MPa
$\gamma_{Mf} \cdot \Delta\sigma_{E,2}$	41.0	46.5	49.4	61.1	77.5	75.9	31.6	MPa
$\Delta\sigma_c$	64.6	63.1	66.0	80.0	80.0	80.0	80.0	MPa

All the details are verified against fatigue. The detail of the transverse weld of the vertical T-shaped stiffener web on the lower flange at mid-span P1-P2 is the most critical. It has become decisive in the designs B and C, whereas it was not in the design A.

11. Shear connection

The shear connection between the concrete slab and the main steel girder should be designed:

- With an elastic design at support P1, where the resistance is checked elastically;
- With a plastic design in the design A in span P1-P2, where the resistance is checked plastically. However, yielding occurs only at mid-span, the shear connection is also designed elastically.

Since the geometric properties of the cross-section vary depending on the type of loading, due to the delayed effects of concrete, the minimum number of shear connectors per unit length N_{min} is:

$$N_{min} = \frac{v_{el,Ed}}{P_{Rd}} = \frac{1}{P_{Rd}} \cdot \sum_i \frac{V_{Ed,i} \cdot S_{c,i}}{I_{b,i} \cdot n_{el,i}} = \frac{1}{P_{Rd}} \cdot \sum_i \frac{V_{Ed,i} \cdot A_c \cdot (z_c - z_{b,i})}{I_{b,i} \cdot n_{el,i}} \quad (11.1)$$

Where P_{Rd} is the resistance of a shear stud; $v_{el,Ed}$ is the shear force per unit length; $V_{Ed,i}$ is the shear forces; $n_{el,i}$ are the modular ratios (from section 5.3); $S_{c,i}$ are the first moments of area of the slab; A_c is the area of the concrete slab; z_c is the neutral axis of the slab; $z_{b,i}$ are the neutral axis of the composite cross-section; $I_{b,i}$ are the second moments of area of the composite cross-section.

The shear force per unit length $v_{el,Ed}$ correspond to the sum of the shear forces per unit length $v_{el,Ed,i}$ calculated with the different modular ratios $n_{el,i}$ and the shear forces $V_{Ed,i}$ in the corresponding resisting cross-section.

The shear force V_{Ed} corresponds to the actions applied on the concrete after its hardening: the non-structural bridge equipment and the variable actions.

At support, the modular ratio is n_{el} = 1.0, since only the reinforcing steel is considered in the cracked zone. To consider the tension stiffening, which is the participation of the concrete in tension between the cracks, $v_{el,Ed}$ is multiplied by an add-on factor k_{maj} = 1.1 according to [8] § 6.6.1.2. At mid-span, since only the variable actions apply a shear force V_{Ed} on the bridge, the modular ratio is $n_{el} = n_0$ = 6.0. The add-on factor k_{maj} is equal to 1.0.

The area A_c of the concrete slab in span is replaced by the area A_s of the reinforcing steel at support.

The elastic resistance P_{Rd} of the shear connectors for C35/45 concrete depends on their diameter, according to [8] § 6.6.3.1. A diameter ϕ = 22 mm is chosen:

Table 62: Elastic resistance of the shear studs

ϕ	13 mm	16 mm	19 mm	22 mm
P_{Rd}	32 kN	49 kN	69 kN	92 kN

The results are detailed in Table 63.

Table 63: Elastic design of the shear connection

	Support P1			Mid-span P1-P2			
Design	A	B	C	A	B	C	
V_{Ed}	3 741	3 701	3 687	1 062	1 062	1 062	kN
n_{el}	1.0	1.0	1.0	6.0	6.0	6.0	[-]
z_b	1 412	1 384	1 558	2 525	2 591	2 592	mm
z_c	3 063	3 063	3 063	3 063	3 063	3 063	mm
A_c, A_s	21.92	21.92	21.92	1 842	1 842	1 842	10^3 mm^2
S_c	36.2	36.8	33.0	991	870	869	10^6 mm^3
I_b	571	274	197	487	416	383	10^9 mm^4
k_{maj}	1.1	1.1	1.1	1.0	1.0	1.0	[-]
$v_{el,Ed}$	237	498	618	360	370	400	kN/m
N_{min}	2.58	5.41	6.72	3.91	4.03	4.35	studs/m
e	700	550	400	500	700	650	mm
N_{studs}	2	3	3	2	3	3	studs/row

Based on the elastic design at ULS, the required number of studs for the shear connection increases from designs A to B, and from designs B to C, both at support P1 and mid-span P1-P2.

The number N_{studs} of shear connectors per row and the spacing e between rows is based on the elastic design at ULS. The shear connection should also be checked at FLS; the spacing may reduce to strengthen the connection between the slab and the steel girders.

For that purpose and to be conservative, the connection is defined as three shear connectors per row, with the spacing e = 200 mm at support and e = 400 mm in span for all designs. The shear connection for all designs is shown in Figure 19.

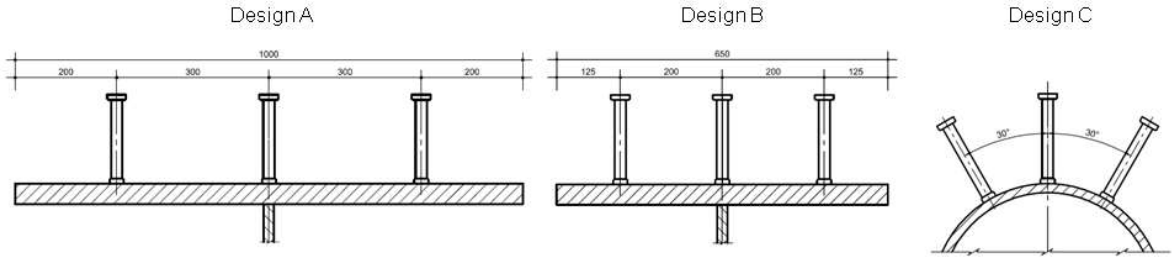

Figure 19: Shear connectors

12. Conclusions and future developments

12.1. Principal conclusions

Several conclusions can be drawn from the comparison of all three designs.

The design B presents several advantages compared to the solution A. The weight of the girders reduces consequently; the use of HSS provides more reserve in resistance at ULS. However, problems related to local buckling of the plates in the section and fatigue become critical in the design.

- Compared to the design A, the weight of the girders in the design B decreases consequently: 50% at support, 22% in span, for a total reduction of 27% of the selfweight. The costs are reduced during the construction, thanks to the lighter deck and the economy of material, as well as welding volumes.

- The increase of the design stresses in the girder, due to the smaller resisting area of the flanges and the web, are largely compensated by the higher yield resistance of steel S690, with a working coefficient around 67% in the lower flange of the design B. Hence the ULS is not critical anymore, as it was in the design A.

- On the other hand, it is not possible to use the plastic moment resistance; instability issues would occur in the web or the compression flanges before they reach the yield strength. Therefore the cross-section must be checked by an effective elastic analysis, for cross-sections in class 4 in the case of the design B.

- The verification regarding flange induced buckling must be adapted by considering the non-symmetry of the composite section. It is also necessary to account for the actual design stresses in the flanges, because the value of the yield resistance of S690 would be too conservative; then it is possible to reduce the thickness of the web.

- The justification against the lateral-torsional buckling of the compression flange is also improved, by using the general check method which considers the reserve in resistance at ULS. The cross-girders used in the bracing frames remain identical, and the vertical stiffeners are smaller. Overall, the safety coefficient related to the stability of the lower flange at support is slightly better than in the design A.

- Fatigue issues become the decisive criterion in the design B. With the increase of the stresses in the flanges, the detail of the transverse weld of the vertical T-shaped stiffener web on the lower flange at mid-span is critical. It limits the reduction of the cross-section area of the girders, more specifically the lower flange, and would require a treatment to improve its FAT category if subjected to higher stresses.

The design C was implemented to try to solve stability and fatigue issues. With a steel weight in the deck similar to solution B, the reserve in resistance at ULS is also high and lateral stability improves greatly. However, the problems related to fatigue remain, and the execution of some constructive details becomes more complex.

- The weight of the girders in the design C also decreases consequently compared to the design A: 56% at support, 24% in span, for a total reduction of 30% of the initial selfweight. When compared to the design B though, it only represents a diminution of 5%. Hence the design C does not improve much the selfweight of the deck.

- The design stresses at ULS are higher in the extreme fibres of the tubular flanges, with a working coefficient between 82% and 97%. Nevertheless, the average stresses in the flanges remain low because the mid-plane of the tube is higher in the section. Besides, the tubes are in class 1 at support, where the design stresses are the greatest. It means a partial plastification of the tubes could be used to increase the resistance of the cross-section at ULS.

- The justification against the lateral-torsional buckling of the compression flange is improved, thanks to the resistance of the tubular flanges against torsion. It allows the cross-girders used in the bracing frames to be lighter, although the vertical stiffeners are even smaller than in the design B.

- The local buckling of the web is improved as well. The connections between the web and the flanges are assumed to be fixed instead of hinged, because of the greater rigidity of the tubes. This enhances the value of the plate buckling coefficient, and thus the limit between cross-sections classes 3 and 4 and the design shear buckling resistance.

- Fatigue issues remain the decisive criterion in the design C. The detail of the transverse weld of the vertical T-shaped stiffener web on the lower flange at mid-span is still critical; the detail is higher in the cross-section, but the design stresses increase.

- Last but not least, some problems related to the construction of the bridge appear. The welds between the vertical stiffeners and the tubular flanges are more difficult to carry out; and the new detail of the butt weld of the lower flange to the vertical plate at support has to be executed. Finally, the length of the tubes is limited in stock for the required diameter and thicknesses, which means more butt welding to assemble the tubular flanges.

12.2. Future developments

Considering the results obtained in this thesis, future developments would be of interest on the following topics:

- The Service Limit State, namely the crack control width of the slab and the deflections, should be verified for all solutions.

- The calculation of the bracing frame rigidity at the final stage has been developed for the case of flat flanges. In this report, it has been used also for the case of tubular flanges. Its validity should be assessed with a shell model and laboratory tests.

- The lateral buckling mode in the design C should be evaluated more precisely, between the torsion mode of the compression flange and the lateral column mode of the girder with no torsion.

- The partial plastification of the tubular flanges at ULS, when the tube section is in class 1, could be studied in order to optimise the design C. It should be pointed out though that the overall design should not change much, because the limiting criterion is at FLS.

- The assumption of a fixed connection between the web and the flanges has led to new values of the plate buckling coefficient, and new limits between the cross-section classes 3 and 4 for a steel girder. The validity of this assumption and of the new equations should be tested.

- The participation of the tubular flanges to the shear resistance has been neglected in the design C. It would be interesting to study their contribution, and their behaviour when subjected to the interaction between the shear force and the stresses due to bending. The participation of the concrete slab to the shear resistance could also be studied in all designs.

- The designs B and C could be optimised, assuming that the critical details in this report are treated in order to enhance their FAT category. New details should become critical and would need to be studied.

- A fourth design could be implemented. Tubular flanges with a welded box section would make the detail of the transverse weld of the vertical T-shaped stiffener web on the lower flange easier to execute. The number of butt welds necessary to assemble the tubes would reduce, although the longitudinal welds along the boxes would be required. A triangular shape could also be studied.

References

[1] SETRA, *Guidance book, Eurocodes 3 et 4, Application to steel-concrete composite road bridges*. Bagneux: Service d'études techniques des routes et autoroutes, 2010.

[2] J.-P. Lebet and M. A. Hirt, *Ponts en acier : Conception et dimensionnement des ponts métalliques et mixtes acier-béton : Traité de Génie Civil 12*. Lausanne: Presses polytechniques et universitaires romandes, 2009.

[3] *EN 10025-3: Hot rolled products of structural steels - Part 3: Technical delivery conditions for normalized/normalized rolled weldable fine grain structural steels*, Comité européen de normalisation CEN. 2004.

[4] *EN 10025-6: Hot rolled products of structural steels - Part 6: Technical delivery conditions for flat products of high yield strength structural steels in the quenched and tempered condition*, Comité européen de normalisation CEN. 2004.

[5] *Eurocode 3: Design of steel structures - Part 1-1: General rules and rules for buildings*, Comité européen de normalisation CEN. Bruxelles, 2005.

[6] *Eurocode 2: Design of concrete structures - Part 1-1: General rules and rules for buildings*, Comité européen de normalisation CEN. Bruxelles, 2004.

[7] *Eurocode 3: Design of steel structures - Part 1-10: Material toughness and through-thickness properties*, Comité européen de normalisation CEN. Bruxelles, 2005.

[8] *Eurocode 4 - Design of composite steel and concrete structures - Part 2: General rules and rules for bridges*, Comité européen de normalisation CEN. Bruxelles, 2005.

[9] *Eurocode 4: Design of composite steel and concrete structures - Part 1-1: General rules and rules for buildings*, Comité européen de normalisation CEN. Bruxelles, 2004.

[10] *Welding - Studs and ceramic ferrules for arc stud welding*. 2008.

[11] *Eurocode 1: Actions on structure - Part 1-1: General actions - Densities, self-weight, imposed loads for buildings*, Comité européen de normalisation CEN. Bruxelles, 2002.

[12] *Eurocode 1: Actions on structures - Part 2: Traffic loads on bridges*, Comité européen de normalisation CEN. Bruxelles, 2003.

[13] *Eurocode 1: Actions on structures - Part 1-5: General actions - Thermal actions*, Comité européen de normalisation CEN. Bruxelles, 2003.

[14] *Eurocode - Basis of structural design. Annex A2*, Comité européen de normalisation CEN. Bruxelles, 2005.

[15] R. Bez and M. A. Hirt, *Construction métallique : Notions fondamentales et méthodes de dimensionnement : Traité de Génie Civil 10*. Lausanne: Presses polytechniques et universitaires romandes, 2006.

[16] *Eurocode 3 - Design of steel structures - Part 1-5: Plated structural elements*, Comité européen de normalisation CEN. Bruxelles, 2006.

[17] *EBPlate*. CTICM, http://downloads.informer.com/ebplate/.

[18] U. Kuhlmann, L. Davaine, B. Braun, and others, *Design of Plated Structures: Eurocode 3: Design of Steel Structures, Part 1-5: Design of Plated Structures*. John Wiley & Sons, 2012.

[19] *Eurocode 3 - Design of steel structures - Part 2: Steel Bridges*, Comité européen de normalisation CEN. Bruxelles, 2006.

[20] OTUA, 'Bulletin Ponts métalliques', no. 11, pp. 150–165, 1986.

[21] *SIA 263 : Construction en acier*, Société suisse des ingénieurs et des architectes. Zurich, 2013.

[22] *Eurocode 3: Design of steel structures - Part 1-9: Fatigue*, Comité européen de normalisation CEN. Bruxelles, 2005.

Annex I. Drawing of design A

LONGITUDINAL VIEW - TYPICAL SPAN

ECH: 1/250

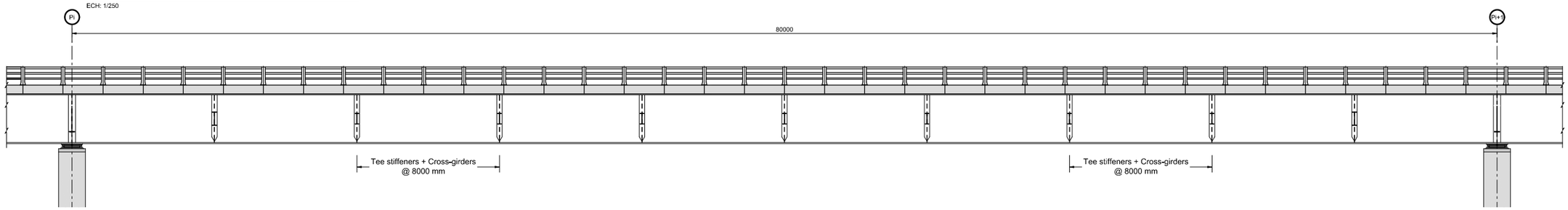

Top Flanges (mm)	1000 x 120 / 12000	1000 x 80 / 8000	1000 x 40 / 40000	1200 x 80 / 8000	1000 x 120 / 12000
Web thickness (mm)	26 / 12000	22 / 8000	18 / 40000	22 / 8000	26 / 12000
Bottom Flanges (mm)	1200 x 120 / 12000	1200 x 80 / 8000	1200 x 40 / 40000	1200 x 80 / 8000	1200 x 120 / 12000
Head Stud Connectors	Stud Connectors 3 Ø22 // 200	Stud Connectors 3 Ø22 // 300	Stud Connectors 3 Ø22 // 400	Stud Connectors 3 Ø22 // 300	Stud Connectors 3 Ø22 // 200
Longitudinal Reinforcement	1.19% / 12000	0.92% / 56000			1.19% / 12000

DECK TYPICAL CROSS-SECTION - SUPPORT

ESC: 1/125

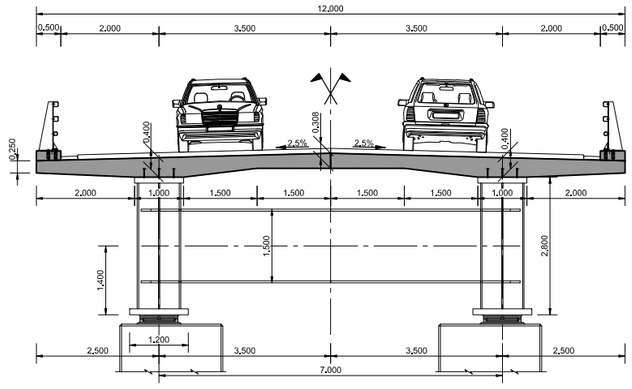

DECK TYPICAL CROSS-SECTION - SPAN

ESC: 1/125

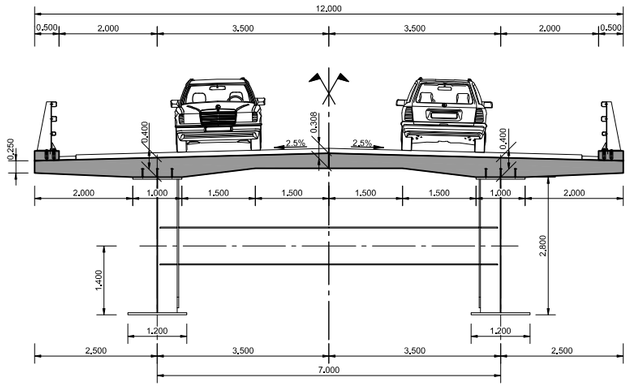

SECTION B-B - CROSS-GIRDERS

ESC. 1/50

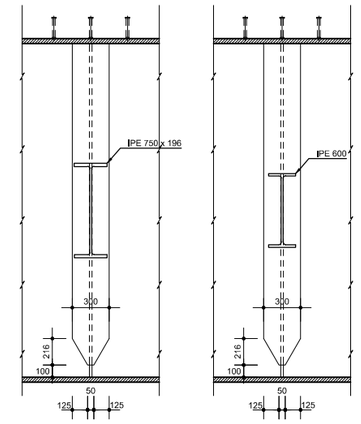

WELDING DETAILS

Scale: 1/10

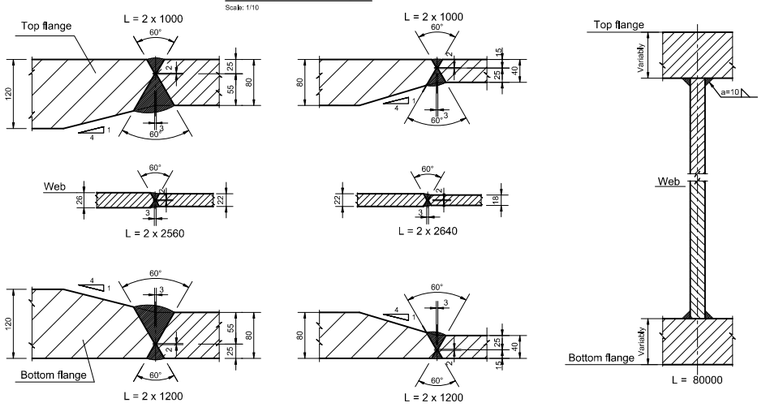

HEAD STUD CONNECTORS

ESC. 1/12,5

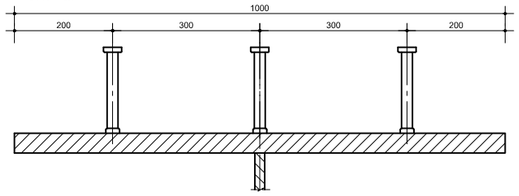

HEAD STUD CONNECTORS

ESC. 1/5

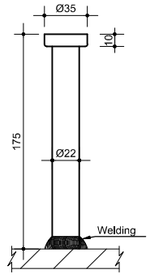

Name	Symbol	Throat	Name	Symbol	Throat
Fillet weld with no bevel			Bevel in half-V		
Fillet weld with bevel			Bevel in K		
Bevel in V			Bevel in Y		
Bevel in X			Bevel in double Y		

(*) The arrow points to the bevelled plate

SECTION A-A - TEE STIFFENERS IN SPAN

ESC. 1/50

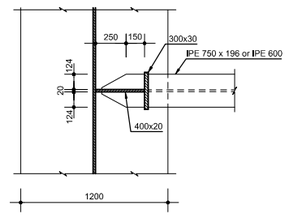

STRUCTURAL MATERIALS

CONCRETE:			
Designation	EN 206-1	Exposure Classes	Cover (mm)
Piers and Foundations	C30/37	XC3 / XF1	45
Deck - Slab	C35/45	XC4/ XF4	40
STEEL:			
Structural Steel	EN10025-2 S355 K2 (40J,-20°C) EN10025-3 S355 N (40J,-20°C) EN10025-3 S355 NL (27J,-50°C)		
Reinforcement	B500B (EN 10080)		
Stud Connectors	EN10025 S235 J2 + C450 (EN ISO 13918)		

SECTION C-C - TEE STIFFENERS AT SUPPORT

ESC. 1/50

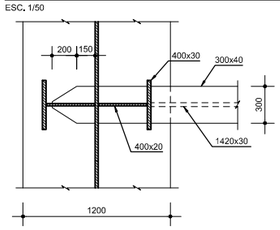

Annex I. Design A

Annex II. Drawing of design B

LONGITUDINAL VIEW - TYPICAL SPAN

ECH: 1/250

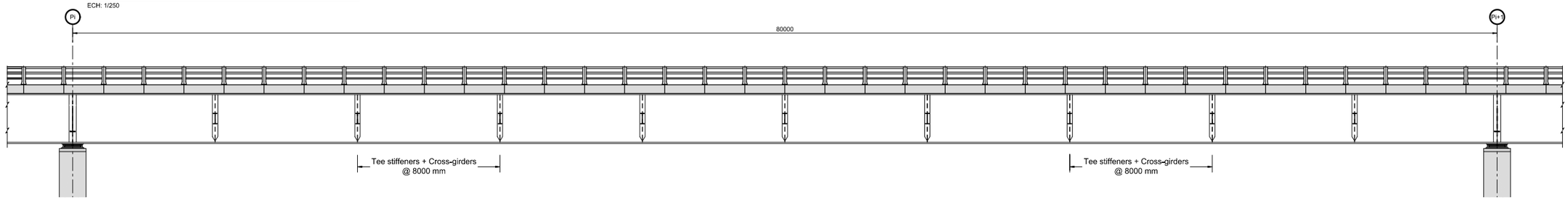

Top Flanges (mm)	650 x 50 / 12000	650 x 35 / 56000			650 x 50 / 12000
Web thickness (mm)	20 / 12000	16 / 8000	14 / 40000	16 / 8000	20 / 12000
Bottom Flanges (mm)	900 x 75 / 12000	900 x 60 / 8000	900 x 45 / 40000	900 x 60 / 8000	900 x 75 / 12000
Head Stud Connectors	Stud Connectors 3 Ø22 // 200	Stud Connectors 3 Ø22 // 300	Stud Connectors 3 Ø22 // 400	Stud Connectors 3 Ø22 // 300	Stud Connectors 3 Ø22 // 200
Longitudinal Reinforcement	1.19% / 12000	0.92% / 56000			1.19% / 12000

DECK TYPICAL CROSS-SECTION - SUPPORT

ESC: 1/125

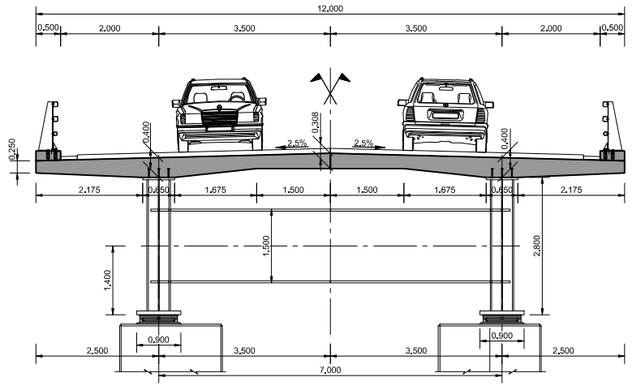

DECK TYPICAL CROSS-SECTION - SPAN

ESC: 1/125

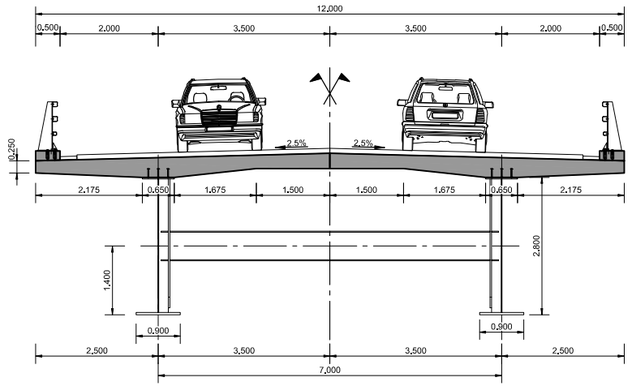

SECTION B-B - CROSS-GIRDERS

ESC. 1/50

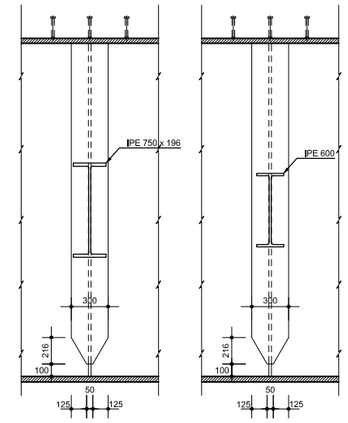

WELDING DETAILS

Scale: 1/10

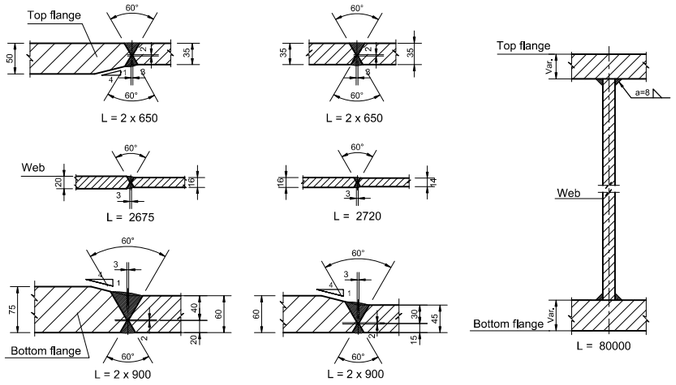

HEAD STUD CONNECTORS

ESC. 1/12,5

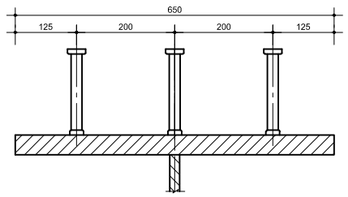

HEAD STUD CONNECTORS

ESC. 1/5

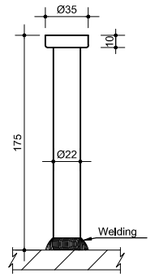

Name	Symbol	Throat	Name	Symbol	Throat
Fillet weld with no bevel			Bevel in half-V		
Fillet weld with bevel			Bevel in K		
Bevel in V			Bevel in Y		
Bevel in X			Bevel in double Y		

(*) The arrow points to the bevelled plate

SECTION A-A - TEE STIFFENERS IN SPAN

ESC. 1/50

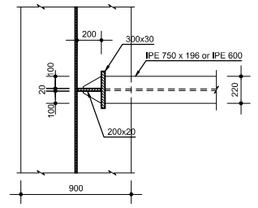

SECTION C-C - TEE STIFFENERS AT SUPPORT

ESC. 1/50

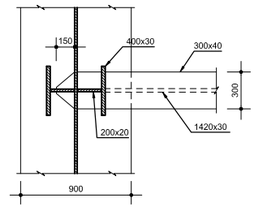

STRUCTURAL MATERIALS

CONCRETE:			
Designation	EN 206-1	Exposure Classes	Cover (mm)
Piers and Foundations	C30/37	XC3 / XF1	45
Deck - Slab	C35/45	XC4/ XF4	40
STEEL:			
Structural Steel	EN10025-6 S690 QL (30J.-40ºC) EN10025-6 S690 QL1 (40J.-40ºC)		
Reinforcement	B500B (EN 10080)		
Stud Connectors	EN10025 S235 J2 + C450 (EN ISO 13918)		

Annex II. Design B

Annex III. Drawing of design C

LONGITUDINAL VIEW - TYPICAL SPAN

ECH: 1/250

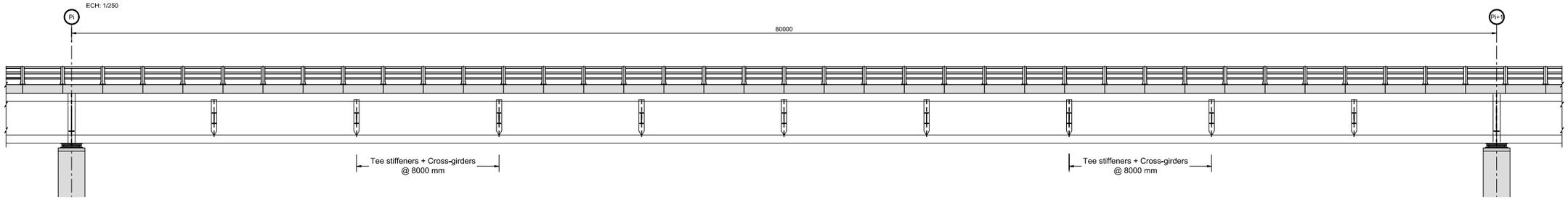

Top Flanges (mm)	Ø 457 x 30 12000	Ø 457 x 17.5 56000			Ø 457 x 30 12000
Web thickness (mm)	20 12000	16 8000	14 40000	16 8000	20 12000
Bottom Flanges (mm)	Ø 457 x 40 12000	Ø 457 x 36 56000			Ø 457 x 40 12000
Head Stud Connectors	Stud Connectors 3 Ø22 // 200	Stud Connectors 3 Ø22 // 300	Stud Connectors 3 Ø22 // 400	Stud Connectors 3 Ø22 // 300	Stud Connectors 3 Ø22 // 200
Longitudinal Reinforcement	1.19% 12000	0.92% 56000			1.19% 12000

DECK TYPICAL CROSS-SECTION - SUPPORT

ESC: 1/125

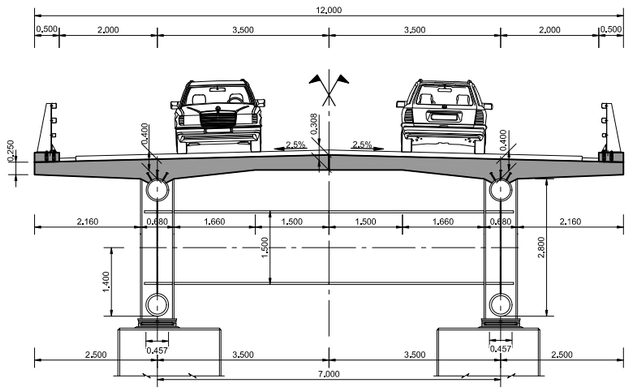

DECK TYPICAL CROSS-SECTION - SPAN

ESC: 1/125

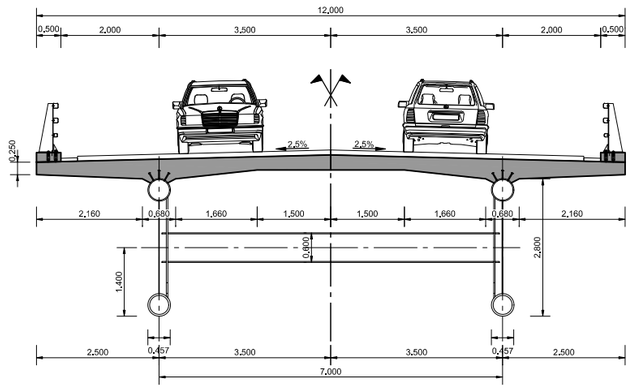

SECTION B-B - CROSS-GIRDERS

ESC. 1/50

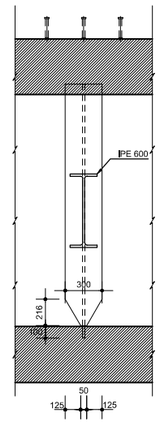

WELDING DETAILS

Scale: 1/10

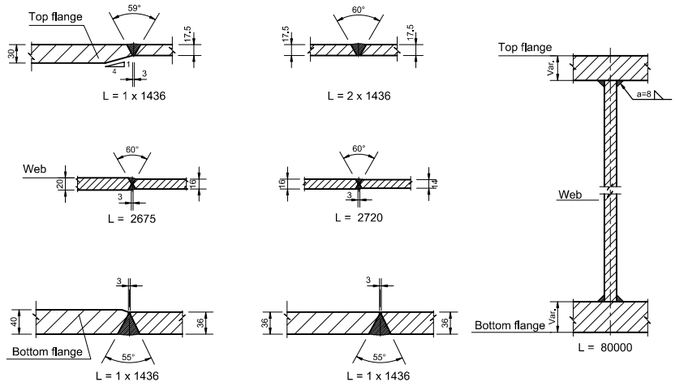

HEAD STUD CONNECTORS

ESC. 1/12,5

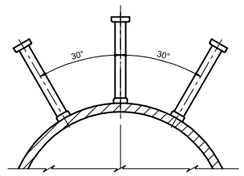

HEAD STUD CONNECTORS

ESC. 1/5

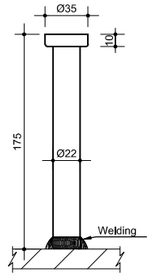

Name	Symbol	Throat	Name	Symbol	Throat
Fillet weld with no bevel			Bevel in half-V		
Fillet weld with bevel			Bevel in K		
Bevel in V			Bevel in Y		
Bevel in X			Bevel in double Y		

(*) The arrow points to the bevelled plate

SECTION A-A - TEE STIFFENERS IN SPAN

ESC. 1/50

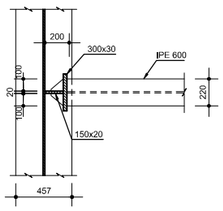

SECTION C-C - TEE STIFFENERS AT SUPPORT

ESC. 1/50

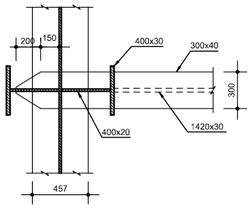

STRUCTURAL MATERIALS

CONCRETE:			
Designation	EN 206-1	Exposure Classes	Cover (mm)
Piers and Foundations	C30/37	XC3 / XF1	45
Deck - Slab	C35/45	XC4/ XF4	40
STEEL:			
Structural Steel	EN10025-6 S690 QL (30J.-40°C) EN10025-6 S690 QL1 (40J.-40°C)		
Reinforcement	B500B (EN 10080)		
Stud Connectors	EN10025 S235 J2 + C450 (EN ISO 13918)		

Annex III. Design C

Annex IV. Transverse influence line of the LM1

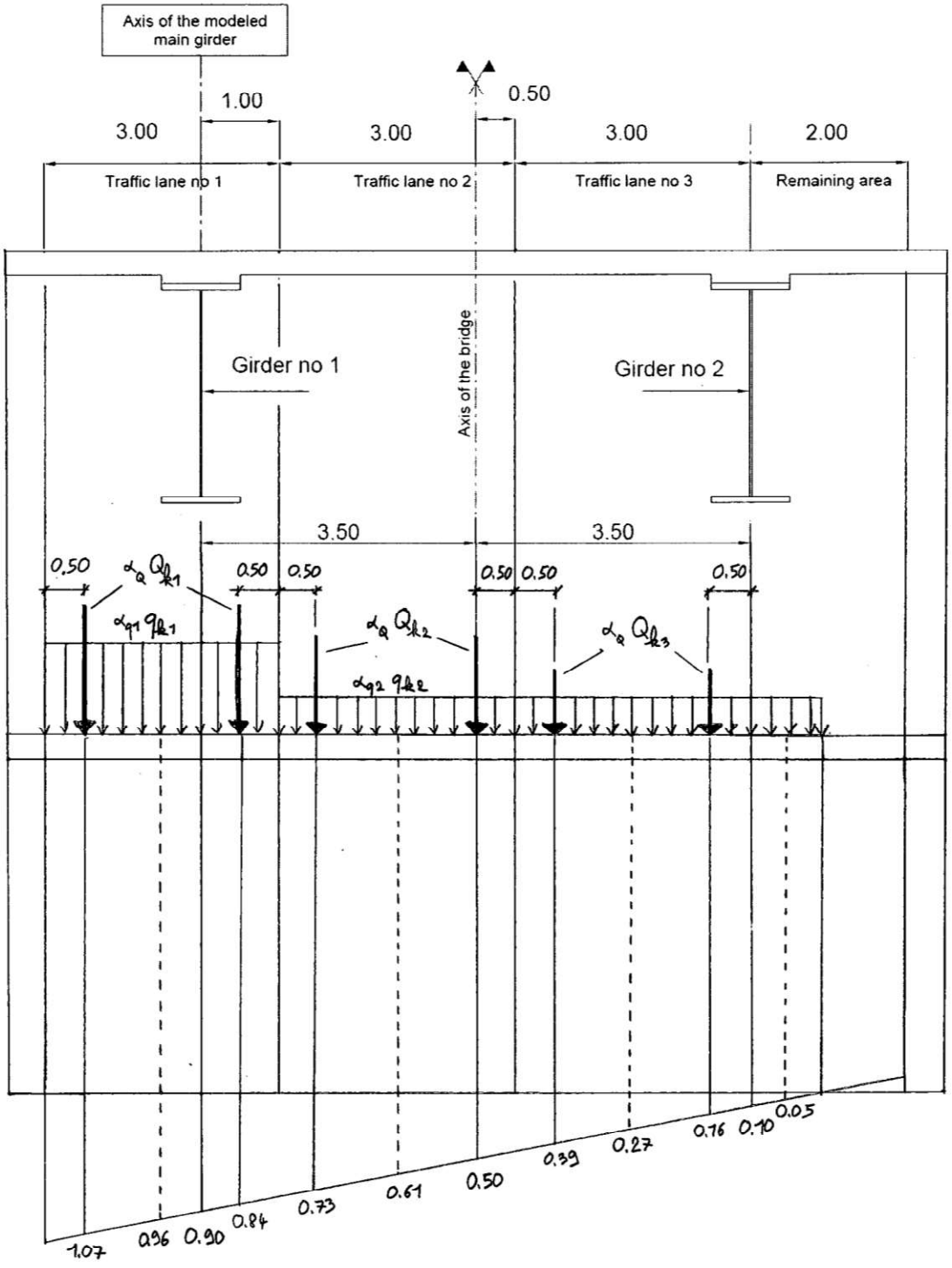

Figure 20: Transverse positioning of the traffic lanes and load distribution (LM1)

Annex V. Transverse influence line of the FLM3

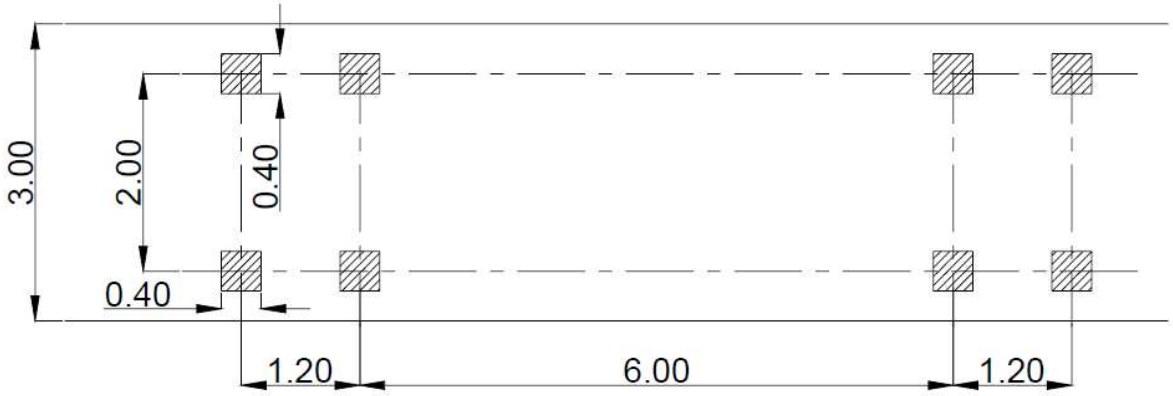

Figure 21: Single-vehicle model with 4 axles from the FLM3

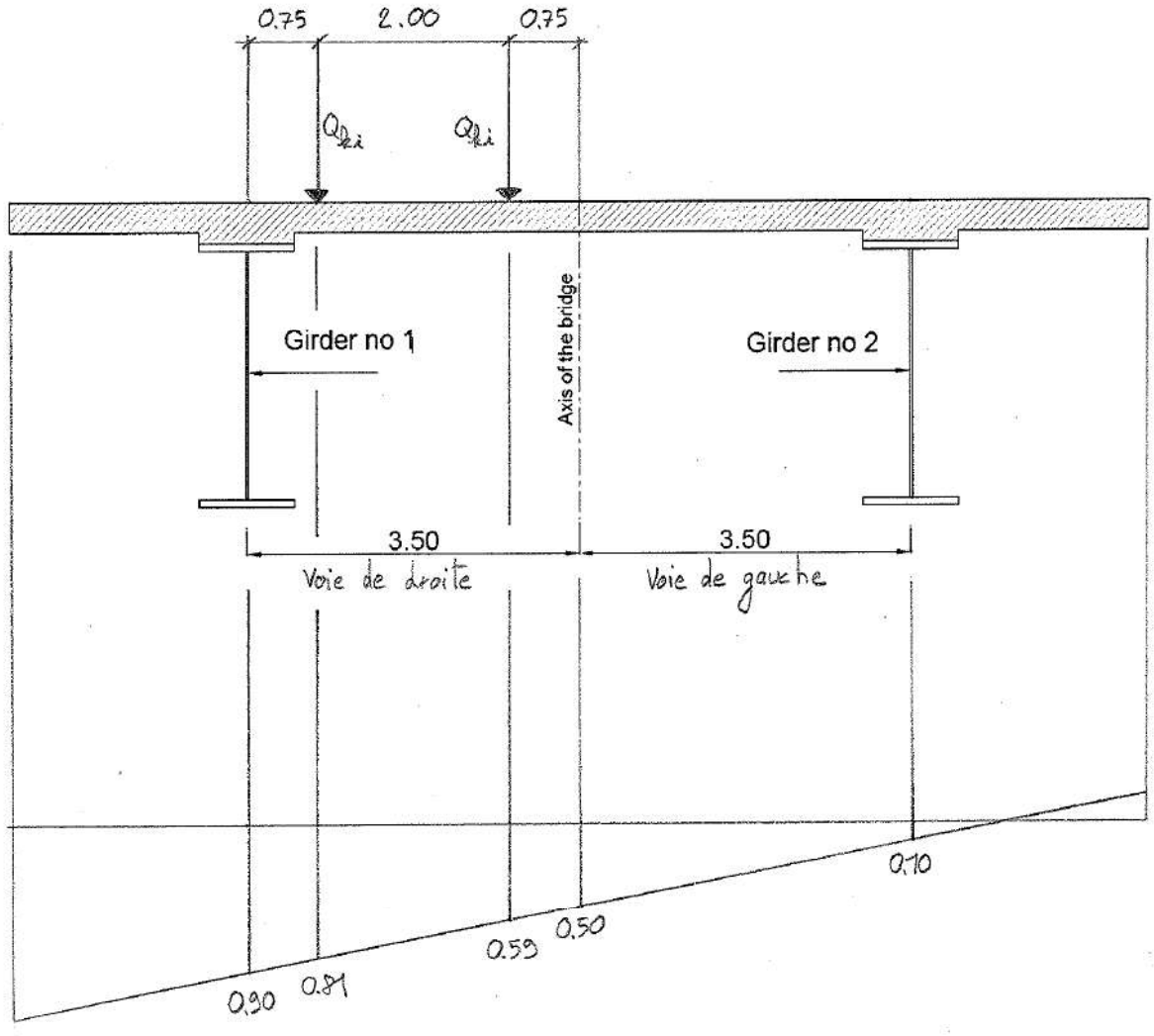

Figure 22: Transverse positioning of the traffic lanes and load distribution (FLM3)

Annex VI. Cross-sections in SAP 2000

Figure 23: Longitudinal elevation of the model

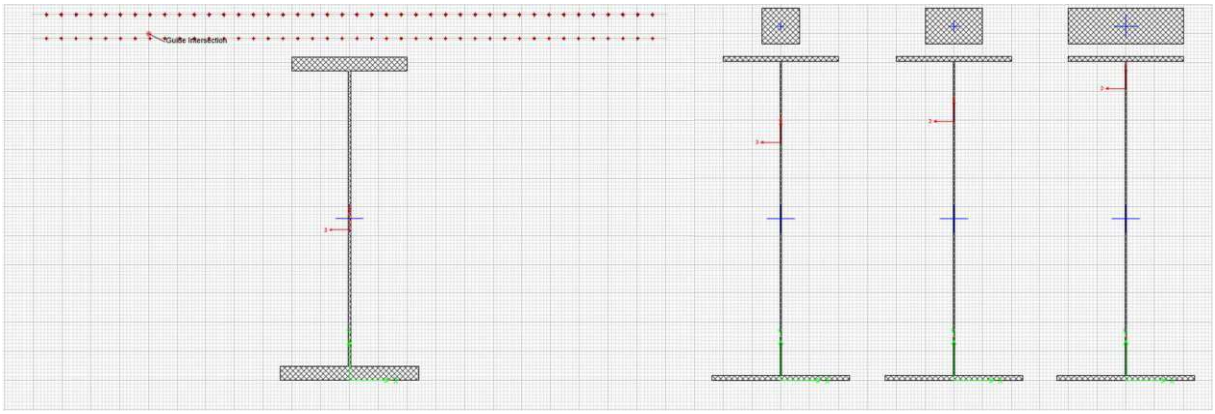

Figure 24: Cross-sections in SAP 2000 for the design A

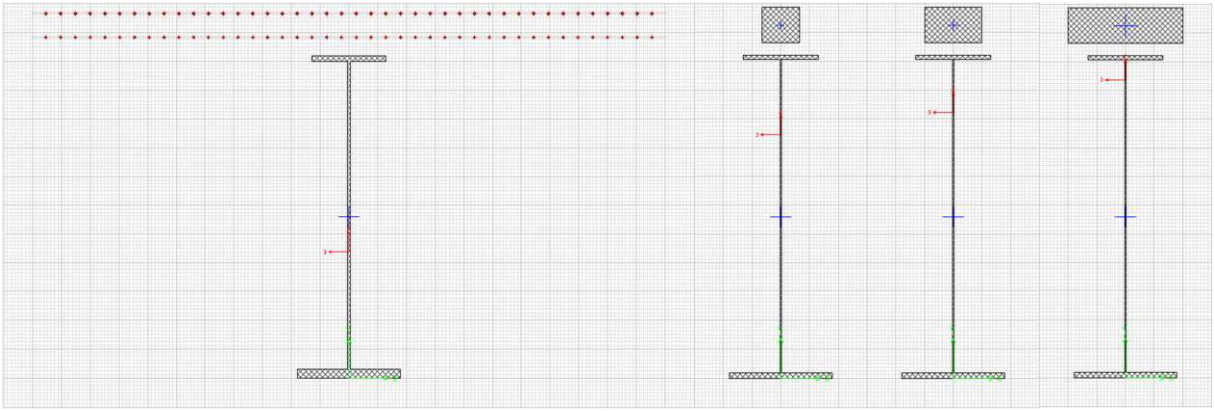

Figure 25: Cross-sections in SAP 2000 for the design B

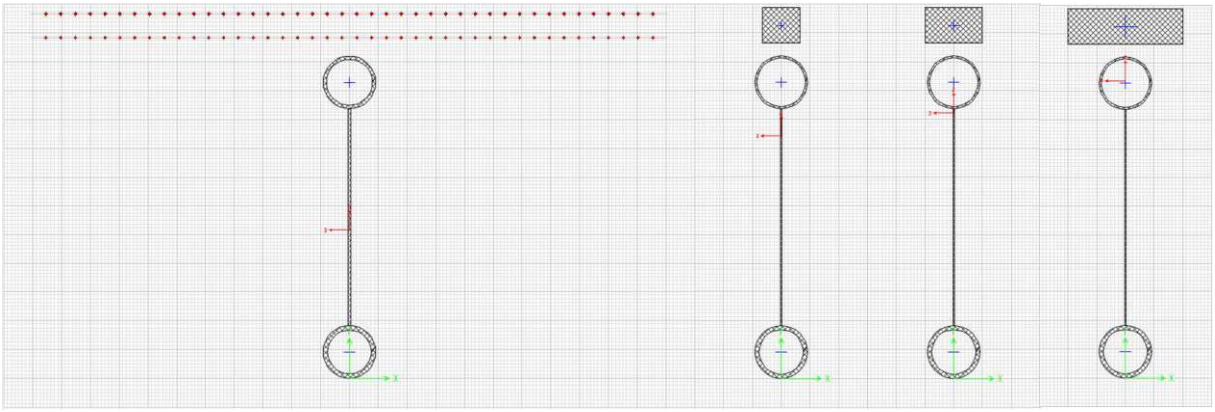

Figure 26: Cross-sections in SAP 2000 for the design C

Annex VII. Loads in SAP 2000

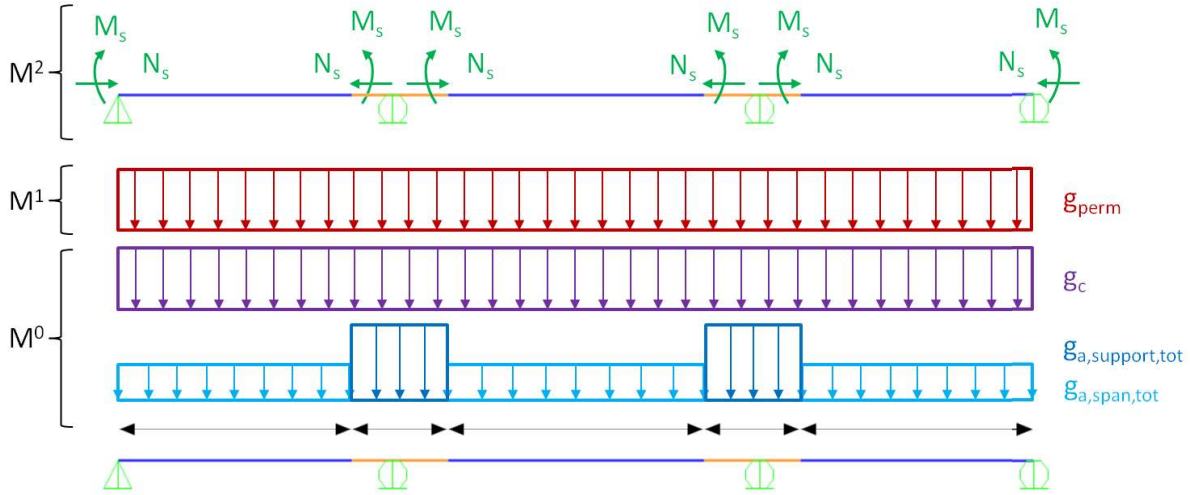

Figure 27: Design models 0, 1 and 2

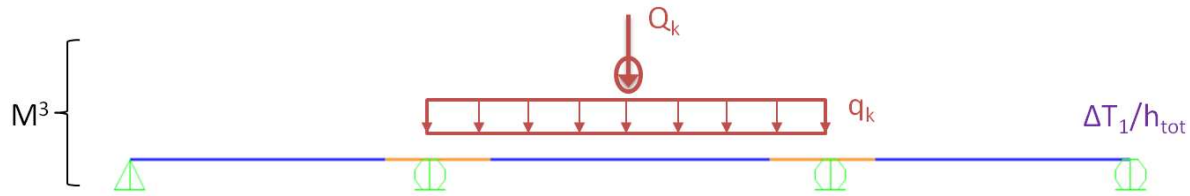

Figure 28: Design model 3 to maximize the bending moment at mid-span

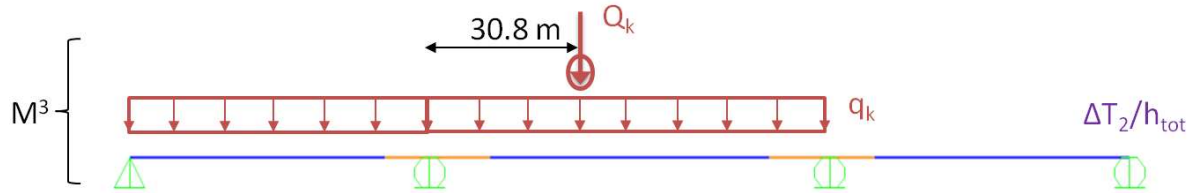

Figure 29: Design model 3 to maximize the bending moment at support

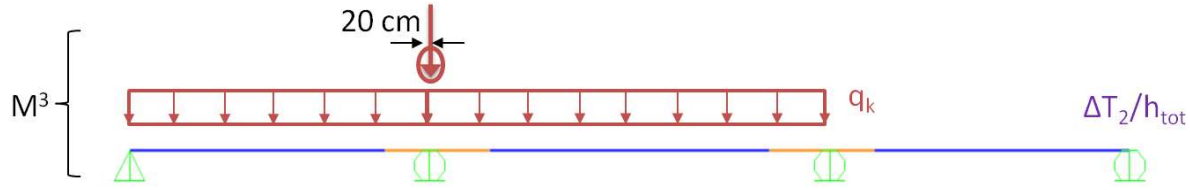

Figure 30: Design model 3 to maximize the shear force at support

Annex VIII. Bending moment diagrams at ULS

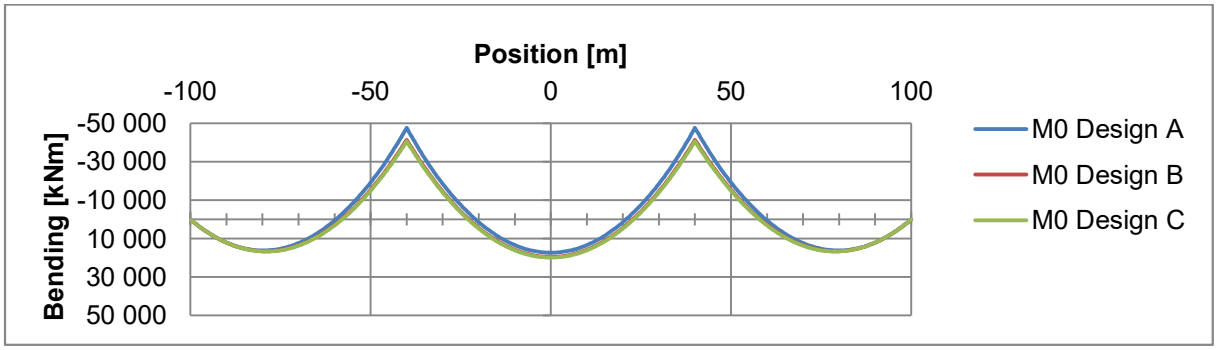

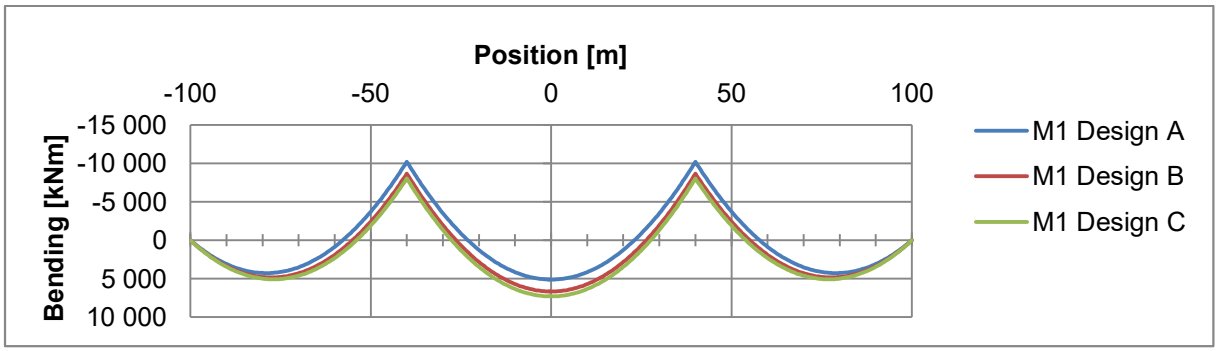

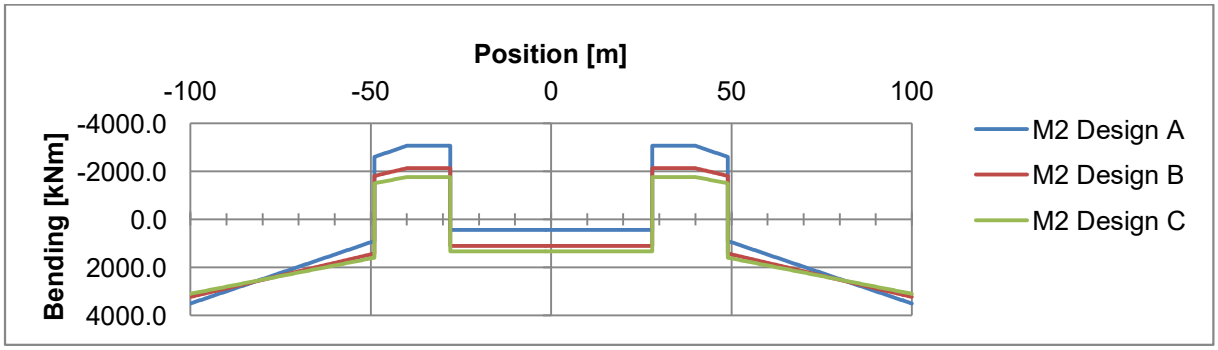

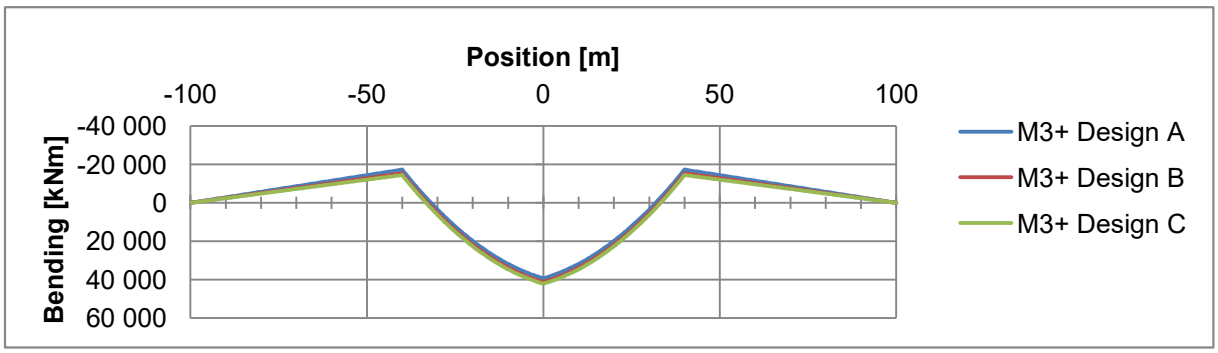

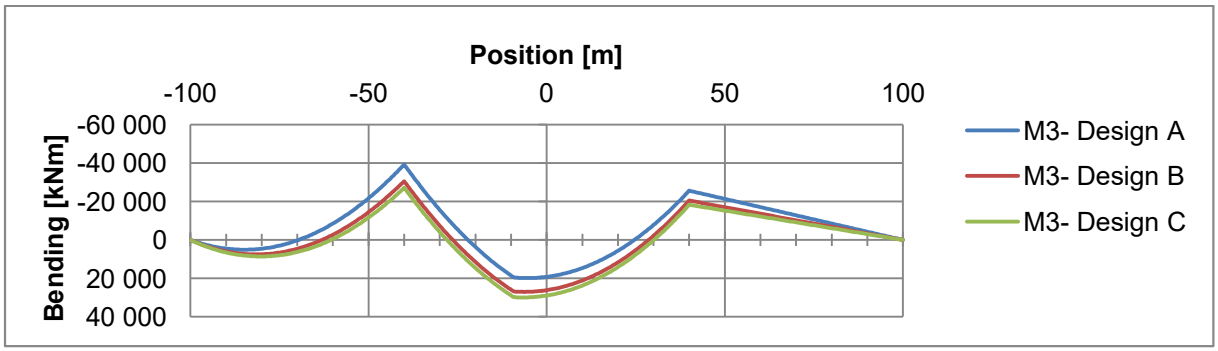

Annex IX. Shear force diagrams at ULS

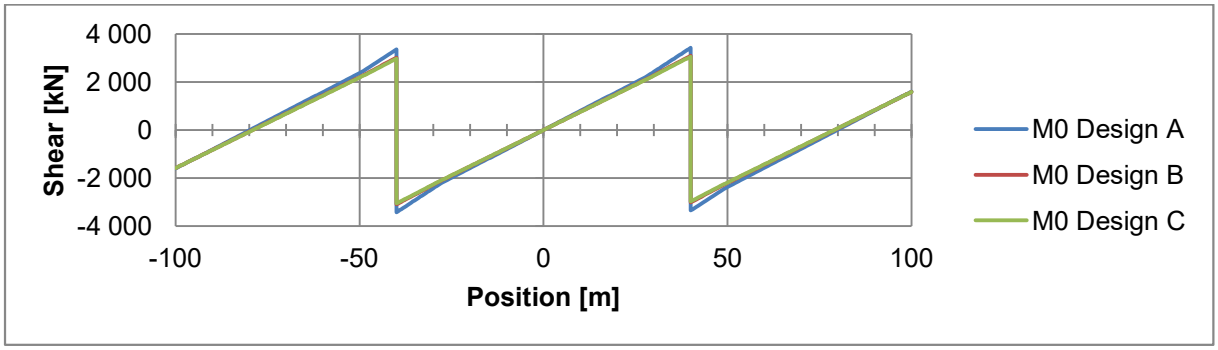

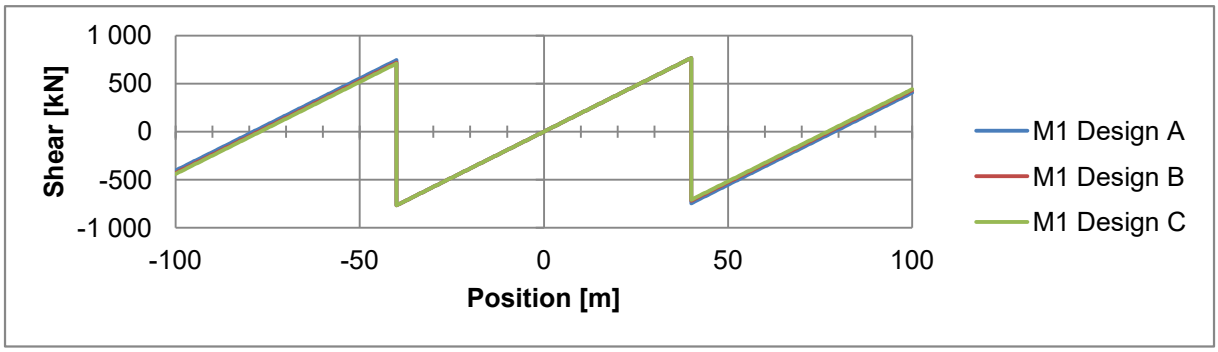

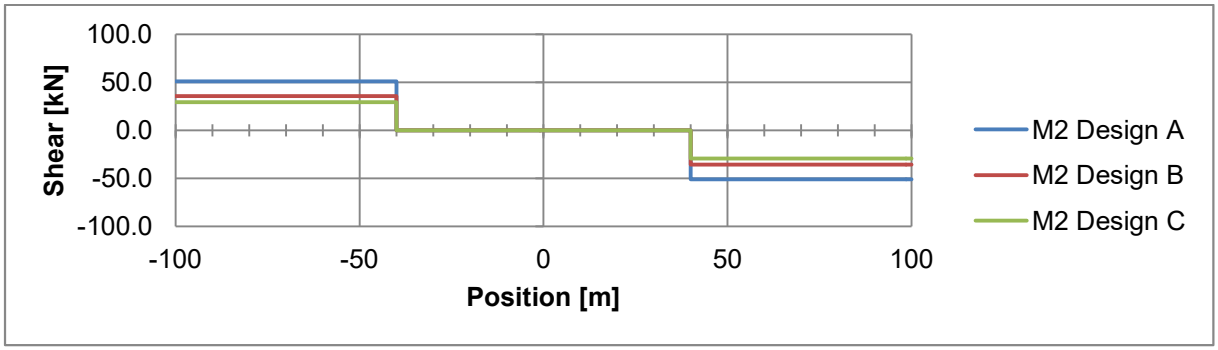

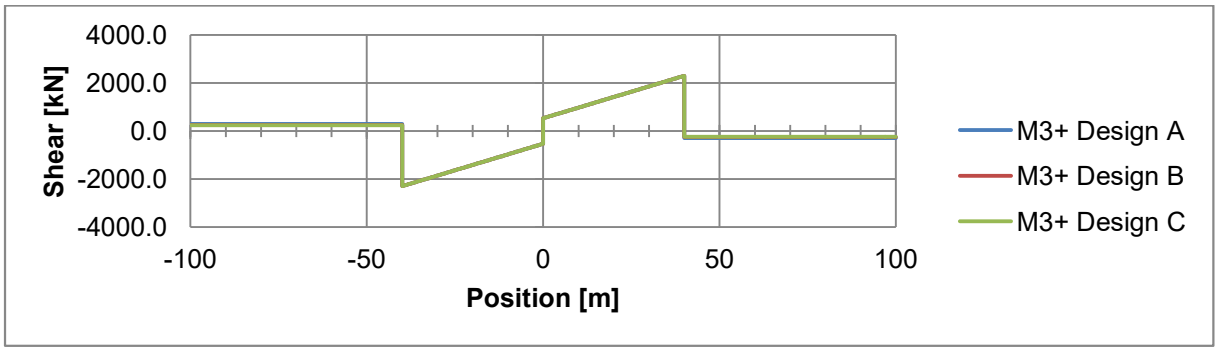

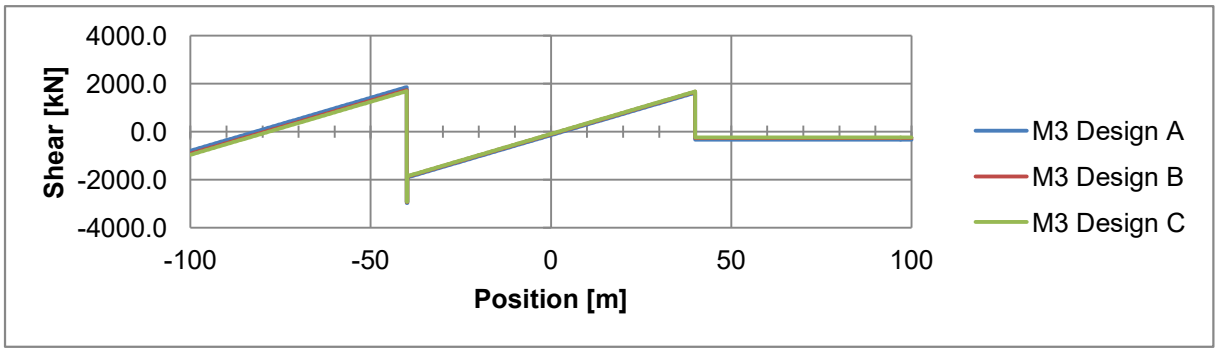

Annex X. Design elastic stresses in the gross cross-sections

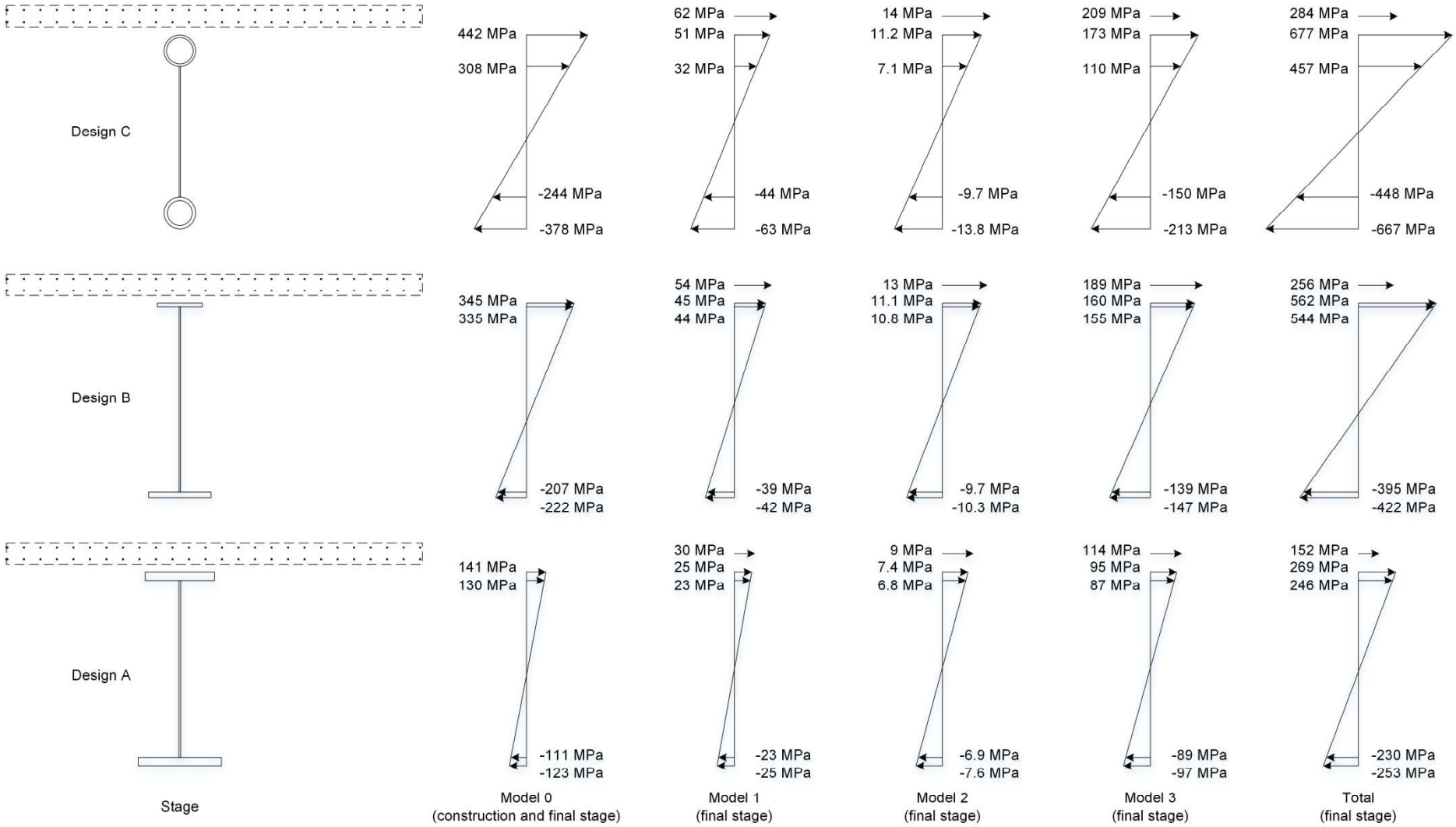

Figure 31: Stress distribution in the gross cross-section at support P1 (all designs, all stages)

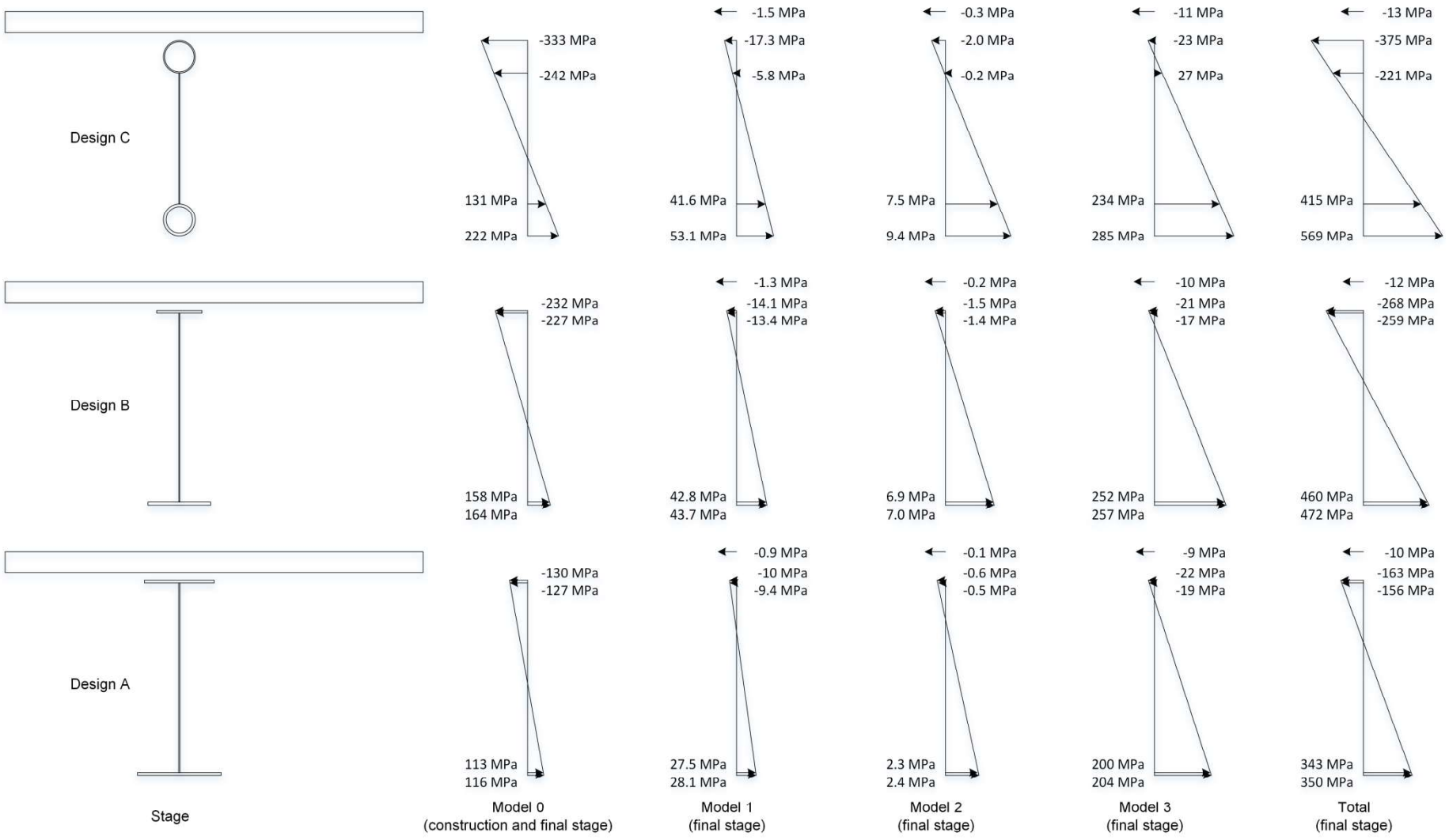

Figure 32: Stress distribution in the gross cross-section at mid-span P1-P2, (all designs, all stages)

Annex XI. Design elastic stresses in the effective cross-sections

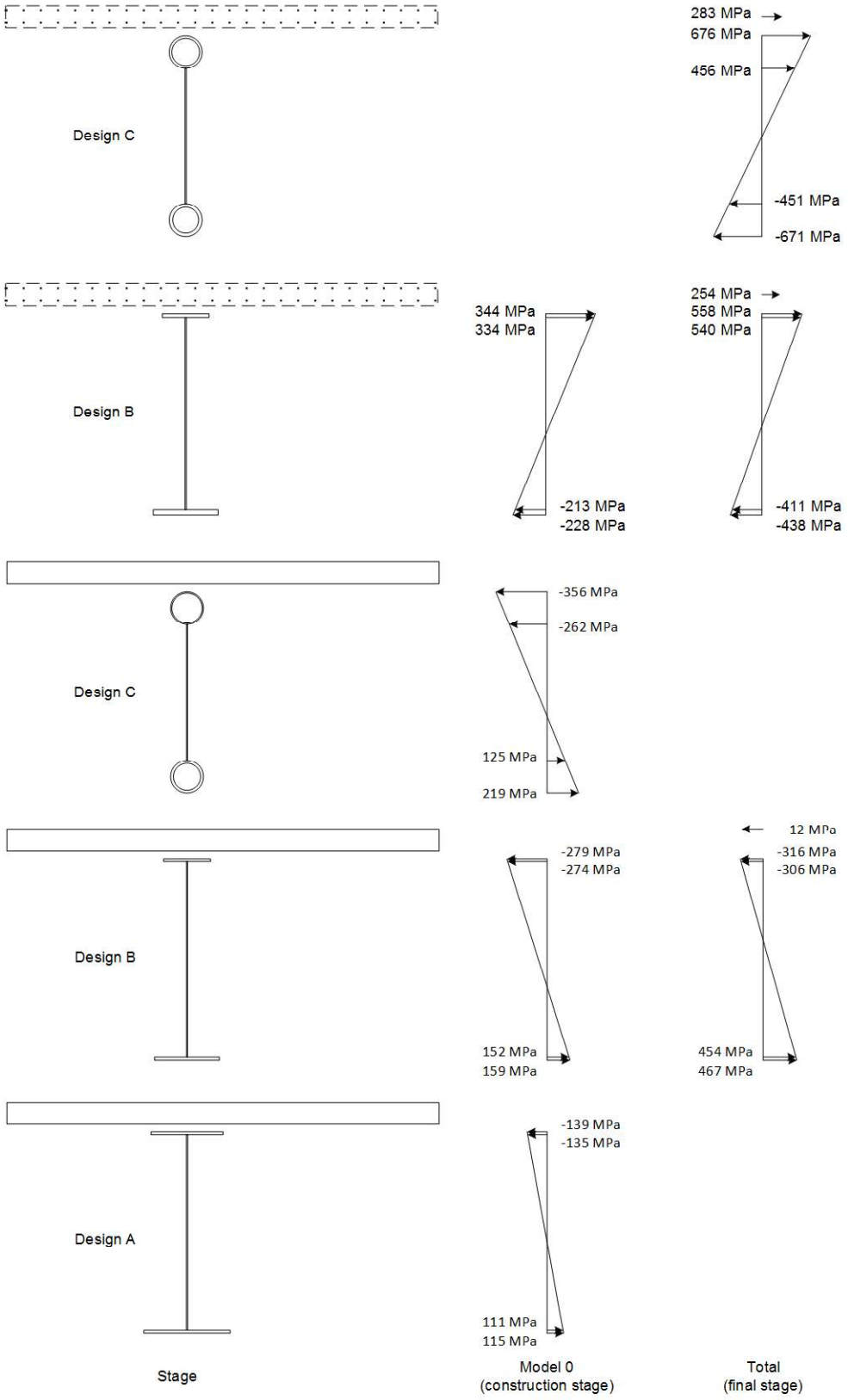

Figure 33: Stress distribution in all effective cross-sections (all designs, all stages)

Annex XII. Design plastic moment resistance

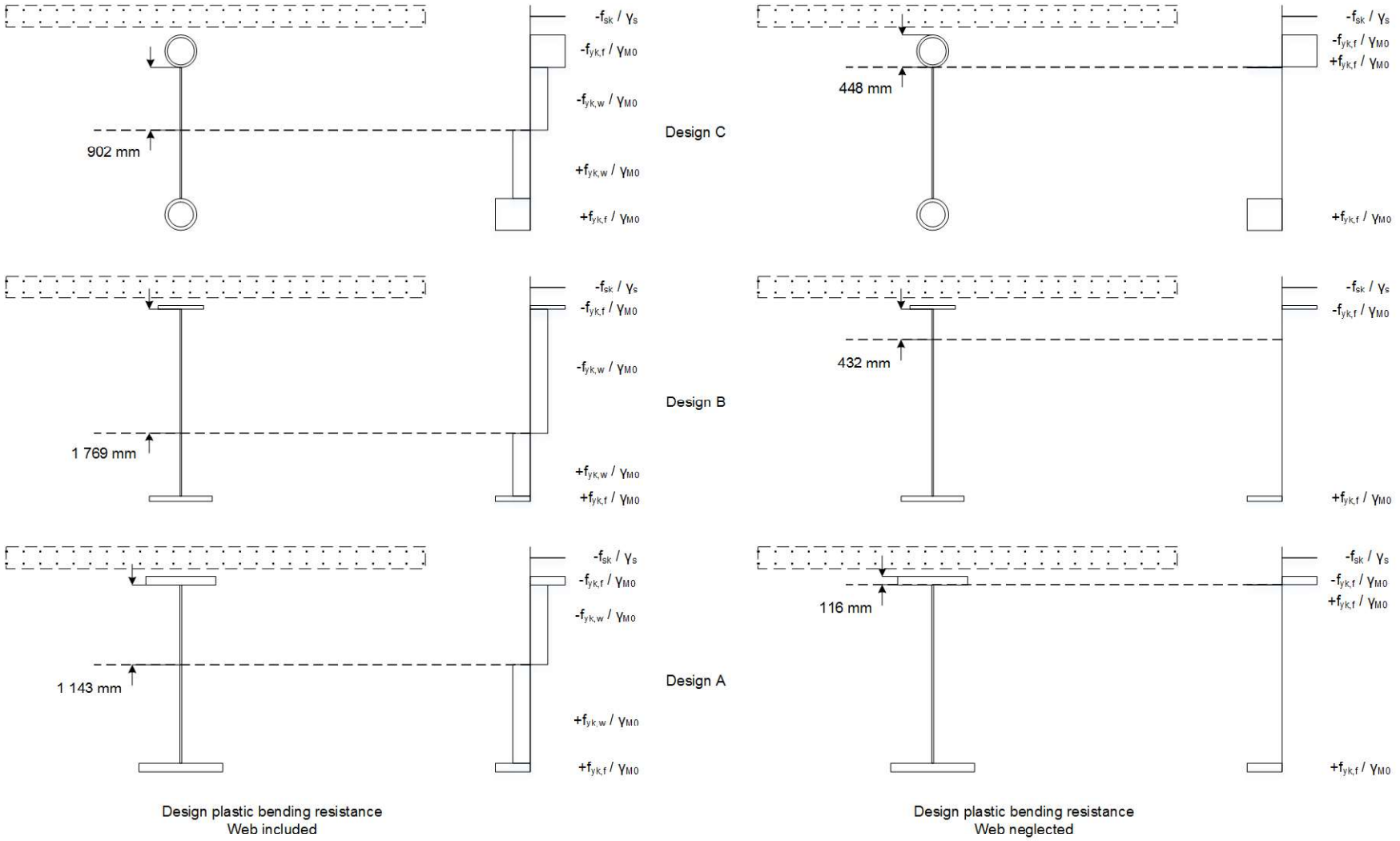

Figure 34: Design plastic moment resistance

Annex XIII. General check method for the LTB justification

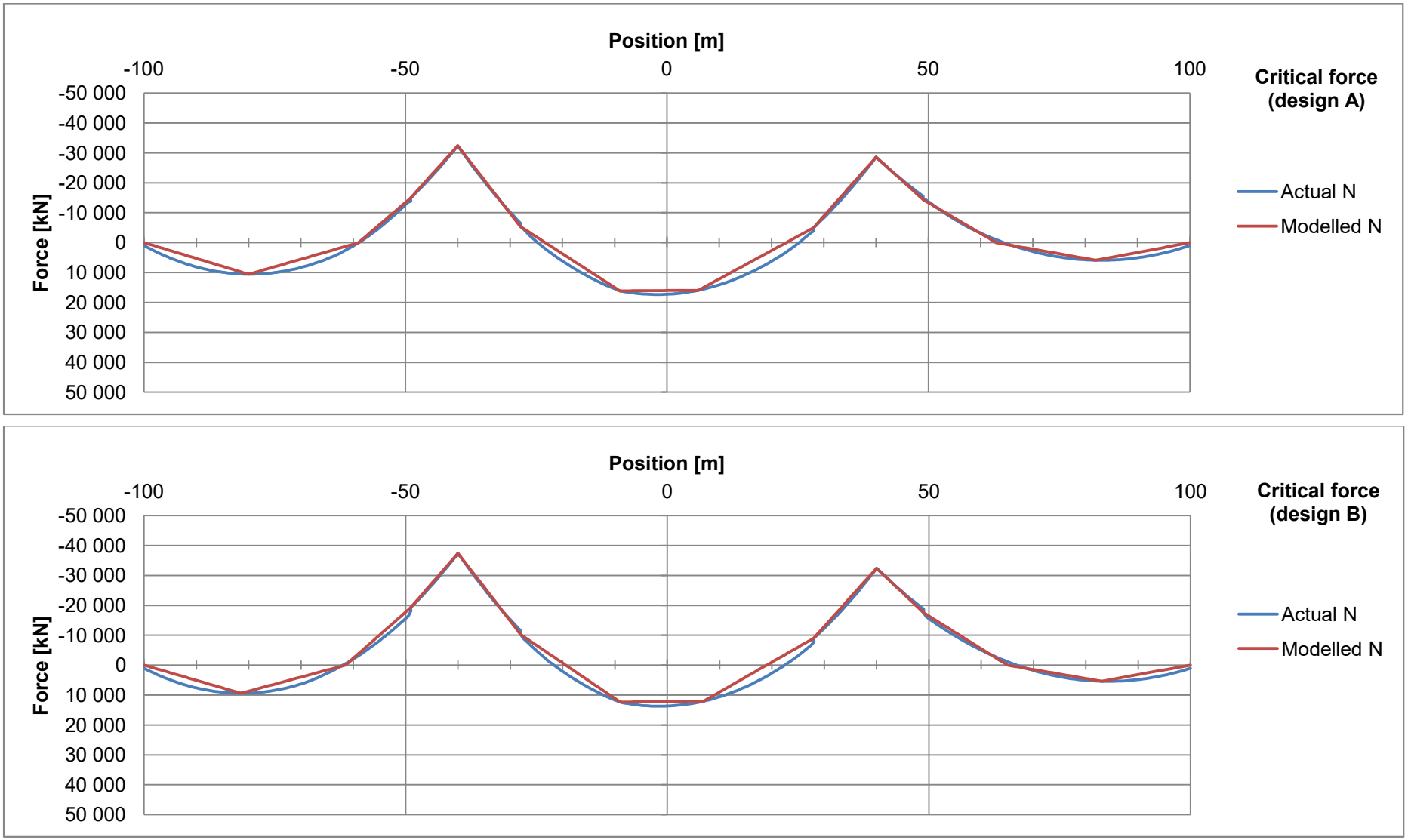

Annex XIV. Bending moment diagrams and influence lines at FLS

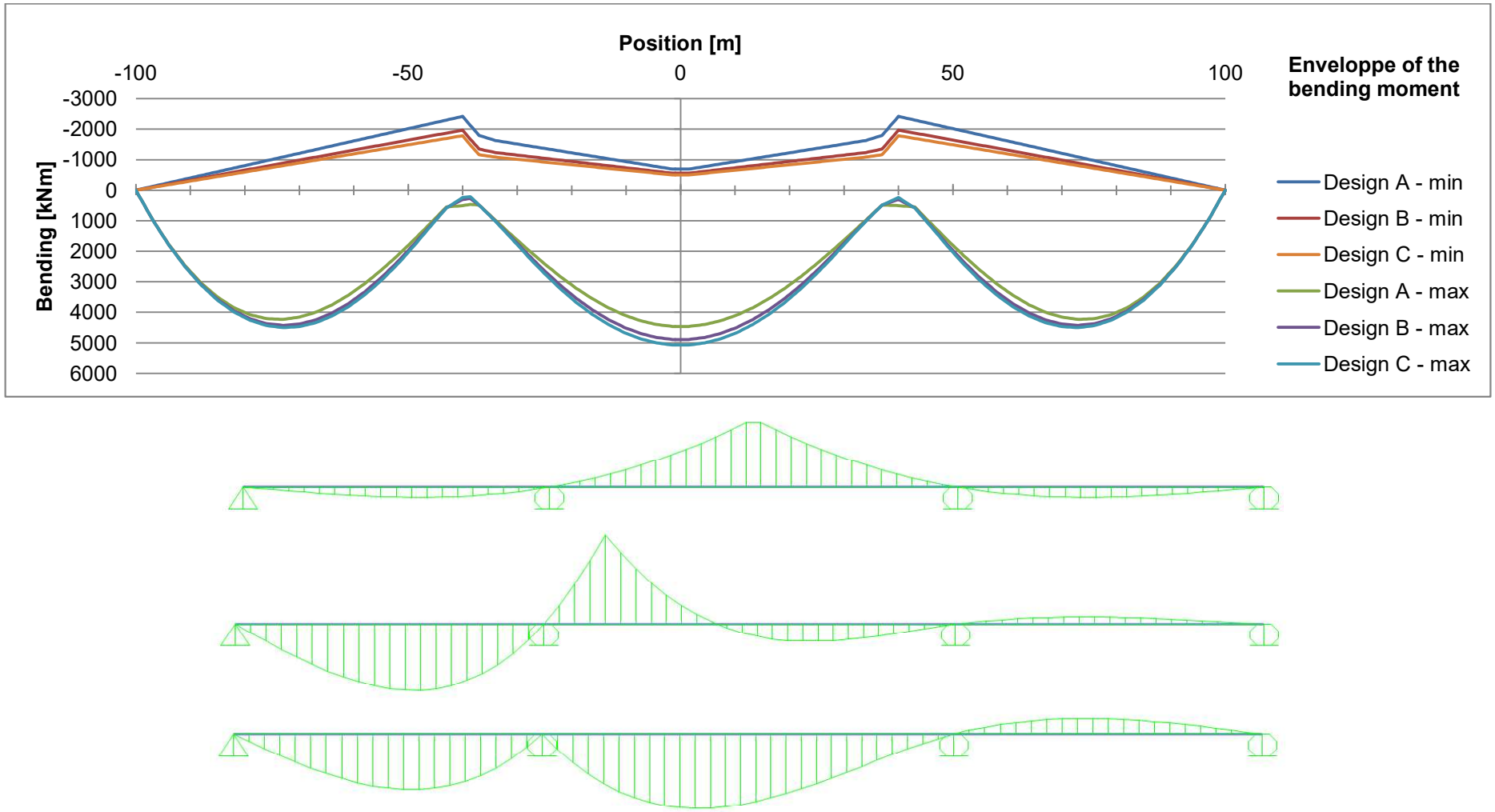

Figure 35: Influence lines for the details 1, 2 and 3